PHYS-633: Introduction to Stellar Astrophysics

Stan Owocki

Version of October 31, 2010

Contents

1. Course Overview: Stellar Atmospheres vs. Interiors

The discussion in DocOnotes1-stars gives a general overview of how the basic observables of stars – position, apparent brightness, and color spectrum – can be used, together with some basic physical principles, to infer or estimate their key physical properties – mass, luminosity, radius, etc. DocOnotes2-spectra show that, while the spectral energy distributions (SED) from observed stars can be roughly approximated by a Planck BlackBody function, the detailed spectrum contains a complex myriad of absorption lines imprinted by atomic absorption of radiation escaping the stellar atmosphere.

The goals of this course, and the notes here, are now to extend these relatively simplifed concepts to gain a more complete understanding of both the atmospheres and interiors of stars.

While the *atmosphere* consists of only a tiny fraction of the overall stellar radius and mass (respectively about 10^{-3} and 10^{-12}), it represents a crucial boundary layer between the dense interior and the near vacuum outside, from which the light we see is released, imprinting it with detailed spectral signatures that, if properly interpreted in terms of the physics principles coupling gas and radiation, provides essential information on stellar properties. In particular, the identities, strengths, and shapes (or profile) of spectral lines contain important clues to the physical state of the atmosphere – e.g., chemical composition, ionization state, effective temperature, surface gravity, rotation rate. However these must be properly interpreted in terms of a detailed model atmosphere that accounts properly for basic physical processes, namely: the excitation and ionization of atoms; the associated absorption, scattering and emission of radiation and its dependence on photon energy or frequency; and finally how this leads to such a complex variation in emitted flux vs. frequency that characterizes the observed spectrum. Such model atmosphere interpretation of stellar spectra form the basis for inferring basic stellar properties like mass, radius and luminosity.

But once given these stellar properties, a central goal is to understand how they interrelate with each other, and how they develop and evolve in time. The first represents the problem of *stellar structure*, that is the basic equations describing the hydrostatic support against gravity, and the source and transport of energy from the deep interior to the stellar surface.

The latter problem of *stellar evolution* breaks naturally into questions regarding the *origin and formation* of stars, their gradual *aging* as their nuclear fuel is expended, and how they eventually *die*.

The first issue regarding origin and formation of stars represents a very broad area of active research; it could readily encompass a course of its own, but is usually part of

a course on the Inter-Stellar Medium (ISM), which indeed provides the source mass, from gas and dust in dense, cold molecular clouds, that is condensed by self gravity to form a proto-star. Apart from some brief discussions, e.g. of the critical "Jean's" length or mass for gravitational collapse of a cloud, we will have little time for discussion of star formation in this course.

Instead, our examination of stellar evolution will begin with the final phases of contraction (on what's known as the "Hayashi track") toward the *Zero-Age Main Sequence* (ZAMS), representing when the core of a star is first hot enough to allow a nuclear-fusion burning of hydrogen into helium. This then provides an energy source to balance the loss by the radiative luminosity, allowing the star to remain on this MS for many millions or even (e.g. for the Sun) billions of years. But the gradual MS aging as this core-H fuel is spent leads ultimately to the *Terminal Age Main Sequence* (TAMS), when the core H is exhausted, whereupon the star actually expands to become a cool, luminous "giant".

A key overall theme is that the luminosity and lifetime on the MS, and indeed the very nature of the post-MS evolution and ultimate death of stars, all depend crucially on their *initial mass*.

1.1. Differences between Atmospheres and Interiors

But our path to this heart of a star and its life passes necessarily through the atmosphere, the surface layers that emit the complex radiative spectrum that we observe and aim to interpet. So let us begin by listing some key differences between stellar atmospheres vs. interiors:

- **Scale:** Whereas a stellar interior extends over the full stellar radius R, the atmosphere is just a narrow surface layer, typically only about $10^{-3}R$.
- **Mean-Free-Path:** By definition an atmosphere is where the very opaque nature of the interior finally becomes semi-transparent, leading to escape of radiation. This transparency can be quantified in terms of the ratio of photon mean-free-path ℓ to a characteristic length to escape. In the interior ℓ is very small (a few cm), much smaller than the stellar radius scale R. But in the atmospheric surface ℓ becomes of comparable to the scale height H (which is also of order $10^{-3}R$), allowing single flight escape.
- **Isotropy:** The opaqueness of the interior means its radiation field is nearly isotropic, with only a tiny fraction (of order $\ell/R \ll 1$) more photons going up than down. By

contrast, the esape from the photosphere makes the radiation field there distinctly anisotropic, with most radiation going up, and little or none coming down from the nearly empty and transparent space above.

- **Radiation Transport:** Given the above distinctions, we can see that the transport of radiative energy out of the interior can be well modeled in terms of a local diffusion; by contrast, the transition to free escape in the atmosphere must be cast in terms of a more general equation of radiative transfer that in principle requires an integral, and thus inherently *non-local*, solution.

- **LTE vs. NLTE:** In the interior extensive absorption of radiation implies a strong radiation-matter coupling that is much like a classical blackbody, and so leads very nearly to a *Local Thermodynamic Equilibrium* (LTE), with the radiation field well characterized by the Planck function $B_\nu(T)$. In contrast, the inherently non-local transport in an atmosphere, particularly in a case with a strong degree of *scattering* that does not well couple the radiation to the thermal properties of the gas, can lead to a distinctly Non Local-Thermodynamic-Equilibrium [1] (NLTE).

- **Temperature:** The escape of radiation makes an atmospheric surface relatively "cool", typically $\sim 10^4$ K, in contrast to the $\sim 10^7$ K temperature of the deep interior, where the opaqueness of overlying matter acts much like a very heavy "blanket".

- **Pressure:** To balance its own self-gravity, a star has to have much higher pressure in the interior than at the surface.

- **Density:** Even with the high temperature, this gravitational compression also leads to a much higher central density.

- **Energy Balance:** While the surface luminosity represents energy *loss* from the atmosphere, the very high density and temperature within the deep stellar core results in a nuclear burning that provides an energy *source* to the interior.

Despite these many important differences, there are a few fundamental concepts that are essential for both atmospheres and interiors. The next few sections cover some key examples, for example the *opacity* that couples radiation to matter, and the balance between pressure gradient and gravity the supports both a star and its atmosphere in *hydrostatic equlibrium*.

---

[1] The negation of the "Non" here is of the whole concept of LTE, and not, e.g., a TE that happens to be non-local (NL).

2. Escape of Radiation from a Stellar Envelope

Most everything we know about a star comes from studying the light it emits from its visible surface layer or "atmosphere". But the energy for this visible emission can be traced to nuclear fusion in the stellar core. As illustrated in fig. 1, to reach the surface, the associated photons must diffuse outward via a "random walk" through the stellar envelope.

To decribe the extent of this diffusion, one needs to estimate a typical photon mean-free-path (mfp) in the stellar interior,

$$\ell \equiv \frac{1}{n\sigma} = \frac{1}{\kappa\rho}\,, \tag{2.1}$$

where mass and number densities (ρ and n) are related through the mean mass per particle μ, i.e. $\rho = \mu n$, and the opacity κ is likewise just the interaction cross section σ per particle mass, i.e. $\kappa = \sigma/\mu$.

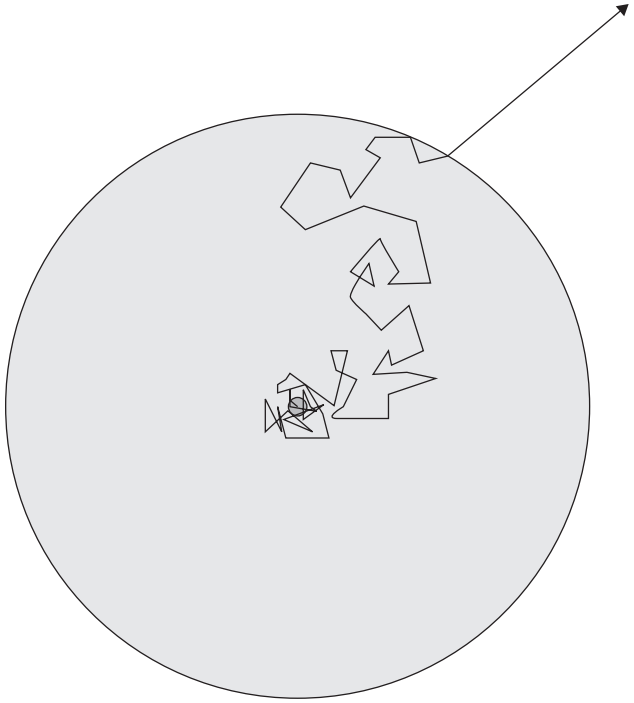

Fig. 1.— Illustration of the random-walk diffusion of photons from the core to surface of a star.

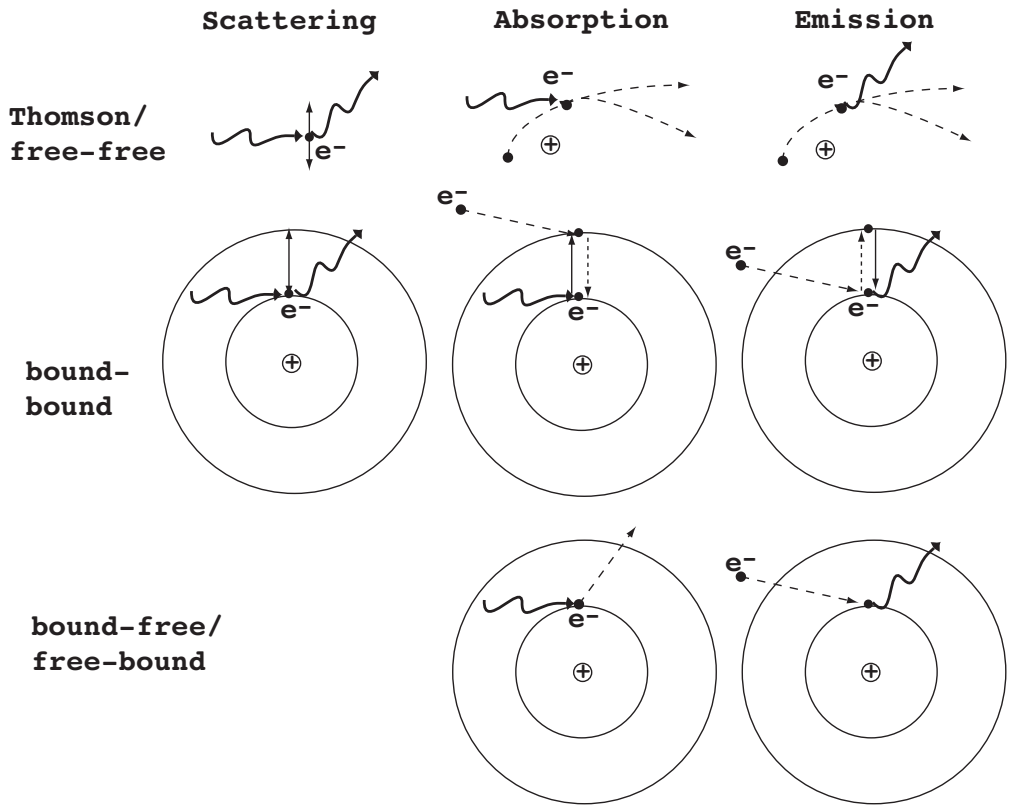

Fig. 2.— Illustration of the free-electron and bound-electron processes that lead to scattering, absorption, and emission of photons.

2.1. Sources of Stellar Opacity

The opacity of stellar material is a central issue for both interiors and atmospheres, so let's briefly summarize the sources of stellar opacity in terms of the basic physical processes. Because light is an electromagnetic wave, its fundamental interaction with matter occurs through the variable acceleration of charged particles by the varying electric field in the wave. As the lightest common charged particle, electrons are most easily accelerated, and thus they are generally key for the interaction of light with matter. But the details of the interaction, and thus the associated cross sections and opacities, depend on the bound vs. free nature of the electron. The relevant combinations are illustrated in figure 2, and are briefly listed as follows:

1. *Free electron (Thomson) scattering*

2. *Free-free (f-f) absorption*

3. *Bound-free (b-f) absorption*

4. *Bound-bound (b-b) absorption or scattering*

Because a completely isolated electron has no way to store both the energy and momentum of a photon, it cannot by itself absorb radiation, and so instead simply scatters, or redirects it. Such "Thomson scattering" by free electrons (item #1) is thus distinct from the "true" absorption of the free-free (item #2) interaction of electrons that are unbound, but near enough to an ion to share the momentum and energy of the absorbed photon. In the latter, the electron effectively goes from one hyperbolic orbital energy to another. Since the hyperbolic orbital energies of such free electrons are not quantized, such f-f absorption can thus in principal occur for *any* photon energy.

Moreover, for photons with sufficient energy to *ionize* or kick off an electron bound to an atom or ion, there is then also bound-free absorption (item #3). This is non-zero for any energy above the ionization threshhold energy.

Lastly, for photons with just the right energy to excite an atom or ion from one discrete bound level to a higher bound level, there can be bound-bound absorption (item #4). This is the basic process behind the narrow absorption lines in observed stellar spectra. Following such initial absorption to excite an electron to a higher bound level, quite often the atom will then simply spontaneously de-excite back to the same initial level, emitting a photon of nearly the same original energy, but in a different direction, representing then a b-b *scattering*. On the other hand, if before this spontaneous decay can occur, another electron *collisionally de-excites* the upper level, then overall there is a "true" absorption, with the energy of the photon ending up in the colliding electron, and thus ultimately shared with the gas.

A key distinction between scattering and true absorption is thus that the latter provides a way to couple the energetics of radiation and matter, and so tends to push both towards thermodynamical equilibrium (TE).

Note finally that the *emission* of radiation generally occurs by the *inverse* of the last 3 absorption processes in the above list, known thus as

1. *Free-free (f-f) emission*

2. *Free-Bound (f-b) emission*

3. *Bound-bound (b-b) emission*

2.2. Thomson Cross-Section and the Opacity for Electron Scattering

In the deep stellar interior, where the atoms are generally highly ionized, a substantial component of the opacity comes just from the scattering off free electrons. This is a relatively simple process that can be reasonably well analyzed in terms of classical electromagnetism, in contrast to the quantum mechanical models needed for photon interaction with electrons that are bound within atoms.

The upper left panel of figure 2 illustrates how the acceleration of an electron induces a corresponding variation of its own electric field, which then induces a new electromagnetic wave, or photon, that propagates off in a new direction. The overall process is called "Thomson scattering", after J.J. Thomson, who in the late 19th century first worked out the associated 'Thomson cross section' using Maxwell's equations for E&M. Details can usually be found in any undergraduate E&M text, but the site here gives a basic summary of the derivation: `http://farside.ph.utexas.edu/teaching/jk1/lectures/node85.html`

Intuitively, the result can be roughly understood in terms of the so-called "classical electron radius" r_e. This is obtained through the equality,

$$\frac{e^2}{r_e} \equiv m_e c^2 \,, \tag{2.2}$$

where again e is the magnitude of the electron charge, m_e is the electron mass, and c is the speed of light. The left side is just the classical energy needed to assemble the total electron charge within a uniform sphere of radius r_e, while the right side is the rest mass energy of an electron from Einstein's famous equivalence formula between mass and energy. Eqn. (2.2) can be trivially solved for the associated electron radius,

$$r_e = \frac{e^2}{m_e c^2} \,. \tag{2.3}$$

In these terms, the Thomson cross section for free-electron scattering is just

$$\sigma_{Th} = \frac{8}{3}\pi r_e^2 = 0.66 \times 10^{-25} cm^2 = 2/3 \text{ barn} \,. \tag{2.4}$$

(The term "barn" represents a kind of physics joke, because compared to the cross sections associated with atomic nuclei, it is a huge, "as big as a barn door".) Thus we see that Thomson scattering has a cross section just 8/3 times greater than the projected area of a sphere with the classical electron radius.

For stellar material to have an overall neutrality in electric charge, even free electrons must still be loosely associated with corresponding positively charged ions, which have much

greater mass. Defining then a mean mass per free electron μ_e, we can then write the electron scattering opacity $\kappa_e \equiv \sigma_{Th}/\mu_e$. Ionized hydrogen gives one proton mass m_p per electron, but for fully ionized helium (and indeed for most all heavier ions), there are two proton masses for each electron. For fully ionized stellar material with hydrogen mass fraction X, we find then that

$$\mu_e = m_p/(1+X)\,. \tag{2.5}$$

Since $m_p \approx 5/3 \times 10^{-24}$ g, we thus obtain

$$\kappa_e = 0.2\,(1+X)\,\frac{cm^2}{g} = 0.34\,cm^2/g\,, \tag{2.6}$$

where the last equality applies a "standard" solar hydrogen mass fraction $X = 0.72$.

Two particularly simple properties of electron scattering are: 1) it is generally almost spatially constant, and 2) it is "gray", i.e. independent of photon wavelength. This contrasts markedly with many other sources of opacity, which can depend on density and temperature, as well as on wavelength, particularly for line-absorption between bound levels of an atom. We discuss such other opacity source and their scalings in greater detail below.

2.3. Random-Walk Model for Photon Diffusion from Stellar Core to Surface

For a star with mass M and radius R, the mean stellar density is $\bar{\rho} = M/((4/3)\pi R^3)$, which for the sun with $M_\odot \approx 2 \times 10^{33}$ g and $R_\odot \approx 7 \times 10^{10}$ cm works out to be

$$\bar{\rho}_\odot = \frac{M_\odot}{4\pi R_\odot^3/3} \approx 1.4\,g/cm^3\,, \tag{2.7}$$

i.e. just above the density of water. Multiplying this by the electron opacity and taking the inverse then gives an average mean-free-path from electron scattering in the sun,

$$\bar{\ell}_\odot = \frac{1}{0.34\ \times\ 1.4} = 2\,cm\,. \tag{2.8}$$

Of course, in the core of the actual sun, where the mean density is typically a hundred times higher than this mean value, the mean-free-path is yet a factor hundred smaller, i.e $\ell_{core} \approx 0.2$ mm!

But either way, the mean-free-path is much, much smaller than the solar radius $R_\odot \approx 7 \times 10^{10}$, implying a typical optical depth,

$$\tau = \frac{R_\odot}{\bar{\ell}_\odot} \approx 3.5 \times 10^{10}\,. \tag{2.9}$$

The total number of scatterings needed to diffuse from the center to the surface can then be estimated from a classical "random walk" argument. The simple 1D version states that after N left/right random steps of unit length, the root-mean-square (rms) distance from the origin is $\sqrt{N}$. For the 3D case of stellar diffusion, this rms number of unit steps can be roughly associated with the total number of mean-free-paths between the core and surface, i.e. τ. This implies that photons created in the core of the sun need to scatter a total of $\tau^2 \approx 10^{21}$ times to reach the surface! Along the way the cumulative path length travelled is $\ell_{tot} \approx \tau^2 \bar{\ell}_\odot \approx \tau R_\odot$. For photons travelling at the speed of light $c = 3 \times 10^{10}$cm/s, the total time for photons to diffuse from the center to the surface is thus

$$t_{diff} = \tau^2 \frac{\bar{\ell}_\odot}{c} \approx \tau \frac{R_\odot}{c} = 3.5 \times 10^{10} \times 2.3\, s \approx 2600\ yr\,, \tag{2.10}$$

where for the last evaluation, it is handy to note that $1\ yr \approx \pi \times 10^7\ s$.

Once the photons reach the surface, they can escape the star and travel unimpeded through space, taking, for example, only a modest time $t_{earth} = au/c \approx 8$ min to cross the 1 au distance from the sun to the earth. The stellar atmospheric surface thus marks a quite distinct boundary between the interior and free space. From deep within the interior, the stellar radiation field would appear nearly isotropic (same in all directions), with only a small asymmetry (of order $1/\tau$) between upward and downward photons. But near the surface, this radiation becomes distinctly anisotropic, emerging upward from the surface below, but with no radiation coming downward from empty space above.

We shall see below that this atmospheric transition between interior and empty space occurs over a quite narrow layer, typically a few hundred kilometers or so, or about a thousandth of the stellar radius.

3. Density Stratification from Hydrostatic Equilibrium

In reality of course stars are not uniform density, because the star's self-gravity attracts material into a higher inward concentration. In a static star, the inward gravitational acceleration $g = GM_r/r^2$ on stellar material of density ρ at local radius r must be balanced by a (negative) radial gradient in the gas pressure P,

$$\boxed{\frac{dP}{dr} = -\rho\, g = -\rho \frac{GM_r}{r^2}}\,, \tag{3.1}$$

a condition known as *Hydrostatic Equilibrium*. This is one of the fundamental equations of stellar structure, with important implications for the properties of both the interior and

atmosphere. For the atmosphere, the mass and radius are fixed at surface values M and R. But within a spherical stellar envelope, the local gravitational acceleration is set by just the total mass *interior* to the local radius r, i.e.

$$M_r \equiv \int_0^r 4\pi\rho(r')r'^2\,dr'\,. \tag{3.2}$$

To relate the density and pressure, a key auxiliary equation here is the *Ideal Gas Law*, which in this context can be written in the form,

$$P = \rho\frac{kT}{\bar{\mu}}\,, \tag{3.3}$$

where $k = 1.38 \times 10^{-16}$erg/K is Boltzmann's constant, T is the temperature, and $\bar{\mu}$ is the average mass of all particles (e.g. both ions and electrons) in the gas. For any given element, the fully ionized molecular weight is just set by the ratio of the nuclear mass to charge. For fully ionized mixture with mass fraction X, Y, and Z for H, He, and metals, the overall mean molecular weight comes from the inverse of the inverse sum of the individual molecular weights,

$$\bar{\mu} = \frac{m_p}{2X + 3Y/4 + Z/2} \approx 0.6m_p \tag{3.4}$$

where the last equality is for the solar case with $X = 0.72$, $Y = 0.27$, and $Z = 0.01$.

The ratio of eqns. (3.3) to (3.1) defines a characteristic scale height for variations in the gas pressure,

$$H \equiv \frac{P}{|dP/dr|} = \frac{kT}{\bar{\mu}g} = \frac{kTr^2}{\bar{\mu}GM}\,. \tag{3.5}$$

The huge differences in temperataure between the interior vs. surface imply a correspondly large differences in the pressure scale height H in these regions.

3.1. Million-Kelvin Virial Temperature of Stellar Interiors

Over the full stellar envelope, the pressure drops from some large central value to effectively zero just outside the surface radius R. This means that, averaged over the whole star, $H \approx R$.

Applying this in eqn. (3.5), and approximating the gravity by its surface value at $r = R$, we can readily estimate a characteristic temperature for a stellar interior,

$$T_{int} \sim \frac{GM\bar{\mu}}{kR} \sim 13 \times 10^6 K\,\frac{M/M_\odot}{R/R_\odot}\,. \tag{3.6}$$

The latter evaluation for stellar mass and radius in units of the solar values shows directly that stellar interior temperatures are typically of order 10 *million* Kelvin!

This close connection between thermal energy of particles in the interior ($\sim kT$) and their stellar gravitational binding energy ($\sim GM\bar{\mu}/R$) turns out to be an example of a general property for bound systems, often referred to as the "*virial theorum*". We will return to this again in our discussion of stellar interiors, but for now you can find further details in in R. Townsend's Stellar Interior notes 01-virial.pdf.

Note that this "virial temperature" for stellar interiors is also comparable to that needed for nuclear fusion of hydrogen into helium in the stellar core, which is about 15 MK. This correspondence is also not a coincidence. As stars contract from interstellar gas, they go through a phase wherein the gravitational energy from contraction powers their radiative luminosity. This contraction stops when the core temperature becomes hot enough for hydrogen fusion to provide the energy for the stellar luminosity. Such processes will be a central focus of our later discussion of stellar structure and evolution in the interiors part of this course.

3.2. Thinness of Atmospheric Surface Layer

In contrast to this million-Kelvin interior, the characteristic temperature in the atmospheric surface layers of a star are typically of order a few *thousand* Kelvin, i.e. near the stellar *effective* temperature, which for a star of luminosity L and radius R is given by

$$T_{eff} = \left[\frac{L}{4\pi\sigma R^2}\right]^{1/4} = 5800\,K\,\frac{(L/L_\odot)^{1/4}}{\sqrt{R/R_\odot}}\,, \tag{3.7}$$

where (as discussed in sec. 5.2 of DocOnotes1-stars) σ here is the Stefan-Boltzmann constant. For the solar surface gravity $g_{grav} = GM_\odot/R_\odot^2 \approx 2.7 \times 10^4\ cm/s^2$, molecular weight $\bar{\mu} \approx 0.6 m_p \approx 10^{-24}$ g, and photospheric temperature $T_\odot = 5800$ K, we thus obtain a surface pressure scale height that is only a tiny fraction of the solar radius,

$$H_\odot \approx 0.0005\,R_\odot \approx 300\ km\,. \tag{3.8}$$

This relative smallness of the atmospheric scale height is a key general characteristic of static stellar atmospheres, common to all but the most extremely extended giant stars. In general, for stars with mass M, radius R, and surface temperature T, the ratio of scale height to radius can be written in terms of the ratio of the associated sound speed $a_* \equiv \sqrt{kT/\bar{\mu}}$ to

surface escape speed $v_e \equiv \sqrt{2GM/R}$,

$$\frac{H}{R} = \frac{2a_*^2}{v_e^2} \approx 5 \times 10^{-4} \, \frac{T}{T_\odot} \, \frac{R/R_\odot}{M/M_\odot} \tag{3.9}$$

For the solar surface, the sound speed is $a_* \approx 9$ km/s, about 1/70th of the surface escape speed $v_e = 620$ km/s.

Because of this relative thinness of atmopheric scale heights, the emergent spectrum from a star can generally be well modeled in terms of a 1D *planar* atmosphere, in which local conditions vary only with vertical height $z = r - R$. While this height is measured relative to some reference layer $z = 0$ near the stellar radius R, the characteristics of the model are themselves largely *independent*[2] of R.

Within the atmosphere itself, the scale length for variation in temperature, $T/|dT/dr|$, is typically much larger than a pressure scale height H. If we thus approximate the atmosphere as being roughly isothermal with a constant temperature $T \approx T_{eff}$, then both the density and pressure will have an exponential stratification with height $z = r - R$,

$$\frac{P(z)}{P_*} \approx \frac{\rho(z)}{\rho_*} \approx e^{-z/H} \, , \tag{3.10}$$

where the asterisk subscripts denote values at the surface layer where $z \equiv 0$.

Once the density drops to a level where the photon mean-free-path becomes comparable to this relatively small atmospheric scale height, radiation no longer diffuses, but rather escapes fully into an unimpeded propagation away from the star. This transition between diffusion and free escape occurs over just a few scale heights $H \ll R$. This explains the very sharp edge to the visible solar photosphere.

4. The Stellar Radiation Field

4.1. Surface Brightness or Specific Intensity I

The radiation field within a star can be fundamentally described in terms of the *specfic intensity*, I. For radiation of frequency ν at some spatial location $\mathbf{r}$, $I_\nu(\hat{\mathbf{n}}, \mathbf{r})$ represents the

[2]Analogously, the properties of earth's atmosphere are quite sensitive to the height above sea level, which is at a central radial distance of roughly an earth's radius. But otherwise, the actual value of earth's radius plays little role in the physics of the atmosphere, which is also much more affected by earth's gravity and characteristic surface temperature.

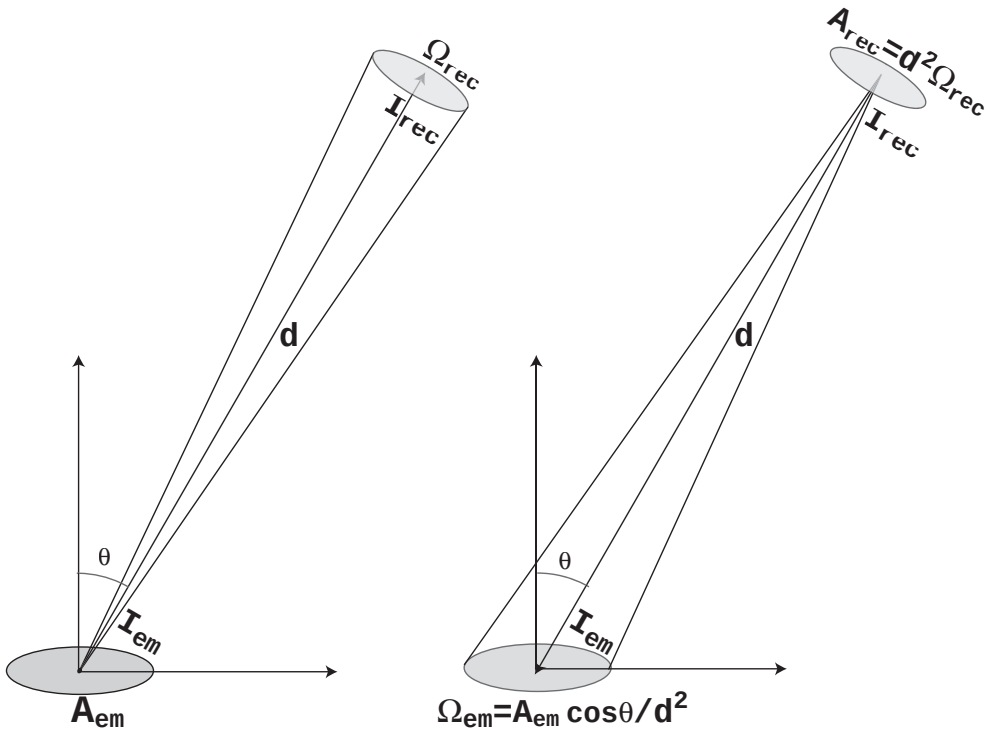

Fig. 3.— Left: The intensity I_{em} emitted into a solid angle Ω_{rec} located along a direction that makes an angle θ with the normal of the emission area A_{em}. Right: The intensity I_{rec} received into an area $A_{rec} = D^2\Omega_{rec}$ at a distance D from the source with projected solid angle $\Omega_{em} = A_{em}\cos\theta/D^2$. Since the emitted and received energies are equal, we see that $I_{em} = I_{rec}$, showing that intensity is invariant with distance D.

energy per-unit-area, per-unit-time, per-unit-frequency, and *per-unit solid angle*[3] about the radiation direction $\hat{\mathbf{n}}$. It can also be thought of the "surface brightness" of a small patch of the sky in a given direction.

As illustrated in figure 3, a key point is that the *specific intensity remains unchanged*

[3]A solid angle is a 2-D generalization of a 1-D angle in a plane. Much as the circumference of a unit circle implies there are 2π radians along the full arc of the circle, so the area of a unit sphere implies that the solid angle of the full sky is 4π steradians. If one imagines a sphere centered on the observer but outside some observed object, then the solid angle of the object is given by the area of the *shadow* the object makes on the sphere divided by the square of the radius of the sphere. For an object with an area A and surface normal that makes an angle θ with the line of sight to observer, the solid angle seen from a large distance D is approximately $\Omega = A\cos\theta/D^2$ steradian.

during propagation through a vacuum, i.e. without any material to absorb or emit radiation. This may seem at first surprising because intuitively we know that the *flux* from a radiative source typically falls off with the inverse square of the distance. But note then the *specific intensity represents a kind of flux per unit solid angle.*

Since the solid angle of a source with fixed size, like the sun, also declines with inverse distance squared, the specific intensity of the resolved source, for example the surface brightness of the sun, remains the same viewed from any distance. When we see the sun in earth's sky, its disk has the same brightness (ignoring absorption by earth's atmosphere) as it would have if we were to stand on the surface of the sun itself!! See §5.1 of DocOnotes1-stars for some further discussion on the constancy of specific intensity and the meaning of solid angle.

In contrast to this constancy of specific intensity for radiation propagating through free space, the specific intensity at any point within the atmosphere or interior of a star depends on the sources and sinks of radiation from its interaction with stellar matter. As we shall see in the discussion below, this can in general quite difficult to determine. But within the very deep stellar interior, it again becomes relatively simple to describe, set by $I_\nu \approx B_\nu$, where the Planck blackbody function depends only on the local temperature T. Note this implies that I_ν in the interior is *isotropic*, i.e. the same in all directions $\hat{\mathbf{n}}$.

Between these simple limits of the isotropic, Planckian intensity of the deep interior and the free-streaming constancy of intensity through empty space, lies the stellar *atmosphere*, where I_ν is generally a complex function of spatial location $\mathbf{r}$, frequency ν, and direction $\hat{\mathbf{n}}$. But if one ignores the complex 3-D spatial structure seen in actual views of, e.g. the solar atmosphere, the overall radial thinness of an atmosphere implies that the directional dependence can be completely described in terms of the projection of the radiation direction onto the local vertical, i.e. $\mu = \hat{\mathbf{n}} \cdot \hat{\mathbf{z}}$, giving then $I_\nu(\mu, z)$.

Moreover, if we defer for now discussion of the dependence on frequency, we can suppress the ν index, and so simply write $I(\mu, z)$.

4.2. Mean Intensity J

In some contexts, it is of interest just to describe the angle-averaged intensity, that is, I integrated over the full 4π steradians of solid angle Ω,

$$J \equiv \frac{1}{4\pi} \oint I(\hat{\mathbf{n}})\, d\Omega = \frac{1}{2} \int_{-1}^{+1} I(\mu) d\mu \,, \tag{4.1}$$

where the latter applies to the case of a planar atmosphere, noting that $d\Omega = -d\mu d\phi$, and carrying out the integral over the 2π radians of the azimuthal angle ϕ, over which I is

assumed to be constant. In such a planar case, the mean intensity depends only on height, $J(z)$.

For light propagating at speed c, the mean intensity gives directly the radiative energy density per unit volume,

$$U = \frac{4\pi J}{c} \,. \tag{4.2}$$

4.3. Eddington Flux H

The *vector radiative flux* is given by

$$\mathbf{F} \equiv \oint \hat{\mathbf{n}}\, I(\hat{\mathbf{n}})\, d\Omega = 2\pi\, \hat{\mathbf{z}} \int_{-1}^{+1} \mu\, I(\mu)\, d\mu \equiv 4\pi H\, \hat{\mathbf{z}}\,, \tag{4.3}$$

where again the second equality applies for the vertical flux in a planar atmosphere. The last equaility defines the *Eddington flux*,

$$H \equiv \frac{1}{2} \int_{-1}^{+1} \mu\, I(\mu)\, d\mu\,, \tag{4.4}$$

which is constructed to have an analogous form to the mean intensity J, but now with a μ factor within the integral.

4.4. Second Angle Moment K

The mean intensity and Eddington flux can also be characterized as the two lowest angle *moments* of the radiation field. For a planar atmosphere, the general "j-th" moment is defined by

$$M_j \equiv \frac{1}{2} \int_{-1}^{+1} \mu^j\, I(\mu)\, d\mu\,, \tag{4.5}$$

by which we see that J and H represent respectively the zeroth and first moments. The next highest, or second moment, is given by setting $j = 2$,

$$K \equiv \frac{1}{2} \int_{-1}^{+1} \mu^2\, I(\mu)\, d\mu\,. \tag{4.6}$$

Physically K is related to the *radiation pressure*, P_R. In a planar atmosphere, this just represents the *vertical* transport of the *vertical momentum* of radiation. Since radiative

momentum is given by the energy divided by light speed, we find

$$P_R \equiv 4\pi \int_{-1}^{+1} \frac{I(\mu)}{c}\, \mu^2\, d\mu = \frac{4\pi K}{c}\,. \tag{4.7}$$

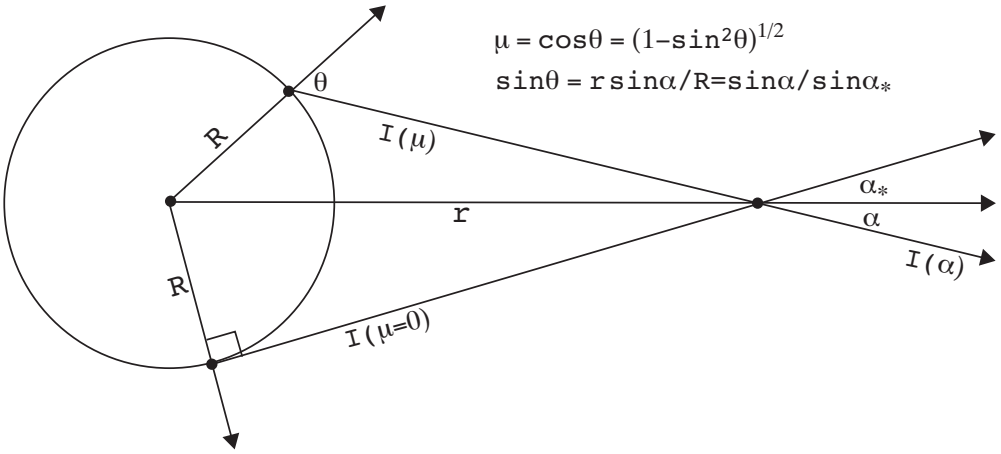

Fig. 4.— A diagram to illustrate how the surface intensity $I(\mu)$ relates to that seen by an observer at distance r from a star of radius R, with the observer angle α and surface angle $\theta = \arccos\mu$ related through the law of signs.

Exercise: As illustrated in figure 4, consider an observer at a distance r from the center of a star of radius R that has an uniformly bright surface, i.e., $I(\mu) = I_o$ = constant for all $\mu > 0$.

a. Derive analytic expressions for $J(r)$, $H(r)$, and $K(r)$ in terms of $\alpha_* \equiv \sin^{-1}(R/r)$.

b. Use these to write expressions for the ratios H/J and K/J in terms of α_*, and in terms of r/R.

c. Plot both ratios vs. r/R over the range $[1, 5]$.

Exercise: The angular diameter of the sun is $\Delta\alpha = 30'$. Suppose that terrestrial atmospheric seeing effects limit our angular resolution to $\delta\alpha = 1$".

a. Show that this sets a lower bound on the μ for which we can infer $I(\mu)$.

b. Derive a formula for this μ_{min} in terms of $\Delta\alpha$ and $\delta\alpha$.

c. Compute a numerical value for the solar/terrestrial parameters given above.

4.5. The Eddington Approximation for Moment Closure

We can in principle continue defining higher and higher moments, but their physical meaning becomes more and more obscure. Instead, it often useful to truncate this moment procedure by finding a *closure* relation between a higher and a lower moment, usually K and J. It then becomes useful to define the ratio $f \equiv K/J$, which was first emphasized by Sir Arthur Eddington, and so is known as the *Eddington factor*. In particular, note that for an isotropic radiation field with $I(\mu) = I_o = \text{constant}$, we have

$$f \equiv \frac{K}{J} = \frac{P_R}{U} = \frac{1}{3}\,. \tag{4.8}$$

This certainly holds very well for the near-isotropic radiation in the stellar interior. But we will see below that the "Eddington approximation", $f \approx 1/3$, or equivalently $J \approx 3K$, is actually quite useful in modeling the stellar atmosphere as well, even though it ultimately becomes harder to justify near, and especially beyond, the stellar surface.

Exercise: Indeed, show that, far from a stellar surface, the intensity approaches a point source form, $I(\mu) = I_o\delta(\mu - 1)$, for which then $J = H = K$ and thus $f = 1$.

Exercise: On the other hand, consider the physically quite reasonable model that, at the stellar surface, $I(\mu) = I_o$ is constant for $\mu > 1$, and zero otherwise. Show that $f = 1/3$, and thus that the Eddington approximation still holds.

The full homework set includes some further illustrative exercises with the Eddington factor f.

5. Radiation Transfer: Absorption and Emission in a Stellar Atmosphere

The atmospheres and interiors of stars are, of course, not at all a vacuum, and so we don't expect in general for I to remain spatially constant through a star. Rather the material absorption and emission of radiation will in general lead to spatial changes in the radiation field I, something known generally as "radiation transport" or "radiative transfer". To derive a general equation for radiative transfer, let us first consider the case with just absorption, ignoring for now any emission source of radiation.

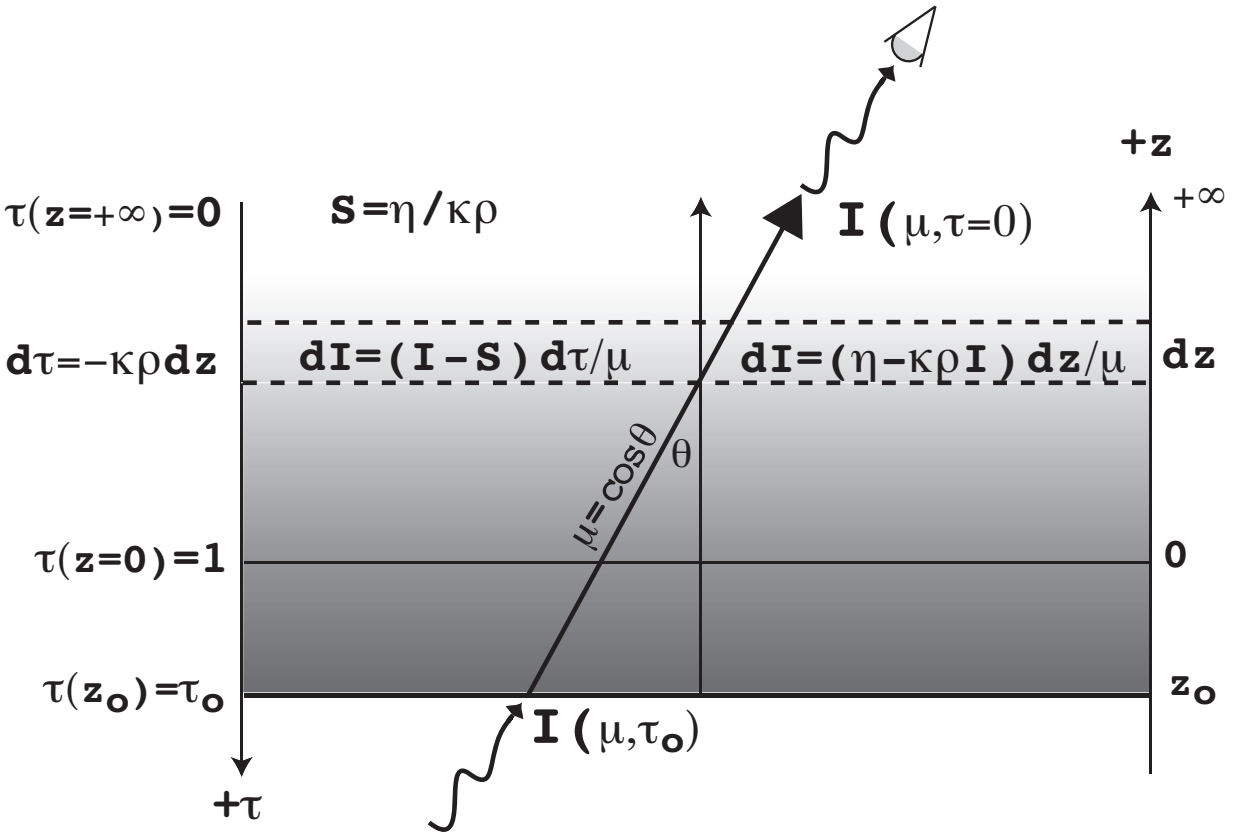

Fig. 5.— Illustration of the emergent intensity from emission and absorption in a stratified planar atmosphere. The lower boundary at $z = z_o$ and $\tau = \tau_o$ is assumed to have an intensity $I(\mu, \tau_o)$, where $\mu = \cos\theta$ is the vertical projection cosine of the ray.

5.1. Absorption in Vertically Stratified Planar Layer

This near-exponential stratification of density over a narrow atmospheric layer near the stellar surface implies a strong increase in absorption of any light emitted from lower heights z. The basic situation is illustrated by figure 5, but for now neglecting any gas emission ($\eta = 0$). For density ρ and opacity κ over a local height interval dz, the differential reduction in specific intensity $I(\mu, z)$ along some direction with projection cosine μ to the vertical gives

$$\mu \frac{dI}{dz} = -\kappa\rho I \, . \tag{5.1}$$

Integration from a lower height z_o, with intensity $I(\mu, z_o)$, to a distant observer at $z = +\infty$ gives an observed intensity,

$$I(\mu, z = +\infty) = I(\mu, z_o) e^{-\tau(z_o)/\mu} \, , \tag{5.2}$$

where the vertical *optical depth* from the observer to any height z is defined generally by

$$\tau(z) \equiv \int_z^\infty \kappa\rho(z')dz' \,. \tag{5.3}$$

In an atmosphere with a constant opacity κ and an exponentially stratified density, $\rho(z) = \rho_* \exp(-z/H)$, this optical depth integral evaluates to

$$\tau(z) = \kappa H \rho_* e^{-z/H} = e^{-z/H} \,. \tag{5.4}$$

where the last equality defines the height $z = 0$ to have a characteristic density $\rho(z = 0) = \rho_* = 1/\kappa H$. Note that this defines this reference height $z = 0$ to have a vertical optical depth $\tau(0) = 1$.

For hot stars with surface temperatures more than about 10,000 K, hydrogen remains almost fully ionized even in the photosphere, and so the opacity near the surface is again roughly set by electron scattering, $\kappa \approx \kappa_e$, while the scale height is again roughly comparable to the solar value $H \approx 300\ km$. This thus implies a typical photospheric density $\rho_* \approx 10^{-7}\, g/cm^3$.

At the much cooler solar surface, hydrogen is either neutral, or even negatively charged, H^-. The latter occurs through an induced dipole binding of a second electron, with ionization potential of just 0.75 eV, i.e. almost a factor 20 lower than the 13.6 eV ionization energy of neutral H. (See, e.g., §3 of DocOnotes2-spectra.) Because a substational fraction of the photons in the photosphere have sufficient energy to overcome this weak binding, it turns out the "bound-free" (b-f) absorption of H^- is a dominant source of opacity in the solar atmosphere, with a characteristic value of $\kappa_{bf} \approx 100\, cm^2/g$, i.e. more than a hundred times the opacity from electron scattering. This implies a solar photospheric density is likewise more than a factor hundred lower than in hotter stars, $\rho_* \approx 3 \times 10^{-10}\, g/cm^3$.

5.2. Radiative Transfer Equation for a Planar Stellar Atmosphere

Let us thus now generalize the above pure-absorption analysis to account also for a non-zero radiative emissivity η, specifying the rate of radiative energy emission *per-unit-volume*, and again into some solid angle. As illustrated in figure 5, this adds now a *positive* contribution $\eta dz/\mu$ to the the change in specific intensity dI defined in eqn. (5.1), yielding a general first-order, ordinary differential equation for the change of intensity with height,

$$\mu \frac{dI}{dz} = \eta - \kappa\rho I \,, \tag{5.5}$$

Commonly known as the *Radiative Transfer Equation* (RTE), this represents the basic controlling relation for the radiation field within, and emerging from, a stellar atmosphere. It can alternatively be written with the optical depth τ as the independent variable,

$$\mu \frac{dI}{d\tau} = I - S \,, \tag{5.6}$$

where the ratio of the emission to absorption, $S \equiv \eta/\kappa\rho$, is called the *source function*. The emissivity η represents an emitted energy/volume/time/solid-angle, and when this is divided by the opacity and density, with combined units of inverse-length, it gives the source function units of specific intensity (a.k.a. surface brightness).

Exercise: Consider a planar slab of physical thickness ΔZ and constant density ρ , opacity κ, and nonzero emissivity η. If the intensity impingent on the slab bottom is $I_o(\mu)$, compute the emergent ($\mu > 0$) intensity $I(\mu)$ at the slab top, writing this in terms of the slab vertical optical thickness $\Delta\tau$ and the source function $S = \eta/\kappa\rho$.

Solution: Since the coefficients in eqn. (5.5) are all constant, straightforward integration (using an integrating factor $\exp[-\kappa\rho z/\mu]$), gives

$$I(\mu) = I_o(\mu)\, e^{-\Delta\tau/\mu} + S\left(1 - e^{-\Delta\tau/\mu}\right) \,. \tag{5.7}$$

In the pure-absorption case $\eta = S = 0$, the second (source) term is zero, and we recover the simple result that the lower boundary intensity is just exponentially attenuated. For no lower boundary intensity, $I_o = 0$, we obtain the emergent intensity from slab emission,

$$\begin{aligned} I(\mu) &= S\left(1 - e^{-\Delta\tau/\mu}\right) \\ &\approx S \qquad\qquad\qquad ; \quad \Delta\tau/\mu \gg 1 \\ &\approx S\Delta\tau/\mu = \eta\Delta z/\mu \quad ; \quad \Delta\tau/\mu \ll 1 \end{aligned}$$

In cases with significant scattering, the source function can depend in an inherently non-local way on the radiation field itself, and thus can only be solved for in terms of some *global* model of the atmospheric scattering.

But the problem becomes much simpler in cases like H^- absorption/emission, for which the LTE detailed balance property (6.1) implies that this source function is just given by the Planck function, $S = B(T)$, which is fixed by the local gas temperature $T(z)$. Indeed, if the opacity, density, and temperature are all known functions of spatial depth z, then the

temperature, and thus the Planck/Source function, can also be written as a known function of optical depth τ. In this case, the radiative transfer equation, which is just a first-order, ordinary differential equation, can be readily integrated.

5.3. The Formal Solution of Radiative Transfer

The resulting integral form of the intensity is commonly called the "Formal Solution", essentially because it can be 'formally' written down even in the case when the source function is non-local, and thus *not* known as an explicit function of optical depth. Multiplying the transfer equation (5.6) by an integrating factor $e^{-\tau/\mu}$, and then integrating by parts with respect to vertical optical depth τ, we find that for upwardly directed intensity rays with $\mu > 0$, the variation of intensity with optical depth in the planar atmosphere model illustrated in figure 5 is given by,

$$I(\mu,\tau) = I(\mu,\tau_o)e^{(\tau-\tau_o)/\mu} + \int_\tau^{\tau_o} S(t)e^{(-t+\tau)/\mu}\,dt/\mu \quad ; \quad \mu > 0,\ \tau < \tau_o\,, \tag{5.8}$$

where τ_o is the total optical thickness of the planar slab under consideration, and t is just a dummy integration variable in optical depth (and *not*, e.g., the *time*!). For downward rays with $\mu < 0$, the solution takes the form

$$I(\mu,\tau) = \int_\tau^{\tau_o} S(t)e^{(-t+\tau)/|\mu|}\,dt/|\mu| \quad ; \quad \mu < 0,\ \tau < \tau_o\,, \tag{5.9}$$

where we've assumed an upper boundary condition $I(\mu,\tau=0) = 0$, i.e. *no* radiation illuminating the atmosphere from above.

5.4. Eddington-Barbier Relation for Emergent Intensity

A particularly relevant case for observations of stellar atmospheres is the emergent intensity ($\mu > 0$) from a semi-infinite slab, i.e. for which $\tau_o \to \infty$. The intensity seen by the external observer at $\tau = 0$ is then given as a special case of eqn. (5.8),

$$I(\mu,0) = \int_0^{\infty} S(t)e^{-t/\mu}\,dt/\mu \quad ; \quad \mu > 0. \tag{5.10}$$

To gain insight, let us consider the simple case that the source function is just a linear function of optical depth, $S(t) = a + bt$. In this case, eqn. (5.10) can be easily integrated analytically (using integration by parts), yielding

$$I(\mu,0) = a + b\mu = S(\tau = \mu)\,. \tag{5.11}$$

Of course the variation of a source function in a stellar atmosphere is usually more complicated than this linear function, but the approximate result,

$$I(\mu, 0) \approx S(\tau = \mu)\,, \tag{5.12}$$

which is known as the *Eddington-Barbier* (E-B) relation, turns out to be surprisingly accurate for a wide range of conditions. The reason is that the exponential attenuation represents a strong localization of the integrand in eqn. (5.10), meaning then that a first-order Taylor expansion gives a roughly linear variation of the source function around the region where the optical depth terms in the exponential are of order unity.

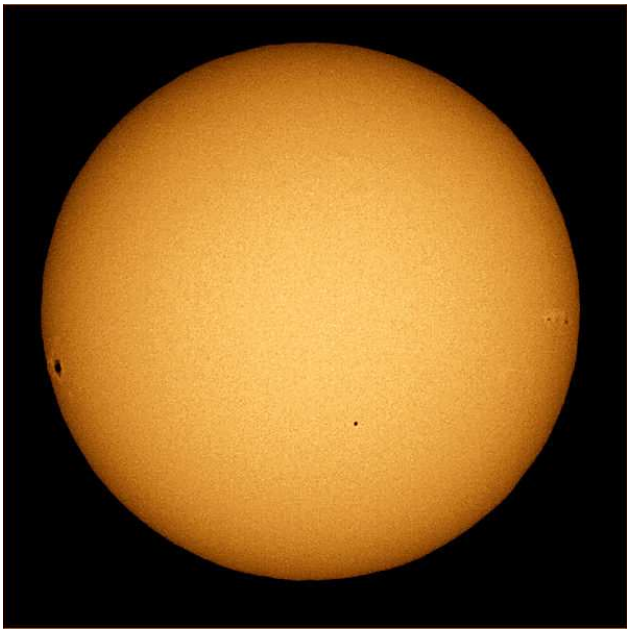

Fig. 6.— Visible light picture of the solar disk, showing the center to limb darkening of the surface brightness.

5.5. Limb Darkening of Solar Disk

A key application of the E-B relation regards the variation of the sun's surface brightness as one looks from the center to limb of the solar disk. At disk center, one is looking vertically down into the local planar atmosphere, i.e. with $\mu = 1$. On the limb, one's view just grazes the atmosphere nearly along the local horizontal, i.e. with $\mu = 0$. The E-B relation gives for

the limb/center brightness ratio,

$$\frac{I(0,0)}{I(1,0)} = \frac{a}{a+b} = \frac{S(0)}{S(0)+dS/d\tau} \approx \frac{B(0)}{B(0)+dB/d\tau}\,. \tag{5.13}$$

The second equality uses the fact that the linear source function coefficients a and b just represent the surface value and gradient of the source function, $a = S(0)$ and $b = S' = dS/d\tau$. The last approximation assumes the LTE case that $S = B$. Since the Planck function depends only on temperature, $B = B(T)$, we have

$$\frac{dB}{d\tau} = -\frac{dT}{dz}\,\frac{1}{\kappa\rho}\,\frac{dB}{dT}\,. \tag{5.14}$$

Since $dB/dT > 0$, and since the temperature of an atmosphere generally declines with height, i.e. $dT/dz < 0$, we see that $dB/d\tau > 0$.

Eqn. (5.13) thus predicts $I(0,0)/I(0,1) < 1$, and so an overall *limb darkening* of the solar surface brightness. As illustrated by the image of the solar disk in figure 6, this is indeed what is observed.

Measurements of the functional variation of solar brightness across the solar disk can even be used to infer the temperature structure of the solar atmosphere. We will consider this further later when we develop solar atmosphere models.

Exercise: For far UV wavelengths $\lambda < 912\mathring{A}$, the photon energy $E > 13.6$ eV is sufficient to ionize neutral hydrogen, and so the associated bound-free absorption by hydrogen makes the opacity in the far UV very high.

a. Compared to visible light with lower opacity, are we able to see to deeper or shallower heights in the far UV?

b. If a far UV picture of the sun shows limb brightening instead of limb darkening, what does that suggest about the temperature stratification of the solar atmosphere?

c. Combining this with results for the limb darkening in optical light, sketch the overall variation of the sun's temperature T vs. height z.

6. Emission, absorption, and scattering: LTE vs. NLTE

In addition to absorption, the material in a stellar atmosphere (or indeed most any matter with a finite temperature) will generally also *emit* radidation, for example through the

inverse processes to absorption. Since microscopic atomic processes in physics are generally all symmetric under time reversal, this can be thought of as somewhat like running the clock backward.

For example, for the sun a dominant source of emission is from the "free-bound"(f-b) recombination of electrons and neutral hydrogen to form the H^-, reversing then the "bound-free" (b-f) absorption that dissociates the H^- ion.

Superficially, the overall process may appear to resemble electron scattering, with absorption of radiation by one H^- ion followed shortly thereafter by remission of radiation during the formation of another H^- ion.

But a key distinction is that, in constrast to the conservative nature of scattering – wherein the energy of the scattered photon essentially[4] remains the same –, the sequence of H^- absorption and emission involves a constant shuffling of the photon energy, very effectively coupling it to the pool of thermal energy in the gas, as set by the local temperature $T(z)$. This is very much the kind of process that tends to quickly bring the radiation and gas close to a *Local Thermodynamic Equilibrium* (LTE). As discussed in §4.2 of DocOnotes1-stars, this means that the local radiation field becomes quite well described by the Planck Blackbody function given in eqns. (I-16) and (I-17).

In contrast, because the opacity of hotter stars is dominated by electron scattering, with thus much weaker thermal coupling between the gas and radiation, the radiation field and emergent spectrum can often deviate quite markedly from what would be expected in LTE. Instead one must develop much more complex and diffult non-LTE (NLTE) models for such hot stars. We will later outline the procedures for such NLTE models, including also some specific features of the solar spectrum (e.g. the so-called "H and K" lines of Calcium) that also require an NLTE treatment.

6.1. Absorption and Thermal Emission: LTE with $S = B$

One important corollary is that processes in LTE exhibit a "detailed balance", i.e. a direct link between each process and its inverse[5]. Thus for example, the thermal emissivity

---

[4]That is, ignoring the electron recoil that really only becomes signifcant for gamma-ray photons with energies near or above the electron rest mass energy, $m_e c^2 \approx 0.5$ MeV.

[5]Einstein exploited this to write a set of relations between the atomic coefficients (related to cross section) for absorption and their emission inverse. As such, once experiments or theoretical computations give one, the inverse is also directly available. See §9.1 below.

η_{th} from LTE processes like H^- f-b emission is given by the associated bound-free absorption opacity κ_{abs} times the local Planck function,

$$\eta_{th} = \kappa_{abs}\, \rho B(T)\,. \tag{6.1}$$

This implies then that, for such pure-absorption and thermal emission, we obtain the simple LTE result,

$$S(\tau) = \frac{\eta_{th}}{\kappa_{abs}\, \rho} = B(T(\tau))\,. \tag{6.2}$$

6.2. Pure Scattering Source Function: $S = J$

In contrast, for the case of pure *scattering* opacity κ_{sc}, the associated emission becomes completely insensitive to the thermal properties of the *gas*, and instead depends only on the local *radiation* field. If we assume (or approximate) the scattering to be roughly isotropic, the scattering emissivity η_{sc} in any direction depends on both the opacity and the angle-averaged mean-intensity,

$$\eta_{sc} = \kappa_{sc}\, \rho J\,. \tag{6.3}$$

This implies then that, for pure-scattering,

$$S(\tau) = J(\tau)\,. \tag{6.4}$$

Since J is the angle-average of I, which itself depends on the global integral given by the formal solution (eqns. 5.8 and 5.9), the solution is inherently *non-local*, representing then a case of non-LTE or NLTE.

6.3. Source Function for Scattering and Absorption: $S = \epsilon B + (1-\epsilon)J$

For the general case in which the total opacity consists of both scattering and absorption, $k \equiv \kappa_{abs} + \kappa_{sc}$, the total emissivity likewise contains both thermal and scattering components

$$\eta = \eta_{th} + \eta_{sc} = \kappa_{abs}\rho B + \kappa_{sc}\rho J\,. \tag{6.5}$$

If we then define an absorption fraction

$$\epsilon \equiv \frac{\kappa_{abs}}{\kappa_{abs} + \kappa_{sc}}\,, \tag{6.6}$$

we can write the general source function in the form

$$S = \epsilon B + (1-\epsilon)J\,. \tag{6.7}$$

6.4. Thermalization Depth vs. Optical Depth

In physical terms, the absorption fraction ϵ can be also thought of as a *photon destruction probability* per encounter with matter. In cases when $\epsilon \ll 1$, a photon that is created thermally somewhere within an atmosphere can scatter many ($N_{sc} \approx 1/\epsilon$) times before it is likely to be absorbed. By a simple random walk argument, the root-mean-square number of mean-free-paths between its thermal creation and absorptive destruction is thus $\sqrt{N} = 1/\sqrt{\epsilon}$, which thus corresponds to an optical depth change of $\Delta\tau = 1/\sqrt{\epsilon}$. This implies that from locations of the atmosphere with total vertical optical depth $\tau < \Delta\tau = 1/\sqrt{\epsilon}$, any photon that is thermally created will generally *escape* the star, instead of being destroyed by a true absorption.

The *thermalization depth*,

$$\tau_{th} = \frac{1}{\sqrt{\epsilon}}\,, \tag{6.8}$$

thus represents the maximum optical depth from which thermally created photons can scatter their way to escape through the stellar surface, without being destroyed by a true absorption.

It is important to understand the distinction here between thermalization depth and optical depth. If we look vertically into a stellar atmosphere, we can say that the photons we see had their last encounter with matter at an optical depth of order unity, $\tau \approx 1$. But the energy that created that photon can, in the strong scattering case with $\epsilon \ll 1$, come typically from a much deeper layer, characterized by the thermalization depth $\tau_{th} \approx 1/\epsilon \gg 1$.

A physical interpretation of the Eddington-Barbier comes from the first notion that we can see vertically down to a layer of optical depth order unity, and so the observed vertical intensity just reflects the source function at that layer, $I(1,0) \approx S(\tau = 1)$.

But in cases with strong scattering, any thermal emission within a thermalization depth of the surface, $\tau < \tau_{th}$ can *escape* to free space. Since this represents a loss or "sink" of thermal energy, the source function in this layer general becomes *reduced* relative to the local Planck function, i.e.

$$S(\tau < \tau_{th}) < B(\tau)\,. \tag{6.9}$$

In particular, since $S(\tau = \mu) < B(\tau = \mu)$, one can no longer directly infer $B(\tau = \mu)$, or the associated surface temperature temperature $T(\tau = \mu)$, by applying the Eddington-Barbier relation to interpetation of observations of the emergent intensity $I(\mu, 0)$.

In general, we must thus go down to deep layer with $\tau \gtrsim \tau_{th}$ to recover the LTE condition,

$$S(\tau \gtrsim \tau_{th}) \approx B(\tau)\,. \tag{6.10}$$

For example, in the atmospheres of hot stars – for which the opacity is dominated by free-electron scattering – the photon destruction probibilty can be quite small, e.g. $\epsilon \approx 10^{-4}$, implying that LTE is only recovered at depths $\tau \gtrsim 100$.

But note in the case of nearly pure-absorption – which is not a bad approximation for the solar atmosphere wherein the opacity is dominated by H^- b-f absorption – we do recover the LTE result quite near the visible surface, $\tau \approx \tau_{th} \approx 1$. So solar limb darkening can indeed be used to infer the temperature stratification of the solar atmosphere.

6.5. Effectively Thick vs. Effectively Thin

Associated with the thermalization depth is the concept of *effective* thickness, to be distinguished from *optical* thickness.

A planar layer of material with total vertical optical thickness τ is said to be optically thin if $\tau < 1$, and optically thick if $\tau > 1$.

But it is only *effectively thick* if $\tau > \tau_{th}$. If $\tau < \tau_{th}$, it is *effectively thin*, even in cases when it is optically thick, i.e. with $1 < \tau < \tau_{th}$.

We will discuss below solutions of the full radiative transfer for planar slabs that are effectively thick vs. thin.

7. Properties of the Radiation Field

7.1. Moments of the Transfer Equation

The radiation field moments J, H, and K defined above provide a useful way to characterize key properties like energy density, flux, and radiation pressure, instead of dealing with the more complete angle dependence given by the full specific intensity $I(\mu)$. To relate these radiation moments to their physical source and dependence on optical depth, it is convenient to carry out progressive angle moments $j = 0, 1, \ldots$ of the radiative transfer equation,

$$\frac{1}{2}\int_{-1}^{+1} d\mu\, \mu^j\, \mu \frac{dI}{d\tau} = \frac{1}{2}\int_{-1}^{+1} d\mu\, \mu^j\, (I - S)\,. \tag{7.1}$$

Since optical depth is independent of μ, we can pull the $d/d\tau$ operator outside the integral. The $j = 0$ or "0th" moment equation then becomes

$$\frac{dH}{d\tau} = J - S\,. \tag{7.2}$$

Note for example that in the case of pure, conservative scattering we have $S = J$, implying $dH/d\tau$ and thus a spatially *constant flux* H. Since scattering neither creates nor destroy radiation, but simply deflects its direction, the flux in a scattering atmosphere must be everywhere the same constant value.

For the first ($j = 1$) moment of the transfer equation, the oddness of the integrand over the (angle-independent) source function S means that the contribution of this term vanishes, leaving

$$\frac{dK}{d\tau} = H \,. \tag{7.3}$$

In both eqns. (7.2) and (7.3), note that a lower moment on the right-hand-side, e.g. J or H, is related to the optical depth derivative of a higher moment, H or K, on the left-hand-side. In principal, one can continue to define higher moments, but both the usefulness and physical interpretation become increasingly problematic.

To truncate the process, we need a *closure* relation that relates a higher moment like K to a lower moment like J. As noted previously, a particular useful example is the Eddington approximation, $J \approx 3K$, which then implies

$$\frac{1}{3}\frac{dJ}{d\tau} \approx H \,, \tag{7.4}$$

which when combined with the zeroth moment eqn. (7.2), yields a 2nd order ODE for J,

$$\frac{1}{3}\frac{d^2J}{d\tau^2} = J - S \,. \tag{7.5}$$

Given $S(\tau)$, this can be readily integrated to give $J(\tau)$.

7.2. Diffusion Approximation at Depth

At sufficiently deep layers of the atmosphere, i.e. with large optical depths beyond the thermalization depth, $\tau \gtrsim \tau_{th} \gg 1$, we expect the radiation field to become isotropic and near the local Planck function, $J \to S \to B$. Let us thus assume that the variation of the Source function near some reference depth τ can be written as a Taylor expansion of the Planck function about this depth,

$$S(t) \approx B(\tau) + \left.\frac{dB}{d\tau}\right|_\tau (t - \tau) + O\left(d^2B/d\tau^2\right) \,, \tag{7.6}$$

where, noting that each higher term is Order $1/\tau$ (commonly written $O(1/\tau)$) smaller than the previous, we truncate the expansion after just the second, linear term. Application in

the formal solution (5.8) then gives for the local intensity,

$$I(\mu,\tau) \approx B(\tau) + \mu \frac{dB}{d\tau} \,. \tag{7.7}$$

Applying this in the definitions of the radiation field moments gives

$$J(\tau) \approx B(\tau) + O\left(d^2B/d\tau^2\right) \tag{7.8}$$

$$H(\tau) \approx \frac{1}{3}\,\frac{dB}{d\tau} + O\left(d^3B/d\tau^3\right) \tag{7.9}$$

$$K(\tau) \approx \frac{1}{3}\,B(\tau) + O\left(d^2B/d\tau^2\right) \,. \tag{7.10}$$

If we keep just the first-order terms, then comparison of eqns. (7.8) and (7.10) immediately recovers the Eddington approximation, $J = 3K$, while the flux H is given by the *diffusion approximation* form,

$$H \approx \frac{1}{3}\,\frac{dB}{d\tau} = -\left[\frac{1}{3\kappa\rho}\frac{\partial B}{\partial T}\right]\,\frac{dT}{dz}\,, \tag{7.11}$$

where the latter equality shows how this diffusive flux scales directly with the vertical temperature gradient dT/dz, much as it does in, e.g., conduction. Indeed, the terms in square bracket can be thought of as a *radiative conductivity*, which we note depends inversely on opacity and density, $1/\kappa\rho$.

7.3. The Rosseland Mean Opacity for Diffusion of Total Radiative Flux

Note that the physical radiative flux is just $F = 4\pi H$. In modeling stellar interiors[6], we will use this corresponding flux form in spherical symmetry, replacing height with radius, $z \to r$,

$$F_\nu(r) \approx -\left[\frac{4\pi}{3\kappa_\nu\rho}\frac{\partial B_\nu}{\partial T}\right]\,\frac{dT}{dr}\,, \tag{7.12}$$

where we now have also reintroduced subscripts ν to emphasize that this, like all the equations above, depends in principal on photon frequency. But to model the overall energy transport in a stellar atmosphere or interior, we need the total, frequency-integrated (a.k.a. *bolometric*) flux

$$F(r) \equiv \int_0^\infty F_\nu \, d\nu \,. \tag{7.13}$$

---

[6]For a lucid summary of radiative transfer in stellar interiors, see Rich Townsend's notes 06radiation.pdf.

Collecting together all of the frequency-dependent terms of F_ν, we have

$$F(r) = -\frac{4\pi}{3\rho}\frac{dT}{dr}\int_0^\infty \frac{1}{\kappa_\nu}\frac{\partial B_\nu}{\partial T}\,\mathrm{d}\nu. \tag{7.14}$$

The required frequency integral can be conveniently represented by introducing the *Rosseland mean opacity*, defined by

$$\kappa_R \equiv \frac{\int_0^\infty \frac{\partial B_\nu}{\partial T}\,\mathrm{d}\nu}{\int_0^\infty \frac{1}{\kappa_\nu}\frac{\partial B_\nu}{\partial T}\,\mathrm{d}\nu} \tag{7.15}$$

We can see that κ_R represents a harmonic mean of the frequency-dependent opacity κ_ν, with $\partial B_\nu/\partial T$ as a weighting function. The numerator can be readily evaluated by taking the temperature derivative outside the frequency integral,

$$\int_0^\infty \frac{\partial B_\nu}{\partial T}\,\mathrm{d}\nu = \frac{\partial}{\partial T}\int_0^\infty B_\nu\,\mathrm{d}\nu = \frac{\partial}{\partial T}\left(\frac{ac}{4\pi}T^4\right) = \frac{acT^3}{\pi}\,, \tag{7.16}$$

where the radiation constant a is given by

$$a = \frac{8\pi^5 k^4}{15c^3h^3}\,. \tag{7.17}$$

We can thus write the integrated flux as

$$\boxed{F(r) = -\left[\frac{4ac}{3}\frac{T^3}{3\kappa_R\rho}\right]\frac{dT}{dr}}\,. \tag{7.18}$$

This final result – which tells us the total radiative flux F given the temperature, its gradient, the density and the Rosseland-mean opacity – is known as the *radiative diffusion equation*. Sometimes it is instructive to write this as

$$F(r) = -\frac{c}{3}\frac{1}{\kappa\rho}\frac{dU}{dr}, \tag{7.19}$$

where

$$U \equiv aT^4 \tag{7.20}$$

is the density of radiative (photon) energy per unit volume.

7.4. Exponential Integral Moments of Formal Solution: the Lambda Operator

Let us now return to the problem of solving for the radiation moments in the full atmosphere where the above diffusion treatment can break down. Applying the definition

of mean intensity J from eqn. (4.1) into the formal solution eqns. (5.8) and (5.9), we find (again suppressing the ν subscripts for simplicity),

$$J(\tau) = \frac{1}{2}\int_0^1 d\mu \int_\tau^\infty S(t)\, e^{-(t-\tau)/\mu}\, dt/\mu - \frac{1}{2}\int_{-1}^0 d\mu \int_0^\tau S(t)\, e^{-(\tau-t)/\mu}\, dt/\mu \quad (7.21)$$

$$= \frac{1}{2}\int_0^\infty S(t)\, E_1\left(|t-\tau|\right)\, dt \quad (7.22)$$

$$= \Lambda_\tau[S(t)]\,. \quad (7.23)$$

Here the second equality uses the first ($n = 1$) of the general *exponential integral* defined by,

$$E_n(x) \equiv \int_1^\infty e^{-xt}\frac{dt}{t^n}\,. \quad (7.24)$$

Some simple exercises in the homework problem set help to illustrate the general properties of exponential integrals. An essential point is that they retain the strong geometric factor attenuation with optical depth, and so can be qualitatively thought of just a fancier form of the regular exponential $e^{-\tau}$.

Exercise: Given the definition of the exponential integral in eqn. (7.24), prove the following properties:

a. $E_n'(x) = -E_{n-1}(x)$.

b. $E_n(x) = [e^{-x} - xE_{n-1}(x)]/(n-1)$.

c. $E_n(0) = 1/(n-1)$

d. $E_n(x) \approx e^{-x}/x$ for $x \gg 1$.

The last equality in (7.23) defines the *Lambda Operator* $\Lambda_\tau[S(t)]$, which acts on the full source function $S[t]$. In the general case in which scattering gives the source function a dependence on the radiation field J, finding solutions for J amounts to solving the operator equation,

$$J(\tau) = \Lambda_\tau[\epsilon B(t) + (1-\epsilon)J(t)]\,, \quad (7.25)$$

which states that the *local* value of intensity at any optical depth τ depends on the *global* variation of $J(t)$ and $B(t)$ over the whole atmosphere $0 < t < \infty$. One potential approach to solving this equation is to simply assume some guess for $J(t)$, along with a given $B(t)$ from the temperature variation $T(t)$, then compute a new value of $J(\tau)$ for all τ, apply this new J into the Lambdda operator, and repeat the whole process it converges on a self-consistent solution for J. Unfortunately, such *Lambda iteration* turns out to have a hopelessly slow convergence, essentially because the ability of deeper layers to influence upper layers scales

as $e^{-\tau}$ with optical depth, implying it can take e^{τ} steps to settle to a full physical exchange that ensures full convergence. However, a modified form known as *Accelerated Lambda Iteration* (ALI) turns out to have a suitably fast and stable convergence, and so is often used in solving radiative transfer problems in stellar atmospheres. But this is rather beyond the scope of the summary discussion here.

One can likewise define a formal solution integral for the flux,

$$H(\tau) = \frac{1}{2}\int_{\tau}^{\infty} S(t)E_2\left(t-\tau\right)\,dt - \frac{1}{2}\int_{0}^{\tau} S(t)E_2\left(\tau-t\right)\,dt\,, \tag{7.26}$$

which can be used to define another integral operator, commonly notated Φ. An analogous equation can be written for the K-moment, which involves E_3, and can be used to define yet another operator, commonly denoted X.

Exercise: Assume a source function that varies linearly with optical depth, i.e. $S(t) = a + bt$, where a and b are constants.

a. Apply this $S(t)$ in eqn. (7.23) and carry out the integration to obtain the optical depth variation of mean intensity $J(\tau)$ in terms of exponential integrals $E_n(\tau)$.

b. Next apply $S(t)$ in eqn. (7.26) and carry out the integration to obtain the optical depth variation of the Eddington flux $H(\tau)$ in terms of exponential integrals $E_n(\tau)$.

c. For the case $a = 2$ and $b = 3$, plot $H(\tau)$ and the ratio $J(\tau)/S(\tau)$ vs. τ over the range $[0, 2]$.

7.5. The Eddington-Barbier Relation for Emergent Flux

For the case of a source function that is linear in optical depth, $S(t) = a + bt$, we can use eqn. (7.26) to derive a formal solution for the emergent flux,

$$H(0) = \frac{1}{2}\int_{0}^{\infty} (a+bt)E_2[t]\,dt = \frac{a}{4} + \frac{b}{6}\,. \tag{7.27}$$

Recalling that the physical flux $F = 4\pi H$, we thus find that

$$F(0) = \pi\left(a + (2/3)b\right) = \pi S(\tau = 2/3)\,, \tag{7.28}$$

which now represents a form of the Eddington-Barbier relation for the emergent *flux*, associating this with the source function at a characteristic, order-unity optical depth $\tau = 2/3$.

This can be used to interpret the observed flux from stars for which, unlike for the sun, we cannot resolve the surface brightness, $I(\mu, 0)$. Indeed, note that the basic Eddington flux relation (7.27) can also be derived by taking the outward flux moment of the Eddington-Barbier relation for emergent intensity (5.11).

7.6. Radiative Equilbrium

Since atmospheric layers are far away from the nuclear energy generation of the stellar core, there is no net energy produced in any given volume. If we further asssume energy is transported fully by radiation (i.e. that condution and convection are unimportant), then the total, frequency-integrated radiative energy *emitted* in a volume must equal the total radiative energy *absorbed* in the same volume. This condition of *radiative equilibrium* can be represented in various alternative forms,

$$\int_0^\nu d\nu \oint d\Omega\, \eta_\nu = \int_0^\nu d\nu \oint d\Omega\, \rho k_\nu I_\nu \tag{7.29}$$

$$\int_0^\nu k_\nu S_\nu\, d\nu = \int_0^\nu k_\nu J_\nu\, d\nu \tag{7.30}$$

$$\int_0^\nu \kappa_\nu B_\nu\, d\nu = \int_0^\nu \kappa_\nu J_\nu\, d\nu\,, \tag{7.31}$$

where $k_\nu = \kappa_\nu + \sigma_\nu$ is the total opacity at frequency ν, with contributions from both absorption (κ_ν) and scattering (σ_ν) opacity components. The second relation uses the isotropy and other basic properties of the volume emissivity,

$$\eta_\nu = k_\nu S_\nu = \kappa_\nu B_\nu + \sigma_\nu J_\nu\,. \tag{7.32}$$

The third relation uses the conservative property of the coherent scattering component at each frequency $J_\nu = 4\pi\eta_\nu^{sc}/\sigma_\nu$, and shows that, when integrated over frequency, the total true absorption of radiation must be balanced by the total thermal emission.

Upon frequency integration of the flux moment of the radiative transfer equation, we find for the bolometric fluxes H or F

$$\frac{dH}{dz} = \frac{dF}{dz} = 0\,, \tag{7.33}$$

which shows that the *bolometric flux is spatially constant* throughout a planar atmosphere in radiative equilibrium.

Indeed, along with the surface gravity, the impingent radiative flux F from the underying star represents a key characteristic of a stellar atmosphere. Moreover, since the flux from a

blackbody defines an *effective temperature* T_{eff} through $F = \sigma T_{eff}^4$, models of planar stellar atmospheres are often characterized in terms of just the two parameters $\log g$ and T_{eff}. By contrast, the overall structure of a star is generally described by *three* parameters, e.g. luminosity L, mass M, and radius R. But because the radius cancels in the ratio of surface gravity to surface flux, just $\log g$ and T_{eff} suffice to characterize a planar atmosphere, whose properties are insenstive to the stellar radius R.

7.7. Two-Stream Approxmation for Radiative Transfer

An alternative to using moment equations is to approximate the radiative field as confined to just two rays, one upward (+) and the other downward (-), with associated intensities I^+ and I_-. In this approach, one has the freedom to choose the magnitude of the projection cosine of these rays, $|\mu| = \mu_1$. In this two-stream model the transfer equation for each of the $\pm$ directions can be written

$$\pm\mu_1 \frac{dI^\pm}{d\tau} = I^\pm - S\,. \tag{7.34}$$

The mean intensity and Eddington flux now reduce from integrals to mere sums,

$$J = \frac{I^+ + I^-}{2}\,, \tag{7.35}$$

and

$$H = \mu_1 \frac{I^+ - I^-}{2}\,. \tag{7.36}$$

Adding the (+) and (-) transfer equations then gives

$$\frac{dH}{d\tau} = J - S = \epsilon(J - B)\,, \tag{7.37}$$

where the latter equality again assumes a source function of the form $S = (1-\epsilon)J + \epsilon B$. Subtracting the two equations gives

$$\mu_1 \frac{dJ}{d\tau} = \frac{H}{\mu_1}\,. \tag{7.38}$$

Combining these gives a second order equation in J,

$$\mu_1^2 \frac{d^2J}{d\tau^2} = J - S = \epsilon(J - B)\,. \tag{7.39}$$

Comparison with eqn. (7.5) shows that, if we set $\mu_1 = 1/\sqrt{3}$, then this two-stream approach becomes fully equivalent to the Eddington approximation.

7.8. Transmission through Planar Layer: Scattering vs. Absorption

We can use this two-stream approximation to estimate the transmission through a pure-scattering layer or cloud, much like the clouds here on earth. For such a pure scattering ($\epsilon = 0$) case, the right side of eqn. (7.37) is zero, implying then that the flux H must be constant; physically, this again reflects the fact that for pure-scattering, radiation can be neither created or destroyed. By integration of eqn. (7.38), we find that the mean intensity must vary linearly with optical depth,

$$J(\tau) = \frac{H\tau}{\mu_1^2} + C\,, \tag{7.40}$$

where C is an integration constant. This can be evaluated by boundary conditions on the $I^{\pm}$ at the cloud's top and bottom.

For a cloud in which the vertical optical depth ranges from $\tau = 0$ at the top to some total cloud optical thickness τ_c at the bottom, let us assume an incoming (downward) intensity $I^-(0) = I_o$ impingent along the direction μ_1 at the top, with zero upward intensity at the bottom, $I^+(\tau_c) = 0$. Note that

$$\begin{aligned} I^{\pm}(\tau) &= J \pm \frac{H}{\mu_1} && (7.41)\\ &= \frac{H}{\mu_1}\left(\frac{\tau}{\mu_1} \pm 1\right) + C && (7.42)\\ &= \frac{H}{\mu_1}\left(\frac{\tau}{\mu_1} \pm 1 + 1\right) + I_o\,, && (7.43) \end{aligned}$$

where the third equality follows from the upper boundary condition $I^-(0) = I_o$. Applying the lower boundary condition $I^+(\tau_c) = 0$ then gives for the (downward) transmitted flux through the cloud

$$H = -\frac{\mu_1 I_o}{\tau_c/\mu_1 + 2} = \boxed{\frac{H_o}{\tau_c/2\mu_1 + 1}}, \tag{7.44}$$

where the latter equality scales the transmitted flux by its value H_o without any cloud layer, i.e., with $\tau_c = 0$. If we assume nearly vertical illumination $\mu_1 \approx 1$ (as would apply near noon around midsummer), then we see that a scattering cloud's reduction of the sun's flux scales as $1/(\tau_c/2 + 1)$. A typically very cloudy day with $\tau_c \approx 10$ would thus have the sun's flux reduced by a factor 1/6. Thus when taking a picture, you might need to increase the exposure time by a factor of 6.

This relatively modest reduction should be contrasted with the much stronger, *exponential* attenuation of the transmitted flux by a pure-*absorbing* cloud with the same optical

thickness,

$$H_{abs} = -(\mu_1 I_o/2)e^{-\tau_c/\mu_1} = H_o e^{-\tau_c/\mu_1} \,. \tag{7.45}$$

For the same example with $\mu_1 = 1$ and $\tau_c = 10$, this would give a much stronger flux reduction of about a factor $e^{-10} \approx 5 \times 10^{-5}$. Thus, for example, if the clouds were made of black absorbing coal dust instead of highly reflective water vapor, a cloudy day would be nearly pitch dark! Thus dust from a volcano, or from the meteor impact that killed the dinosaurs, could make the affected surface quite dark, and cold.

This difference in flux attenuation is one of the key physical distinctions between a scattering vs. absorption layer.

8. Radiative Transfer for Gray Opacity

In general, the complex frequency dependence of stellar opacity greatly complicates the full solution for the radiation field. But we can gain great insight into the overall properties of an atmosphere and its radiation if we make the (strong) simplifying assumption that the opacity is *gray*, i.e. independent of frequency or wavelength. In this case the Rosseland mean opacity is just given by this constant, gray opacity, $\kappa_R = \kappa$. If we now identify unsubscripted symbols for the intensity I and its angle moments J, H, and K with their *bolometric* values, then the transfer equation and its moments have the basic forms defined above,

$$\mu \frac{dI}{d\tau} = I - S \tag{8.1}$$

$$\frac{dH}{d\tau} = J - S \tag{8.2}$$

$$\frac{dK}{d\tau} = H \,. \tag{8.3}$$

8.1. Gray Atmospheres in Radiative Equilibrium: the Hopf Function

Now if we further assume a condition of radiative equilibrium, we have generally $S = J$, regardless of the admixture of absorption and thermal emission vs. scattering. As such, the second equality above immediately implies a constant flux H. This allows us to immediately integrate to obtain for the K-moment

$$K(\tau) = H(\tau + c) \,, \tag{8.4}$$

where c is an integration constant. A complete solution requires now that we relate K to J. So recall again that at large depth $\tau \gg 1$ we recover a diffusion limit for which the radiation field has only a small deviation from isotropy, giving then the Eddington approximation $J \approx 3K$. This suggests we write the solution for mean intensity in the form,

$$J(\tau) = 3H(\tau + q(\tau)) \,, \tag{8.5}$$

where $q(\tau)$ is called the "Hopf function", and use of the Eddington approximation at large optical depth $\tau \to \infty$ shows that $q(\infty) = c$. Application of $S = J$ from eqn. (8.5) in the formal solution for mean intensity (7.23) means that finding the Hopf function requires solving the integral equation,

$$\tau + q(\tau) = \frac{1}{2} \int_0^\infty (t + q(t)) \; E_1 \left[|t - \tau| \right) \; dt \,. \tag{8.6}$$

8.2. The Eddington Gray Atmosphere

While it is possible to tabulate full solutions of the integral equation (8.6), a more analytically tractable approach is to assume validity of the Eddington approximation everywhere. Recalling from the exercises in problem set #1 that the Eddington approximation nearly holds for a wide range range of forms for $I(\mu)$, such an *Eddington gray atmosphere* approach, while not exact, turns out to give pretty accurate, and very insightful, results.

Using $J = 3K$, let us now rewrite eqn. (8.4) as a solution for the Eddington approximation for mean intensity

$$J_E(\tau) = 3H\tau + c' \,, \tag{8.7}$$

where $c' = 3Hc$ is just an alternative definition for the integration constant. Using the formal solution eqn. (7.26), we find that the surface flux is

$$\begin{aligned} H(0) &= \frac{1}{2} \int_0^\infty J(t) E_2(t) \, dt & (8.8) \\ &= \frac{1}{2} \int_0^\infty (3H\, t + c') \, E_2(t) \, dt & (8.9) \\ &= \frac{c'}{4} + \frac{H}{2} \,. & (8.10) \end{aligned}$$

Setting $H(0) = H$, we find $c' = 2H$, implying $c = 2/3$, and thus that for the Eddington approximation, the Hopf function is just a constant, $q_E(\tau) = 2/3$. This gives a simple analytic form for the mean intensity in an Eddington gray atmosphere,

$$J_E(\tau) = 3H \left(\tau + \frac{2}{3} \right) \,. \tag{8.11}$$

Using then $J_E = B(T) = \sigma T^4/\pi$ and $H = \sigma T_{eff}^4/4\pi$, we find that the temperature in a gray atmosphere varies according to

$$T^4(\tau) = \frac{3}{4} T_{eff}^4 \left(\tau + \frac{2}{3}\right) . \tag{8.12}$$

This shows that the temperature increases in the inner regions with large optical depth, giving $T \approx T_{eff}\,\tau^{1/4}$ for $\tau \gg 1$. Note moreover that $T(\tau = 2/3) = T_{eff}$, showing again that such τ of order unity corresponds to rougly to the visible photosphere. On the other hand, for very small optical depth, we find a "surface temperature" $T_o \equiv T(0) = T_{eff}/2^{1/4} \approx 0.841\,T_{eff}$. This agrees pretty closely with the exact value for a non-Eddington gray model $T_o/T_{eff} = (\sqrt{3}/4)^{1/4} \approx 0.8114$.

8.3. Eddington Limb-Darkening Law

Let us next apply this Eddington gray atmosphere result into the formal solution (5.10) for the surface intensity,

$$\begin{aligned} I_E(\mu, 0) &= 3H \int_0^\infty (t + 2/3)\, e^{-t/\mu}\, dt/\mu & (8.13)\\ &= 3H(\mu + 2/3)\,. & (8.14) \end{aligned}$$

This gives the *Eddington limb-darkening law*

$$\frac{I_E(\mu, 0)}{I_E(1, 0)} = \frac{3}{5}\left(\mu + \frac{2}{3}\right) . \tag{8.15}$$

For example, this predicts a limb-to-center brightness ratio $I_E(0, 0)/I_E(1, 0) = 2/5 = 0.4$, which is in good agreement with optical observations of the solar disk.

8.4. Lambda Iteration of Eddington Gray Atmosphere

It is important to realize that, while very helpful for providing insight, this Eddington gray atmosphere model is not a fully self-consistent solution for the radiation transport. To see this, let us compute a new intensity from the Lambda operator form of the formal solution (7.23),

$$\begin{aligned} J_E^{(1)}(\tau) &= \Lambda_\tau \left[J_E^0(t)\right] & (8.16)\\ &= 3H\,\Lambda_\tau \left[t + 2/3\right] & (8.17)\\ &= 3H\ (\tau + 2/3 + E_3(\tau)/2 - E_2(\tau)/3)\ , & (8.18) \end{aligned}$$

where the superscript indicates that this is a first-order iteration on the basic Eddington solution, $J_E^{(0)}$. For large optical depth $\tau \gg 1$ the exponential integral terms all vanish, and so we find $J_E^{(1)} \to J_E^{(0)}$, showing that this Lambda iteration does not affect the solution deep in the atmosphere, where the Eddington approximation is indeed well justified. But at the surface we find $J_E^{(1)}(0)/J_E^{(0)}(0) = 7/8$, so the solution has changed by 1/8, or 12%. This now gives a surface temperature $T_o^{(1)}/T_{eff} = (7/16)^{1/4} = 0.813$, which is substantially closer to the exact result $T_o/T_{eff} = 0.8114$ than the earlier result $T_o^{(0)}/T_{eff} = 1/2^{1/4} = 0.841$.

As shown in the exercise below, a similar application of the Eddington solution for mean intensity into the formal solution for the flux shows that the flux is not constant, as required by radiative equilibrium. This thus represents an inherent insconsistency in the Eddington gray atmosphere model, but as shown in the exercise, the relative error is quite small, at most only a few percent.

Exercise:

a. Apply $S(t) = J_E(t)$ in the formal integral solution for the flux given by eqn. (7.26), and obtain thereby an integral expression for the next-order iteration for the radiative flux, $H^{(1)}(\tau)$.

b. Evaluate the required integral using properties of the exponential integrals, and show thereby that $H^{(1)}(\tau)$ is *not constant*.

c. Using your favorite analysis and plotting software, e.g. *Maple* or *Mathematica*, plot the relative flux error $H^{(1)}/H - 1$ vs. τ for $\tau = 0$ to $\tau = 5$.

d. What is the maximum error, and at about what optical depth does it occur?

In principal one can continue to reapply the Lambda operator to get an sequence of higher iterations of J, but the process requires difficult integrals involving product of exponential integrals, and moreover converges very slowly. To see this, let us focus on the Hopf function $q(\tau)$, and specifically assume that some guess for this differs from the "exact" solution by a constant, i.e. $q(t) = q_{exact}(t) + C$. Application of the Lambda operator to both sides gives

$$\Lambda_\tau[t + q(t)] = \Lambda_\tau[t + q_{exact}(t) + C] \tag{8.19}$$

$$\tau + q^{(1)}(\tau) = \tau + q_{exact}(\tau) + \Lambda_\tau[C] \tag{8.20}$$

$$\Delta q^{(1)}(\tau) \equiv q^{(1)} - q_{exact} = C(1 - E_2(\tau)/2)\,. \tag{8.21}$$

From this we see that the new error is reduced by half at the surface, i.e. $\Delta q^{(1)}(0) = C/2$, whereas at large optical depth there is essentially no improvement, i.e. $\Delta q^{(1)}(\infty) = C$.

Physically, this failure to improve the solution much beyond the surface can be traced to the fact that a photon mean-free-path corresponds to $\Delta\tau = 1$, which then essentially represents the depth of influence for each Λ-iteration. As such the full convergence of Λ-iteration is very slow, especially at great depth.

8.5. Isotropic, Coherent Scattering + Thermal Emission/Absorption

In this context of a gray atmosphere, a formally similar, but conceptually distinct, form for radiation transport arises in the case when the radiation remains "self-contained" within a single "coherent" frequency ν. The opacity in this case need not be gray, and indeed, we will see below such an approach can provide a first approximation for treating spectral lines with a highly frequency-dependent opacity. Nonetheless, such coherent frequency transport has many similarities to the gray case developed above.

As a specific example, consider a case in which the source function is given by

$$S_\nu(\tau_\nu) = \epsilon B_\nu(\tau_\nu) + (1-\epsilon) J_\nu(\tau_\nu)\,. \tag{8.22}$$

This first term on the right represents thermal emission for a (now assumed known) depth variation of the Planck function $B_\nu(\tau_\nu)$. The second terms represents isotropic, coherent[7] scattering that depends on the mean intensity J_ν at the same frequency ν, for which the optical depth variation must be derived from a global solution of the scattered radiation transport.

Let us thus write the flux and K-moments of the tranfer equation as

$$\frac{dH_\nu}{d\tau_\nu} = J_\nu - S_\nu = \epsilon(J_\nu - B_\nu) \tag{8.23}$$

and

$$\frac{dK_\nu}{d\tau_\nu} = H_\nu = \frac{1}{3}\frac{dJ_\nu}{d\tau_\nu}\,, \tag{8.24}$$

where the last equality again assumes the Eddington approximation $J_\nu = 3K_\nu$. If we next assume a Planck function that is linear in optical depth, i.e.

$$B_\nu(\tau_\nu) = a + b\tau_\nu\,, \tag{8.25}$$

[7] "Coherent" here refers to frequency, i.e. that the energy and thus frequency of the photon is not changed through the scattering process. In practice, line-scattering by ions leads to a "frequency redistribution" associated with the Doppler effect from thermal motions of the ions. We will return to this in our discussion of line-scattering below.

we can combine these first-order ODE's into a single second-order one,

$$\frac{1}{3}\,\frac{d^2}{d\tau_\nu^2}(J_\nu - B_\nu) = \epsilon(J_\nu - B_\nu)\,. \tag{8.26}$$

This can be readily integrated to give

$$J_\nu - B_\nu = \alpha e^{-\sqrt{3\epsilon}\,\tau_\nu} + \beta e^{\sqrt{3\epsilon}\,\tau_\nu}\,, \tag{8.27}$$

where α and β are integration constants. Since we know the solution is bounded at large optical depth, we must have $\beta = 0$. The other boundary condition comes from the gray-atmosphere surface condition $J_\nu(0) = \sqrt{3}H_\nu(0) = (1/\sqrt{3})(dJ_\nu/d\tau_\nu)_0$, which here implies $a + \alpha = b/\sqrt{3} - \alpha\sqrt{\epsilon}$, or

$$\alpha = \frac{b/\sqrt{3} - a}{1 + \sqrt{\epsilon}}\,. \tag{8.28}$$

The *fully analytic* solution for the mean intensity is thus

$$J_\nu(\tau_\nu) = a + b\tau_\nu + \frac{b/\sqrt{3} - a}{1 + \sqrt{\epsilon}}\, e^{-\sqrt{3\epsilon}\,\tau_\nu}\,. \tag{8.29}$$

Eqn. (8.29) quantifies nicely the above physical arguments about thermalization in an atmosphere with non-zero scattering. For example, note that the LTE condition $J \approx B$ is generally only recovered for optical depths of order the thermalization depth, i.e. for $\tau_\nu \gtrsim \tau_{th} \approx 1/\sqrt{\epsilon}$.

In contrast, at the $\tau_\nu = 0$ surface we find, for the simple case of an isothermal atmosphere with $b = 0$ and so $B_\nu = a$ =constant, that the mean intensity is

$$J_\nu(0) = \frac{\sqrt{\epsilon}}{1 + \sqrt{\epsilon}}\, B_\nu\,. \tag{8.30}$$

For $\epsilon \ll 1$, with thus a substantial level of scattering, we obtain $J_\nu/B_\nu \ll 1$, reflecting the exensive "leakage" of radiative energy due to the diffusive loss to empty space.

Figure 7 plots $J_\nu - B_\nu$ vs. $\log\tau_\nu$ for various ϵ, assuming the standard Eddington atmosphere coefficients $a = 2$ and $b = 3$. Note that for small ϵ, representing weak absorption and strong scattering, the mean intensity remains well below the Planck function from the surface down to optical depths of order the thermalization depth, $\tau_{th} = 1/\sqrt{\epsilon}$.

Exercise: Assume a *two-stream* approximation in which the radiation field is characterized by the specific intensities $I_\nu^\pm$ along just two discrete directions $\mu = \pm\mu_1$, where μ_1 is fixed.

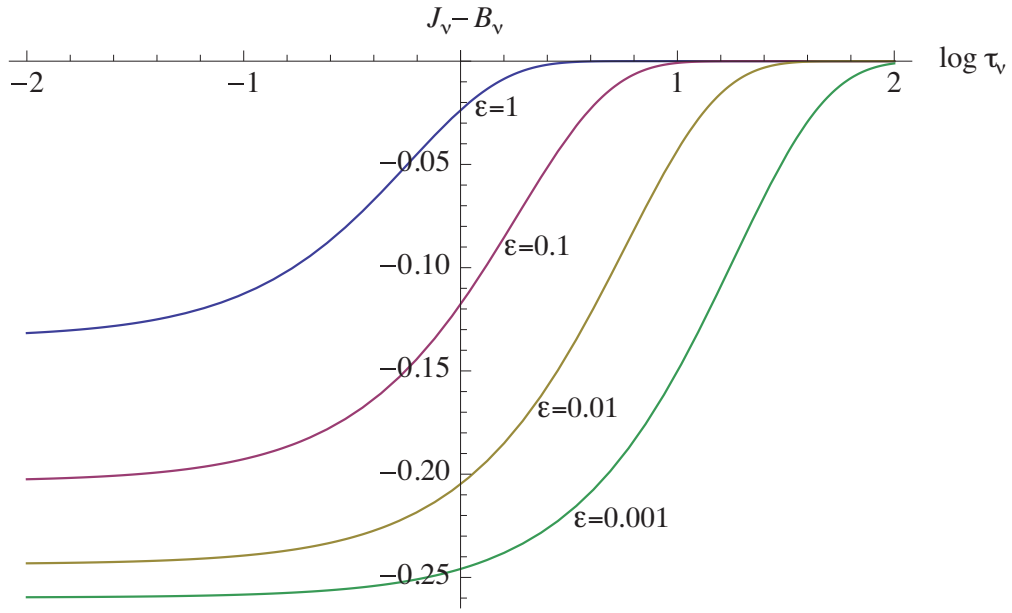

Fig. 7.— $J - B$ vs. $\log \tau_\nu$ for mean-intensity solution (8.29), assuming $a = 2$, $b = 3$, and various absorption fractions ϵ.

a. Write down the discrete angle forms for both the mean intensity J_ν and the flux H_ν in terms of the $I_\nu^\pm$ and μ_1.

b. By adding and subtracting the separate transfer equations for I_ν^+ and I_ν^-, derive equations for $dJ_\nu/d\tau_\nu$ and $dH_\nu/d\tau_\nu$.

c. Now combine these to get a second-order equation for J_ν. For what value of μ_1 does this become equivalent to the second-order equation for J_ν in the Eddington approximation?

d. For a finite slab of optical thickness $\tau_s = 2\tau_m$, write out boundary conditions for the $I^\pm$ at the appropriate surfaces $\tau_\nu = 0$ and $\tau_\nu = \tau_s$.

e. Assume a source function of the form $S_\nu = \epsilon B_\nu + (1 - \epsilon)J_\nu$, appropriate to coherent scattering plus thermal emission. For the case $B_\nu = \textit{constant}$ and ϵ =constant, use symmetry arguments to replace one of the surface B.C.'s with a B.C. at the slab midpoint $\tau = \tau_m$. Then derive an expression for the ratio J/B at the slab midpoint in terms of ϵ and τ_m.

f. A slab for which this midpoint ratio is approximately unity is called *effectively thick*. What then is the requirement for such a slab to be "effectively thick"?

Compare this to the requirement for the slab to be "optically thick".

9. Line Opacity and Broadening

9.1. Einstein Relations for Bound-Bound Emission and Absorption

Let us now focus on cases wherein the opacity has a significant contribution from bound-bound processes. Because this leads to narrow "lines" of modified flux or intensity in a stellar spectrum, the overall process is call "line transfer". There are 3 basic kinds of line processes associated with bound-bound transitions of atoms or ions:

1. *Direct Absortion.* In which the absorbed photon induces a bound electron to go into a higher energy level.

2. *Spontaneous Emission.* In which an electron in a higher energy level spontaneously decays to lower level, emitting the energy difference as a photon.

3. *Stimulated Emission.* In which an incoming photon induces an electron in a higher energy level to decay to a lower level, emitting in effect a second photon that is nearly identical in energy (and even phase) to the original photon.

For lower and upper levels i and j, we can associate with these three processes the Einstein coefficients, written B_{ij}, A_{ji}, and B_{ji}. The first of these is related to the opacity κ_ν via the associated energy removed from an intensity beam I_ν,

$$\rho\kappa_\nu I_\nu \equiv n_i B_{ij} \frac{h\nu_{ij}}{4\pi} \phi_\nu I_\nu \,, \tag{9.1}$$

where n_i is the number of atoms or ions in the lower atomic state i, and ϕ_v is called the *profile function*, defining just how the opacity varies for frequencies ν near the resonance (a.k.a. "line-center") value ν_{ij}. It is normalized to unity when integrated over all frequencies,

$$\int_0^\infty \phi_\nu \, d\nu = 1 \,. \tag{9.2}$$

In the idealized case that both the upper and lower energy levels are infinitesmally sharp and well defined, the profile function meansured in the rest-frame of the atom can be written as a Dirac delta functiion, $\phi_\nu = \delta(\nu - \nu_{ij})$. In practice, the Heisenberg uncertainty principal means a level with a finite lifetime has energy uncertainty, giving the profile what is known as "natural broadening". Moreover, the perturbative effect of other atoms and ions leads

to a kind of "pressure" (a.k.a. "Stark") broadening. These both act on the intrinsic profile in the atom's frame, but if one accounts for the random thermal motion of atoms, then the Doppler effect leads to an additional "thermal Doppler broadening" for the profile measured in the rest frame of the overall stellar atmosphere. We will discuss these further below.

The Einstein coefficients for emission have to be divided between spontaneous and stimulated components,

$$\eta_\nu^{spon} \equiv n_j A_{ij} \frac{h\nu_{ij}}{4\pi} \psi_\nu \,, \tag{9.3}$$

and

$$\eta_\nu^{stim} \equiv n_j B_{ji} \frac{h\nu_{ij}}{4\pi} \psi_\nu I_\nu \,, \tag{9.4}$$

where n_j is the number density of ions in the upper level j, and ψ_ν is the *emission profile*. In practice, one can often assume $\psi_\nu = \phi_\nu$, which implies a randomization or *complete redistribution* (CRD)[8] of the photon frequencies between absorption and emission within the line profile ϕ_ν.

To proceed, let us consider the case of a gas in strict thermodynamic equilibrium (TE), with $I_\nu = B_\nu$, and the ratio of the population in upper and lower levels set by

$$\frac{n_j^*}{n_i^*} = \frac{g_i}{g_j} \, e^{-h\nu_{ij}/kT} \,, \tag{9.5}$$

where g_i and g_j are the statistical weights of the lower and upper levels, and the asterisks emphasize that we're specifically referring to TE level populations. The exponential term is the "Boltzmann factor", with eqn. (9.5) then known as the "Boltzmann relation". It is one of the fundamental underpinnings of thermodynamics and statistical mechanics.

In TE, the principal of detailed balance requires $\phi_\nu = \psi_\nu$. It also requires that the energy absorbed be equal to that emitted,

$$n_i^* \, B_{ij} B_\nu = n_j^* \, (A_{ji} + B_{ji} B_\nu) \,, \tag{9.6}$$

Solving for the Planck function, we find

$$B_\nu = \frac{A_{ji}/B_{ji}}{\frac{g_i B_{ij}}{g_j B_{ji}} e^{h\nu/kT} - 1} = \frac{2h\nu^3/c^2}{e^{h\nu/kT} - 1} \,. \tag{9.7}$$

---

[8]More generally, one needs to consider a frequency *redistribution function* $R(\nu, \nu') \equiv \phi_\nu \psi_{\nu'}$, describing the probability that absorption of a photon of initial frequency ν is followed by reemission of a photon of different frequency ν'. In CRD, $R(\nu, \nu') = \phi_\nu \phi_{\nu'}$.

But because the Einstein coefficients don't depend on temperature or, for that matter the conditions of LTE, in order to recover the proper form for the Planck function, we must require these two *Einstein relations*

$$A_{ji} = \frac{2h\nu_{ij}^3}{c^2} B_{ji} \,, \tag{9.8}$$

and

$$g_i B_{ij} = g_j B_{ji} \,. \tag{9.9}$$

It should be emphasized again that these Einstein relations are quite general, and *do not depend on an assumption of LTE*. At a base level, they really stem from the time-reversal nature of microscopic laws of physics, since running a clock backwards on an absorption looks like an emission, and vice versa. It is the basis of the general rule of thumb: "a good absorber is a good emitter". In general then, once we know the absorption coefficient B_{ij}, we can use these Einstein relations to obtain the stimulated and spontaneous emission coefficents B_{ji} and A_{ji}.

9.2. The Classical Oscillator

A key issue in line-transfer is computing the line-absorption opacity,

$$\kappa_\nu = \frac{n_i}{\rho} \sigma_\nu \,, \tag{9.10}$$

in terms of the level population n_i for the lower level i, and the associated bound-bound cross section,

$$\sigma_\nu = \sigma_{tot} \, \phi_\nu \,, \tag{9.11}$$

where σ_{tot} is the total, frequency-integrated cross section, with units $cm^2\,\mathrm{Hz}$. For complex atoms with many electrons and energy levels, it can be quite difficult to calculate these cross sections, and often they are best determined by experiment.

But within the context of a basic classical model of an atom, one can derive a quite simple scaling, known as the "classical oscillator", for which the frequency-integrated cross section is just

$$\sigma_{cl} \equiv \frac{\pi e^2}{m_e c} = \pi r_e c \,, \tag{9.12}$$

where again e and m_e are the electron charge and mass, and the latter equality casts this in terms of the classical electron radius $r_e = e^2/m_e c^2$. More complete calculations based on

modern quantum mechanics are generally written with the integrated cross sections scaled by this classical oscillator,

$$\sigma_{tot} = f_{ij}\,\sigma_{cl} = B_{ij}\,\frac{h\nu_{ij}}{4\pi}\,, \tag{9.13}$$

where f_{ij} is a dimensionless "oscillator strength", typically of order unity for quantum mechanically allowed transitions, but very small for "forbidden" transitions that violate some first-order selection rule. The latter equality above shows the relationship to the Einstein absorption coefficient B_{ij}.

Collecting these relations together, we have for the frequency-dependent line-opacity,

$$\kappa_\nu = \frac{n_i}{\rho}\,f_{ij}\,\sigma_{cl}\,\phi_\nu\,. \tag{9.14}$$

9.3. Gaussian Line-Profile for Thermal Doppler Broadening

Let us now derive a form for the line-profile function ϕ_ν that results from the Doppler broadening by the thermal motion of atoms in an (otherwise static) atmosphere. If v is the speed of an atom's thermal motion in the direction of a photon with rest frequency ν, then by the standard formula for Doppler shift, the frequency in the atom's frame is

$$\nu_a = \nu(1 - v/c)\,. \tag{9.15}$$

For gas of temperature T, the mean kinetic energy due to random thermal motion is $kT = mv_{th}^2/2$, where v_{th} is the average thermal speed, and m is the mass of the absorbing atom. The fraction of atoms in a speed interval between v and $v + dv$ is then given by a simple Gaussian distribution,[9]

$$f(v)dv = \frac{e^{-(v/v_{th})^2}}{\sqrt{\pi}v_{th}}\,dv\,, \tag{9.16}$$

The line-profile in the star's frame ϕ_ν can be obtained by convolving this distribution with the profile in atom's frame ϕ_{ν_a}.

For the idealized case that the atomic-frame profile is represented by a Dirac delta-

[9]This is another application of the Boltzmann distribution discussed above, which says that the distribution of states of energy E is proportional to $e^{-E/kT}$, where here the energy is just the kinetic energy of the individual atoms of speed v, i.e. $E = mv^2/2$, with the thermal speed given by $v_{th} = \sqrt{2kT/m}$.

function $\delta(\nu_a - \nu_o)$, the convolution integral becomes quite straightforward to evaluate,

$$\phi_D(\nu) = \int_{-\infty}^{\infty} \delta[\nu(1 - v/c) - \nu_o] \, \frac{e^{-(v/v_{th})^2}}{\sqrt{\pi} v_{th}} \, dv \tag{9.17}$$

$$= \frac{e^{-(\nu-\nu_o)^2/\Delta\nu_D^2}}{\sqrt{\pi}\Delta\nu_D} \, , \tag{9.18}$$

where

$$\Delta\nu_D = \frac{v_{th}}{c}\nu_o = \frac{\sqrt{2kT/m}}{c}\,\nu_o \tag{9.19}$$

represents a characteristic *thermal Doppler width* for the line. Thus lines from a gas with finite temperature are broadened by $\pm\Delta\nu_D$ on both the lower (red) and higher (blue) frequency side of line-center frequency ν_o.

> **Exercise:** Fill in the steps in the integral evaluation between (9.17) and (9.18), by making variable substitutions and accounting explicitly for the dimensions of the delta function. Then integrate eqn. (9.18) over all frequencies to confirm that the Doppler profile $\phi_D(\nu)$ has the proper unit normalization from eqn. (9.2).

Sometimes the profile function is instead defined in terms of the photon wavelength λ instead of frequency ν. But to keep the proper units and normalization, note that one requires $\phi_\nu d\nu = \phi_\lambda d\lambda$. It is often convenient to write a thermally broadened line-profile in terms of thermal Doppler widths x from line center,

$$\phi_D(x) \equiv \frac{e^{-x^2}}{\sqrt{\pi}} \, . \tag{9.20}$$

Depending on the context, the variable x can either be in wavelength, $x_\lambda = (\lambda/\lambda_o - 1)c/v_{th} = (\lambda - \lambda_o)/\Delta\lambda_D$ or in frequency, $x_\nu = (\nu - \nu_o)/\Delta\nu_D$. But for the usual case that $\Delta\lambda_D/\lambda_o = \Delta\nu_D/\nu_o = v_{th}/c \ll 1$, these two definitions are just related by a simple sign flip.

> **Exercise:** For narrow lines characterized by fractional width $v_{th}/c \ll 1$, show that indeed $x_\lambda \approx -x_\nu$.

For hydrogen atoms at the solar effective temperature $T = 5800\ K$, $v_{th} \approx 7$ km/s, and even in hotter stars the dominant lines from partially ionized "metals" typically have $v_{th} \sim 10$ km/s. Comparing this to the speed of light $c = 3 \times 10^5$ km/s, we conclude that the fractional thermal width of lines is thus typically of order

$$\frac{\Delta\lambda_D}{\lambda_o} = \frac{\Delta\nu_D}{\nu_o} = \frac{v_{th}}{c} \approx 3 \times 10^{-5} \, . \tag{9.21}$$

9.4. The Resonant Nature of Bound vs. Free Electron Cross Sections

The concentration of line-opacity into such very narrow seqments in frequency or wavelength is one key factor is making line absorption strong relative to continumm processes at frequencies near an atomic resonance. But this is not the whole, or even main, reason for the inherent strength of line opacity. In particular, even if one averages the total line cross section over a much larger frequency interval given by its own resonance frequency, i.e. σ_{tot}/ν_o, this turns out to be much greater than a characteristic continuum cross section, like the Thomson cross section for electron scattering σ_{Th}. For example, for an allowed line transition with oscillator strength $f_{ij} \approx 1$, we can define a characteristic line-strength ratio Q_λ in terms the classical oscillator σ_{cl},

$$Q_\lambda \equiv \frac{\sigma_{cl}}{\nu_o \, \sigma_{Th}} = \frac{\pi r_e c}{\nu_o \, (8/3) \pi r_e^2} \tag{9.22}$$

$$= \frac{3}{8} \frac{\lambda_o}{r_e} \tag{9.23}$$

$$= 7.5 \times 10^8 \, \lambda_{5000} \, , \tag{9.24}$$

where $r_e = e^2/m_e c^2 \approx 2.5 \times 10^{-13}$ cm is the classical electron radius discussed previously. The last equality shows that, in terms of a wavelength scaled by a typical optical value, i.e. $\lambda_{5000} \equiv \lambda/5000 \, \mathring{A}$, this ratio is *very large*. By this measure, one can thus think of line cross sections as being roughly a *billion* times stronger than for electron scattering!

The basic physical reason for this great intrinsic strength of lines lies in the ability of bound electrons to resonate with narrow bands of the incident radiation, greatly increasing the total cross section. This is much the same principle that makes a whistle loud, with a response tuned to a specific frequency, in contrast to the softer, broadband noise from just blowing into open air. Indeed, by next examining the finite lifetime and damping of the resonance, we will see that the ratio Q_λ is closely related to *quality* of the resonance[10].

9.5. Frequency Dependence of Classical Oscillator: the Lorentz Profile

This simple classical model of a bound oscillator can also be used to derive the *frequency-dependent* cross section, measured in the rest frame of the atom, σ_ν. Multiplied by the

[10]I am indebted to Ken Gayley for first pointing out to me this very deep insight into the resonant nature of line absorption. The discussion in this and the next two sections is largely taken from unpublished notes he shared with me. But for some interesting applications of this general property in the context of radiative driving in stellar winds, I highly recommend Gayley (1995, ApJ 454, 410).

oscillator strength f_{ij} to account for quantum mechanical effects, the result is (from Mihalas 1968, eq. [4-32]):

$$\sigma_\nu \;=\; f_{ij}\,\sigma_{Th}\,\frac{\nu^4}{(\nu^2-\nu_o^2)^2+\nu^2(\Gamma/2\pi)^2}\,, \tag{9.25}$$

where

$$\Gamma \;=\; \frac{8\pi^2}{3}\,\frac{r_e\nu_o^2}{c} = \frac{g_j}{g_i}\,\frac{A_{ji}}{3f_{ij}} \tag{9.26}$$

is a rate parameter for the *damping* of the oscillator. The latter equality makes use of the Einstein relations and eqn. (9.13) to show this classical damping rate is closely related to the quantum mechanical transition rate A_{ji}.

Eqn. (9.25) yields physically different behavior over three regimes in ν:

1. *Thomson scattering* ($\nu \gg \nu_o$). For high frequencies well away from the resonance, we recover (with $f = 1$) the simple Thomson cross section for free electron scattering,

$$\sigma_\nu \approx \sigma_{Th} \quad ; \quad \nu \gg \nu_o\,. \tag{9.27}$$

2. *Rayleigh scattering* ($\nu \ll \nu_o$). In the opposite limit of low frequency well below the resonance, we obtain the Rayleigh scattering limit, with

$$\sigma_\nu \approx \sigma_{Th}\left(\frac{\nu}{\nu_o}\right)^4 \quad ; \quad \nu \ll \nu_o\,. \tag{9.28}$$

   The strong frequency dependence of Rayleigh scattering leads to a substantially reddenng of a light source, with the scattered, diffuse light dominated by bluer color. In the context of scattering by molecules in the earth's atmosphere, such Rayleigh scattering makes the sky blue, and leads to the distinct redness of the solar disk at sunset.

3. *Line absorption* ($\nu \approx \nu_o$). When ν is very close to ν_o, we obtain a line-opacity of the form

$$\sigma_\nu = f_{ij}\sigma_{cl}\,\phi_L(\nu)\,, \tag{9.29}$$

   where

$$\phi_L(\nu) \;= \frac{\Gamma/4\pi^2}{(\nu-\nu_o)^2+(\Gamma/4\pi)^2} \tag{9.30}$$

   is known as the normalized *Lorentz* profile.

Exercise: Derive the Lorentz profile (9.30) from the general eqn. (9.25) in the case that $\nu \approx \nu_o$. *Hint:* Note that in this case, $(\nu^2-\nu_o^2)^2 \cong 4\nu_o^2(\nu-\nu_o)^2$.

Note that *all three* regimes are present for any resonator, and free electrons can be treated simply by taking ν_o and Γ to be zero, with unit oscillator strength, in eqn. (9.25). This suggests that eqn. (9.25) can be rewritten in a simple approximate form that underscores these points,

$$\sigma_\nu \cong f_{ij}\sigma_{Th}\,\min\{1, \nu^4/\nu_o^4\} + f_{ij}\sigma_{cl}\phi_L(\nu). \tag{9.31}$$

Eqn. (9.31) allows us to examine the relative importance of bound and free electrons. It shows that the Thomson cross section is present even for bound electrons. Thus the use of the Lorentz profile is actually an approximation to eqn. (9.25) in the vicinity of the resonance. Using eqn. (9.25) instead eliminates the confusion between the units of σ_{Th} and σ_{cl}, and it is readily seen from eqn. (9.31) that the presence of a resonance merely enhances the cross section in the vicinity of ν_o, and sets up a wide Rayleigh regime where the cross section is somewhat reduced. These are constructive and destructive interference effects, respectively, and the constructive effects far outweigh the destructive ones for a flat continuum. The oscillator strength is an overall multiple that applies in all three regimes, and effectively gives the probability that the oscillator in question is quantum mechanically realized.

9.6. The High "Quality" of Line Resonance

As shown in eqn. (9.26), the damping rate Γ is closely related to the transition rate A_{ji}, meaning $1/\Gamma$ effectively characterizes the lifetime of the state, or equivalently, the duration of the resonance. As such, we can readily define the classical "Q" or *quality* of the resonance,

$$Q \;=\; \frac{\nu_o}{\Gamma} \;=\; \frac{3}{8\pi^2}\,\frac{\lambda_o}{r_e} \;= \frac{Q_\lambda}{\pi^2} \approx 8\times 10^7\,\lambda_{5000}\,, \tag{9.32}$$

which effectively gives the number of cycles required to damp the oscillation after external driving is turned off. It also gives the number of cycles over which the oscillator can retain phase coherence, which measures its potential for constructive interference. This interference allows the bound electrons to dominate the free electrons by essentially the factor QA, where A is the relative fraction of bound vs. free electrons in the stellar atmosphere.

For example, in the atmosphere of a cool star like the sun, most electrons are still bound to hydrogen, and so photons with a frequency near the resonance for one of the bound-bound transitions of a hydrogen, the opacity can be enormous compared to electron scattering. Hydrogen lines in the sun are thus typically very strong, even greater than $Q \sim 10^8$ times the opacity for free electrons.

On the other hand, in hotter stars, hydrogen is fully ionized, and the dominant lines come from various incomplete ionization states of much less abundant "metals", e.g. carbon,

nitrogen, oxygen and iron. With relative abundance of bound electrons thus of order $A \sim 10^{-4}$, the strengths of lines relative to electron scattering is somewhat reduced, but still large, $QA \sim 10^3$.

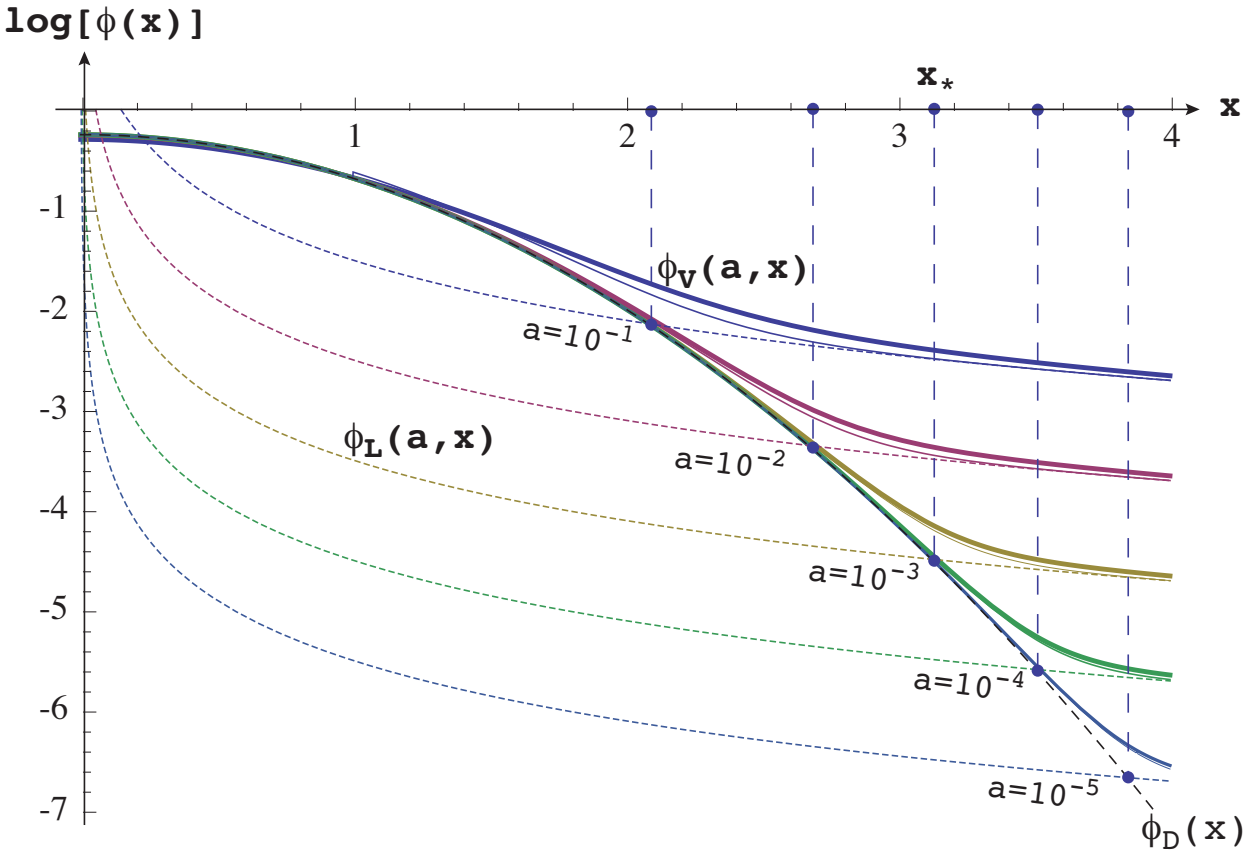

Fig. 8.— $\log[\phi(x)]$ vs. x for Voigt (heavy solid), Doppler (medium dashed) and Lorentz (light dotted) profiles with various damping parameters a_v. The intersection points x_* at which $\phi_D(x_*) \equiv \phi_L(a_v, x_*)$ mark the transition frequency between Doppler core and Lorentz damping wings. The light solid curves show that the sum of the Doppler and Lorentz profiles gives a good, simple approximation to the full Voigt profile for $x > 1$, as noted in eqn. (9.41).

9.7. The Voigt Profile for Combined Doppler and Lorentz Broadening

The above shows that the intrinsic profile in the atom's frame is not completely sharp like a delta-function, but rather, due to the finite liftetime of the state, has an inherent broadening characterized by the Lorentz profile $\phi_L(\nu)$, as given by eqn. (9.30). To obtain

the overall profile in the frame of the stellar atmosphere, we must convolve this Lorentz profile with the Gaussian distribution of speeds that give thermal Doppler broadening,

$$\phi_V(\nu) = \int_{-\infty}^{\infty} \phi_L[\nu(1 - v/c)] \, \frac{e^{-(v/v_{th})^2}}{\sqrt{\pi} v_{th}} \, dv \, . \tag{9.33}$$

For such a "Voigt profile", it is traditional to define a parameterized *Voigt* function,

$$H(a_v, x) \equiv \frac{a_v}{\pi} \int_{-\infty}^{\infty} \frac{e^{-y^2}}{(x-y)^2 + a_v^2} \, dy \tag{9.34}$$

$$= \frac{e^{a_v^2 - x^2}}{2} \Re \left[e^{2ia_v x} \mathrm{erfc}(a_v + ix) + e^{-2ia_v x} \mathrm{erfc}(a_v - ix) \right] \, , \tag{9.35}$$

where the latter analytic form was obtained from *Mathematica*. Here we have again used a Doppler-unit frequency difference from line-center,

$$x \equiv \frac{\nu - \nu_o}{\Delta\nu_D} \, , \tag{9.36}$$

and we have now defined a scaled damping parameter,

$$a_v \equiv \frac{\Gamma}{4\pi \Delta\nu_D} \, , \tag{9.37}$$

which is typically quite small, $a_v \sim 10^{-4} \ll 1$. In these scaled units, the Doppler profile is given by eqn. (9.20), while the Lorentz profile is

$$\phi_L(a_v, x) = \frac{a_v/\pi}{x^2 + a_v^2} \, . \tag{9.38}$$

Figure 8 compares log plots of the frequency variation of Voigt, Doppler, and Lorentz profiles, for various values of a_v.

Exercise: Show that the dimensionless damping parameter a_v can be written in terms of the resonance quality Q defined in eqn. (9.32), and the ratio of thermal speed to light speed v_{th}/c. For the typical values quoted above for Q of an allowed transition with wavelength in the optical, and for thermal speed v_{th} in a stellar atmosphere, estimate an associated numerical value of a_v, confirming thereby that it is indeed very small, $a_v \ll 1$.

We can now write a Doppler-unit Voigt profile

$$\phi_v(a_v, x) = \frac{H(a_v, x)}{\sqrt{\pi}} \tag{9.39}$$

$$\approx \phi_D(x) \quad ; \quad |x| \leq 1 \tag{9.40}$$

$$\approx \phi_D(x) + \phi_L(a_v, x) \quad ; \quad |x| > 1\,. \tag{9.41}$$

Figure 8 compares the full Voigt profile with Doppler and Lorentz profiles, and also their sum. As illustrated by the vertical dashed lines, the frequency x_* – defined implicitly as the outer root of $\phi_D(x_*) = \phi_L(a_v, x_*)$ – marks the transition from the Doppler core to the Lorentz damping wings. This can be solved explicitly using the "Lambert" or "ProductLog" function[11], but for the usual case of a very small damping parameter, $a_v \ll 1$, figure 8 shows that typically $x_* = 2 - 4$. Using $x_* \approx 3$ as first approximation, we can write an explicit next approximation in the form

$$x_* \approx \sqrt{\ln(3\sqrt{\pi}/a_v)}\,. \tag{9.42}$$

For example, for a typical value $a_v = 10^{-4}$, this approximation gives $x_* \approx 3.3$, whereas the exact solution is $x_* = 3.5$.

10. Classical Line Transfer: Milne-Eddington Model for Line + Continuum

Let us now derive the emergent intensity and/or flux from an atmosphere in which the opacity has contributions from both line and continuum. For this, note that in §8.5 we have already solved the radiative transfer for thermal emission plus coherent, scattering at a single, fixed, isolated frequency ν. In that solution, no restriction was made for what the source of the opacity might be at the chosen frequency, and so we are free now to specify this, using both the continuum and line opacity sources we have been examining above.

So consider now a case where at the given frequency ν the total opacity k_ν stems from a combination of both continuum and line processes,

$$k_\nu = k_c + k_l\,\phi_\nu\,, \tag{10.1}$$

with also correponding emissivities

$$\eta_\nu = \eta_c + \eta_l\,\phi_\nu\,. \tag{10.2}$$

---

[11] See `http://mathworld.wolfram.com/LambertW-Function.html` or `http://en.wikipedia.org/wiki/Lambert_W_function` .

Let us further assume that these opacities are divided between scattering and absorption components, with associated photon destruction probabilities.

$$k_c = \kappa_{cs} + \kappa_{ca} \tag{10.3}$$
$$k_l = \kappa_{ls} + \kappa_{la} \tag{10.4}$$
$$\epsilon_c = \kappa_{ca}/k_c \tag{10.5}$$
$$\epsilon_l = \kappa_{la}/k_l \,. \tag{10.6}$$

We can then define a frequency-dependent destruction probability

$$\epsilon_\nu = \frac{\epsilon_c + \epsilon_l \, \beta_\nu}{1 + \beta_\nu} \,, \tag{10.7}$$

where the relative strength of the total line to continuum opacity is defined by

$$\beta_\nu = \frac{k_l}{k_c} \, \phi_\nu \,. \tag{10.8}$$

This still gives a source function of the form in eqn. (8.22),

$$S_\nu(\tau_\nu) = \epsilon_\nu B_\nu(\tau_\nu) + (1 - \epsilon_\nu) J_\nu(\tau_\nu) \,. \tag{10.9}$$

As in §8.5, let us assume a Planck function that is linear in optical depth, defined now by the continuum opacity,

$$B_\nu(\tau_c) = a + b \, \tau_c \tag{10.10}$$
$$\equiv a + p_\nu \, \tau_\nu \,, \tag{10.11}$$

where the second equality gives the variation with frequency-dependent optical depth through the coefficient

$$p_\nu \equiv b \, \frac{k_c}{k_\nu} = \frac{b}{1 + \beta_\nu} \,. \tag{10.12}$$

An essential point here is that, with just these redefinitions, the solution is entirely analogous to that given by eqn. (8.29),

$$J_\nu(\tau_\nu) = a + p_\nu \tau_\nu + \frac{p_\nu/\sqrt{3} - a}{1 + \sqrt{\epsilon_\nu}} \, e^{-\sqrt{3\epsilon_\nu} \, \tau_\nu} \,. \tag{10.13}$$

We can use this to obtain the emergent flux

$$H_\nu(0) = \frac{J_\nu(0)}{\sqrt{3}} = \frac{1}{3} \, \frac{\sqrt{3\epsilon_\nu} \, a + p_\nu}{1 + \sqrt{\epsilon_\nu}} \,. \tag{10.14}$$

For continuum opacity, we have $\beta_\nu \to 0$, $\epsilon_\nu = \epsilon_c$, and $p_\nu = b$, yielding

$$H_c(0) = \frac{1}{3}\,\frac{\sqrt{3\epsilon_c}\,a + b}{1+\sqrt{\epsilon_c}}\,. \tag{10.15}$$

The ratio of these gives the *residual flux* of the line,

$$\boxed{R_\nu \equiv \frac{H_\nu(0)}{H_c(0)} = \left(\frac{\sqrt{3\epsilon_\nu}\,a + b/(1+\beta_\nu)}{\sqrt{3\epsilon_c}\,a + b}\right)\left(\frac{1+\sqrt{\epsilon_c}}{1+\sqrt{\epsilon_\nu}}\right)\,.} \tag{10.16}$$

This general result contains interesting behaviors in various special cases, as we now explore.

10.1. Scattering line with thermal continuum

Let us first consider the case of a pure-scattering line, with $\epsilon_l = 0$, coupled with a pure-aborption, thermal continuum, $\epsilon_c = 1$, which together also imply $\epsilon_\nu = 1/(1+\beta_\nu)$. We then find

$$R_\nu = 2\,\frac{\sqrt{3}a + b/\sqrt{1+\beta_\nu}}{(\sqrt{3}\;a+b)\,(1+\sqrt{1+\beta_\nu})}\,. \tag{10.17}$$

Note then that for a very strong scattering line, i.e. with $\beta_\nu \to \infty$, we obtain $R_\nu \to 0$, meaning it becomes completely saturated or dark.

10.2. Absorption line with thermal continuum

For the case of pure-absorption in both continuum and line, with $\epsilon_c = \epsilon_l = 1$, eqn. (10.16) becomes

$$R_\nu = \frac{\sqrt{3}a + b/(1+\beta_\nu)}{\sqrt{3}\;a+b}\,. \tag{10.18}$$

Now for the limit of strong absorption line, $\beta_\nu \to \infty$, we find

$$R_\nu = R_o = \frac{1}{1+b/\sqrt{3}a}\,, \tag{10.19}$$

which is generally nonzero. Very strong absorption lines thus do not become completely dark.

Figure 9 compares line profiles for this absorption case (left) with the scattering case above (right), for a Voigt parameter $a_v = 10^{-3}$, and Eddington gray atmosphere values for the ratio $b/a = 3/2$. The overplots are for line-center strength $\beta_o = 1$ to 10^6 in steps of factor

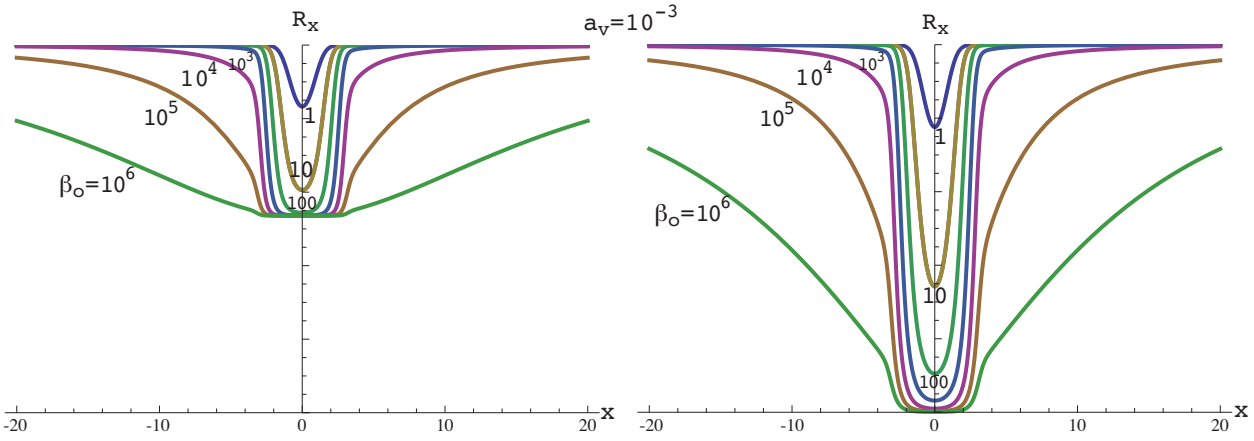

Fig. 9.— The residual flux R_x vs. Doppler-scaled frequency x for the case of pure-absorption continuum $\epsilon_c = 1$ with $b/a = 3/2$, and Voigt line damping parameter $a_v = 10^{-3}$. The left panel is for pure-absorption lines ($\epsilon_l = 1$) and the right is for pure-scattering lines ($\epsilon_l = 0$), with the overplots showing profiles for central line strengths from $\beta_\nu = 1$ to $\beta_o = 10^6$ in step factors of one decade.

10. Note that the strong scattering lines become black at line center, while absorption lines saturate to a level that depends on b/a.

Strong lines have a dual profile character, with a saturated Doppler core, and broad, gradual Lorentz damping wings. Once lines saturate in core, the additional growth of absorption with increasing line opacity β_o occurs through a very gradual (logarithmic) expansion of the core. But with further increase in β_o, there develops a stronger growth in absorption with the expansion of the damping wings. Further details are given in the "curve of growth" discussion below.

Exercise: Consider the analytic Milne-Eddington model for the case of a pure-absorption continuum ($\epsilon_c = 1$). Assume $\beta_\nu = \beta_o \phi_v(x)$ and $B_\nu(\tau_c) = a + b\tau_c$ with $b/a = 3/2$.

a. For pure-scattering lines ($\epsilon_l = 0$), plot the residual flux profiles R_x vs. Doppler-unit frequency displacement x over the range $[-10, 10]$, overplotting curves for $\beta_o = 100$ and 10^4, and for $a_v = 10^{-4}$, 10^{-3}, and 10^{-2}.

b. Do the same for pure-absorption lines ($\epsilon_l = 1$).

c. For the case $\beta_o = 100$ and $av = 10^{-2}$, compute the source function S_ν at optical depth $\tau_\nu = 2/3$ for both a pure-scattering and a pure-absorption line. Use the Eddington-Barbier relation to relate these to the residual fluxes obtained for this case in parts (a) and (b). Do the same for the $\beta_o = 10^4$ case.

10.3. Absorption lines in a Gray Atmosphere

For a gray atmosphere, we have $S_c = J_c = B_\nu$, with

$$B_\nu(\tau) = B_\nu(T_o) + \frac{dB_\nu}{d\tau_c}\tau_c = a + b\tau_c\,, \tag{10.20}$$

and [cf. eqn. (8.12)]

$$T^4 = T_o^4\left(1 + \frac{3}{2}\tau_c\right)\,, \tag{10.21}$$

where $T_o \approx T_{eff}/2^{1/4}$ is the surface temperature. From these relations we see that

$$\frac{b}{a} = \frac{3}{8}\,X_o = \frac{3}{8}\,\frac{h\nu/kT_o}{e^{h\nu/kT_o} - 1}\,. \tag{10.22}$$

For a strong absorption line in such a gray atmosphere, we find residual flux

$$R_o = \frac{1}{1 + \sqrt{3}X_o/8}\,. \tag{10.23}$$

For example, $T_o = 4800$ K, and for $\lambda \approx 5000\,\mathring{A}$, we get $X_o \approx 6$, which applied to eqn. (10.23) gives $R_o = 1/(1 + 3\sqrt{3}/4) = 0.44$. This is in good agreement with the central depth of the Hydrogen Balmer line, Hα, which as a "subordinate line" (originating from an upper level), behaves ~~like~~ almost like a pure absorption.

In contrast, strong "resonances lines", which start at the ground level, tend to behave like scattering lines, and when very strong, they do indeed become nearly black at line center.

10.4. Center to Limb Variation of Line Intensity

The formal solution gives for the emergent intensity,

$$I_\nu(\mu, 0) = \int_0^\infty \left[B_\nu + (1-\epsilon_\nu)(J_\nu - B_\nu)\right] e^{-t/\mu}\, dt/\mu \tag{10.24}$$

$$= a + p_\nu\mu + \frac{(p_\nu - \sqrt{3}a)(1-\epsilon_\nu)}{\sqrt{3}(1+\sqrt{\epsilon_\nu})(1+\sqrt{3\epsilon_\nu}\mu)}\,. \tag{10.25}$$

For pure-absorption continuum with $\beta_\nu = 0$ and $\epsilon_c = 1$, we find again $I_c = a + b\mu$, from which we can now define the residual *intensity* profile

$$r_\nu(\mu) \equiv \frac{I_\nu(\mu, 0)}{I_c(\mu)} \,. \tag{10.26}$$

For a pure-absorption line with $\epsilon_l = \epsilon_c = \epsilon_\nu = 1$, we find

$$r_\nu(\mu) \equiv \frac{a + b\mu/(1+\beta_\nu)}{a + b\mu} \to 1 \quad \text{as} \quad \mu \to 0 \,, \tag{10.27}$$

from which we see that the scattering lines disappear at the limb, regardless of the value of β_ν.

By contrast, for a scattering line with $\epsilon_l = 0$ and thus $\epsilon_\nu = 1/(1+\beta_\nu)$, we find that for $\beta_o \to \infty$, $r_\nu(\mu) \to 0$ for all μ. Thus strong scattering lines are dark all across the solar disk.

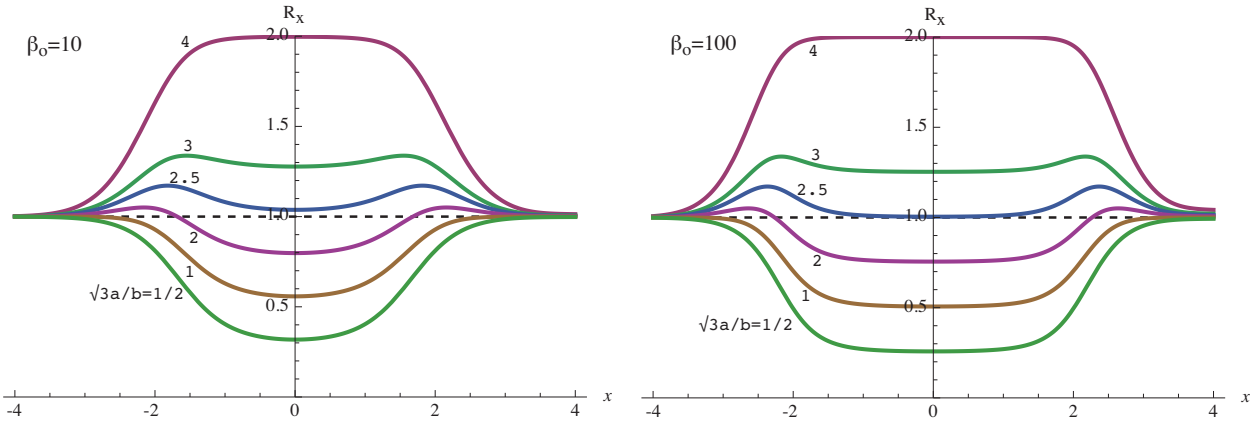

Fig. 10.— Line profiles for Schuster model for an LTE line ($\epsilon_l = 1$) in a pure-scattering continuum ($\epsilon_c = 0$). The Voigt parameter is fixed at $a_v = 10^{-4}$, and the line-center strength is set to $\beta_o = 10$ (left) or $\beta_o = 100$ (right). The overplots show results for various values for the ratio of constants a/b, illustrating how a large a/b causes the line to go into *emission*.

10.5. Schuster Mechanism: Line Emission from Continuum Scattering Layer

In a star's spectrum, the lines most commonly appear in *absorption*, meaning the intensity or flux in the line is *lower* than in the nearby continuum. But occasionally lines can also appear in *emission*, with the intensity or flux *higher* than in the continuum. One of a

handful of processes for producing emission lines is known as the Schuster mechanism, which results when the *continuum* opacity is dominated by *scattering*, such as from free electrons.

Supposing that the continuum is pure scattering, $\epsilon_c = 0$, then $\epsilon_\nu = \epsilon_l \beta_\nu/(1+\beta_\nu)$. Plugging these into eqn. (10.16), the resulting residual flux profile becomes

$$R_\nu = \frac{1/(1+\beta_\nu) + \sqrt{3\epsilon_\nu}\, a/b}{1+\sqrt{\epsilon_\nu}}\,. \tag{10.28}$$

If the line opacity is also pure scattering, with $\epsilon_l = 0$, then the residual flux is given by

$$R_\nu = \frac{1}{1+\beta_\nu} < 1\,, \tag{10.29}$$

which thus is always in absorption.

But for an absorption line with $\epsilon_l = 1$, we find for strong lines $\beta_o \to \infty$,

$$R_\nu \to \frac{\sqrt{3}}{2}\,\frac{a}{b}\,, \tag{10.30}$$

which, for a weak temperature gradient with small b/a, can exceed unity, implying a net line *emission* instead of absorption.

Physically this can be understood from the fact that scattering makes the continuum source function low near the surface, $S_c(0) = J_c(0) \ll B(0)$, which by the Eddington-Barbier relation implies a weak continuum flux. By comparison, the absorption nature of the line means its surface source function is at the much higher Planck level, $S_l(0) \approx B(0)$. This indicates the line can potentially be brighter, but only if the decline from the negative temperature gradi.ent term is not too steep.

Figure 10 plots sample line profiles for a moderate and strong line ($\beta_o = 10$, left; and $\beta_o = 100$, right), assuming various values for the ratio a/b. Note that for $a/b < 1/\sqrt{3}$, the lines remain always in absorption, while for $a/b > \sqrt{3}/2$ they are always in emission. For theintermediate case, the profiles have a mixed character, with emission wings that has a *central reversal* toward the line-core, sometimes even going below the continuum at line center. The critical case $a/b = 5/2\sqrt{3}$ shows a case where the center of a strong line reverses just down to the continuum, with the rest of the line in emission.

Exercise

In the *Schuster-Schwarzschild model*, line formation is assumed confined to a finite "*reversing layer*", of optical thickness T_ν, and illuminated from below by an incident intensity I_o. In the reversing layer, there is no continuum absorption or scattering, and $B_\nu(\tau_\nu) = a + b\tau_\nu$. Assume a *two-stream approximation*, in which $I_\nu(\mu) = I_\nu^\pm$, with only two discrete $\mu = \pm\frac{1}{2}$.

a. For pure, coherent, line-*scattering*, show that $H_\nu \equiv \frac{1}{4}(I_\nu^+ - I_\nu^-) = \text{constant} = \frac{1}{4}I_o/(1+T_\nu)$, and that $J_\nu(\tau_\nu) = 2H_\nu(1+2\tau_\nu)$, where $0 \le \tau_\nu \le T_\nu$. Why are these results independent of the Planck function parameters a and b?

b. Now derive H_ν and J_ν for a pure absorption line. Contrast the dependence here on a and b with that from part (a), and briefly discuss the physical reasons for the difference.

11. Curve of Growth of Equivalent Width

11.1. Equivalent Width

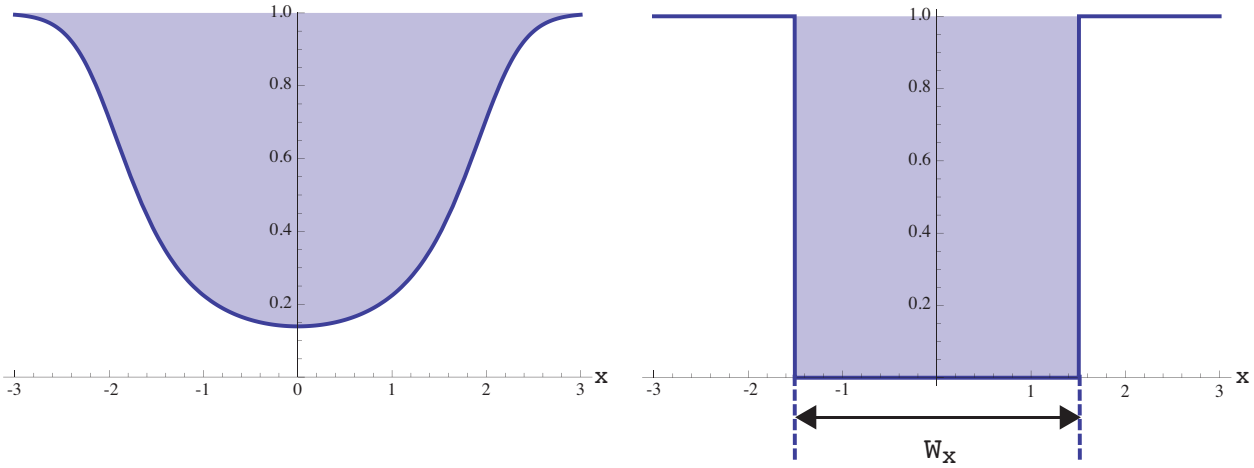

Fig. 11.— Illustration of the definition of equivalent width W_x. The left panel plots the residual flux for a sample line (here with parameters $\beta_o = 100$, $\epsilon_c = 1$, $\epsilon_l = 0$, $b/a = 3/2$, and $a_v = 10^{-3}$), with the shaded area illustrating the total fractional reduction of continuum light. The right panel plots a box profile with width W_x, defined such that the total absorption area is the same for the curve to the left. In this example, $W_x = 3.01$.

Because lines are so typically very narrow, with fractional widths $\Delta\nu_D/\nu_o = v_{th}/c \lesssim 10^{-4}$, being able to actually resolve individual line profiles in a star's spectrum demands a very high spectral resolution, $R \equiv \nu/\Delta\nu \approx \lambda/\Delta\lambda \gtrsim 10,000$, which requires some combination of a very bright star, a very large aperture telescope, or a very long exposure, to attain a sufficient number of photons within each frequency (or wavelength) resolution element. In lower-resolution survey spectra of stars, the individual line profiles are not discernible, and so the information about a given line is limited to some measure of its over strength,

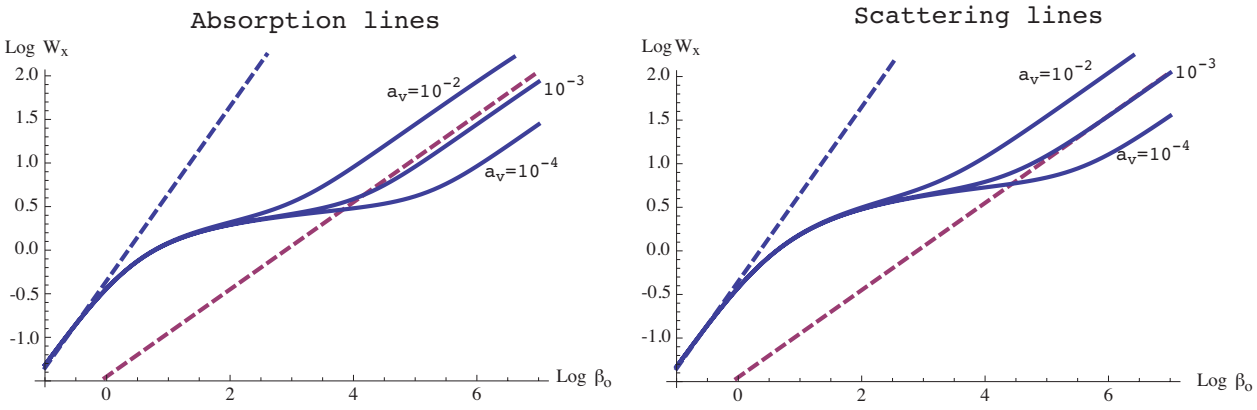

Fig. 12.— Curves of growth for the case of pure-absorption continuum $\epsilon_c = 1$, with $b/a = 3/2$, and Voigt line damping parameters $a_v = 10^{-4}$, 10^{-3}, and 10^{-2}. The left panel shows the pure absorption case given by eqn. (11.7), while the right panel is for the MIlne-Eddington model for scattering lines with $\epsilon_l = 0$. The dashed lines compare linear (blue) and square root (red) functions, to show the limiting forms for very weak and very strong lines. The flatter portion bridging between these limits shows the "logarithmic" growth from intermediate strength lines with saturated Doppler cores, but no significant Lorentz damping wings.

meaning the total fraction of the continuum flux that has been reduced near the line.

This reduction can be characterized in terms of the *equivalent width*, defined mathematically as the frequency integral over the absorption fraction $A_\nu \equiv 1 - R_\nu$,

$$W_\nu \equiv \int_0^\infty A_\nu \, d\nu \, . \tag{11.1}$$

As illustrated in figure 11, W_ν can be intuitively thought of as the width of a box profile with the same total flux reduction as the actual line.

11.2. Curve of Growth for Scattering and Absorption Lines

Given the residual flux R_ν and thus the absorption fraction A_ν, the W_ν can be computed from direct (usually numerical) integration from eqn. (11.1). In practice, it convenient to scale this width by the thermal Doppler width, $W_x \equiv W_\nu/\Delta\nu_D$, with the Doppler-scaled frequency $x = (\nu - \nu_o)/\Delta\nu_D$ used to define the frequency variation of line strength through $\beta_\nu = \beta_o \phi_v(x)$. Here $\phi_v(x)$ is the scaled Voigt profile, and β_o a measure of line-strength at

line-center, defined in terms of basic line parameters by

$$\beta_o = \sigma_{cl} f_{ij} \frac{n_i}{\rho \kappa_c} \frac{1}{\Delta\nu_D} \,. \tag{11.2}$$

This is proportional to the number of line absorbing atoms, and so the increase in of W_x with increasing β_o, known as the *curve of growth*, represents how the integrated line attenuation from lines depends on the total number of absorbers.

The right panel of figure 12 shows such a theoretical curve of growth, computed from direct frequency integration of $A_\nu = 1 - R_\nu$, as derived from the above Milne-Eddington model of a pure *scattering* line with $\epsilon_l = 0$ in pure-absorbing continuum. The left panel shows correponding curves of growth for a pure *absorption* line. Note that the basic forms of the curves of growth is quite similar in both the scattering and absorption cases, and indeed we will now see that this results mainly from the characteristics of the Voigt line profile.

To see this, it is helpful to focus on this relatively simple case of pure-absorption in both line and continuum, with again a linear Planck function $B(\tau) = a + b\tau_c$. But rather than use the above Milne-Eddington scalings that assume the Eddington approximation, in this pure-absorption case we can apply the moment form of the formal solution to compute directly the emerging flux,

$$H_\nu(0) = \frac{1}{2} \int_0^\infty (a + bt)\, E_2[(1+\beta_\nu)t](1+\beta_\nu) dt \tag{11.3}$$

$$= \frac{1}{4} \left(a + \frac{b}{1+\beta_\nu} \right) . \tag{11.4}$$

From the ratio to the continuum, we obtain for the absorption strength

$$A_\nu = 1 - H_\nu(0)/H_c = \frac{\beta_\nu}{1+\beta_\nu} \frac{1}{1+3a/2b} \equiv A_o \frac{\beta_\nu}{1+\beta_\nu} \,, \tag{11.5}$$

and thus the equivalent width

$$W_\nu = A_o \int_0^\infty \frac{\beta_\nu}{1+\beta_\nu} d\nu = 2A_o \Delta\nu_D \beta_o \int_0^\infty \frac{\phi_v(x)}{1+\beta_o \phi_v(x)} dx \,. \tag{11.6}$$

11.3. Linear, Logarithmic, and Square-Root Parts of the Curve of Growth

To isolate just this dependence on the number of absorbers through β_o, it is convenient to define a "reduced equivalent width",

$$\frac{W_\nu}{2A_o \Delta\nu_D} \equiv W^*(\beta_o) = \beta_o \int_0^\infty \frac{\phi_v(x)}{1+\beta_o \phi_v(x)} dx \,. \tag{11.7}$$

Note that this reduced equivalent width depends only on β_o and the *form* of the (Voigt) profile function $\phi_v(x)$. Knowing that form, we can readily understand the various parts of the theoretical curves of growth in figure 12.

First, for weak lines with $\beta_o \lesssim 1$, we can generally ignore the β_o term in the denominator of the integrand, implying that the integral just become the unit normalization of the profile function, and thus that the equivalent width just scales linearly with number of absorbers, $W^* \sim \beta_o$. Referring to the pure-absorption line profiles plotted in figure 9, this weak line regime corresponds to cases when the absorption is just started to appear within the Doppler core of the line. Such relatively weak lines are said to lie on the "linear" part of the curve of growth.

But as we increase the number absorbers, we soon come to a regime where this Doppler core becomes *saturated*, whereupon adding more absorbers hardly increases the total attenuation, since this requires expanding the width of the Doppler core against its strong Gaussian dependence on frequency. The increase in equivalent width for such intermediately strong lines is thus very slow, as $W^* \sim \sqrt{\log \beta_o}$, and so this regime is known as the "logarithmic" part of the curve of growth.

If, however, we increase β_o still further, we now find that the line is becoming optically thick in the Lorentz damping wings, for which the line profile now scales only with the inverse square power of frequency displacement from line center, $\phi_v(x) \sim a_v/x^2$. As the increased number of absorbers extends the optical thick wings against this Lorentz scaling, the equivalent width approachs a scaling $W^* \sim \sqrt{\beta_o}$, and so this very strong lines with Lorentz damping lines represent a "square root" part of the curve of growth.

These separate domains are apparent for both the absorption (left) and scattering (right) line cases plotted in figure 12, but note that the transition from the logarithmic to square-root parts depends on the value of the Voigt damping parameter a_v.

Exercise:

a. For the case $a_v = 10^{-2}$, sketch a plot of W^* vs. β_o by estimating W_* in limiting regimes appropriate to the "linear", "logarithmic", and "square root" parts of this *curve of growth*, marking the values for the transitions between these regimes.

b. Considering the definitions of W^* and β_o, for each of these regimes discuss the dependencies of the actual equivalent width W_ν on the Doppler width $\Delta\nu_D$ and the number of absorbers n_i.

c. Based on your answer to (b), which part of an empirical curve of growth

do you expect to be most appropriate for inferring the presence of "micro-turbulent" velocity fields? Which part for inferring elemental abundances? Explain the reasoning for your answers.

11.4. Doppler Broadening from Micro-turbulence

In our previous analysis of Doppler-broadening of a line profile, we assumed that the only speed to consider was that due to the random thermal motion of individual atoms, with an average thermal speed given in terms of the temperature T and atomic mass m, $v_{th} = \sqrt{kT/m}$. But in practice, a stellar atmosphere is typically not completely static, but can include a spatially complex collection of eddies and swirls, for example associated with convective transport of energy from the interior, or from stellar pulsations, or from localized disturbances like flares. In lieu of developing a detailed model of a specific type of motion and its spatial character, it is often assumed that the motions can themselves be characterized in some simple statistical way, for example taking the fraction of atoms with a given turbulent speed v to again scale as a Gaussian function, $e^{-(v/v_{turb})^2}$, where v_{turb} now characterizes a root-mean-square measure of the turbulent velocity amplitude. Under the further assumption that the spatial scale of such turbulence is much smaller than a typical photon mean-free-path, then the net effect would be add to the Doppler broadening of a line profile. Indeed, since the thermal motion of atoms and the random motion of such "microturbulence" are likely to be uncorrelated, the individual speeds should be added in quadrature, giving then a total average speed

$$v_{tot} = \sqrt{v_{th}^2 + v_{turb}^2}\,, \tag{11.8}$$

which then implies a total Doppler broadening

$$\Delta\nu_D = \nu_o \frac{v_{tot}}{c}\,. \tag{11.9}$$

Since the reduced curve of growth is scaled by the Doppler width, matching an observed curve of growth can allow one to infer $\Delta\nu_D$. If v_{th} can then be inferred from the known stellar temperature $e.g., T \approx T_{eff}$ and known atomic mass, then such a measure of $\Delta\nu_D$ can provide an estimate of the micro-turbulent velocity v_{turb}. The details here are left as an exercise.

12. NLTE Line Transfer

While very helpful for insight, the classical line transfer models of the previous sections have been deficient is several respects, and so now let us develop a physically more realistic model, with emphasis on two particularly important improvements:

1. *CRD vs. Coherent Scattering.* Instead of assuming a "coherent" scattering in which each frequency remains isolated from all others, let us allow for *frequency redistribution*, specifically the opposite assumption to coherent scattering, namely that the photons undergo a randomization or *Complete ReDistritrubition* (CRD) in frequency within the line.

2. *Atomic Physics with Statistical Equilibrium.* Moreover, instead of assuming that the absorption and scattering opacities are given as fixed parameters – which then also set the line destruction probability $\epsilon_l = \kappa_{abs}/(\kappa_{abs} + \kappa_{scat})$–, let us now *compute* these from basic atomic physics properties of absorbers, given also a solution to the ionization and excitation fractions of the ions based an general assumption of *statistical equilibrium.*

12.1. Two-Level Atom

A relatively simple example for this can be given by an approximate model of an atom that assumes it consists of just two bound energy states, representing an upper (u) and lower (l) level. In terms of the Einstein coefficients for excitation from the lower level, and spontaneous and stimulated decay from the upper level, the equation of radiative transfer can be written as

$$\mu \frac{dI_\nu}{dz} = \left[-n_l B_{lu} + n_u (A_{ul} + B_{ul} I_\nu)\right] \phi_\nu \, \frac{h\nu}{4\pi} \,, \tag{12.1}$$

where here we have effectively assumed CRD in invoking an equivalence between the emission and absorption profiles, $\psi_\nu = \phi_\nu$. Let us next define a line-averaged opacity by

$$\rho \kappa_{lu} = (n_l B_{lu} - n_u B_{ul}) \frac{h\nu}{4\pi \Delta\nu} \tag{12.2}$$

$$= \sigma_{cl} \, \frac{f_{lu}}{\Delta\nu} \left(n_l - \frac{g_l}{g_u} n_u \right) \,, \tag{12.3}$$

where $\Delta\nu$ is the line width, and the second term from stimulated emission now represents a kind of "negative absorption"[12]. To cast the transfer equation in its familiar form,

$$\mu \frac{dI_\nu}{d\tau} = I_\nu - S_l \,, \tag{12.4}$$

we now define the line source function by

$$S_l \equiv \frac{n_u A_{ul}}{n_l B_{lu} - n_u Bul} = \frac{2h\nu^3/c^2}{\frac{n_l g_u}{n_u g_l} - 1} \,, \tag{12.5}$$

where the latter equality uses the Einstein relations. In the special condition of thermodynamic equilibrium (TE), the level populations follow the Boltzmann distribution,

$$\frac{n_l g_u}{n_u g_l} = e^{h\nu/kT} \,, \tag{12.6}$$

in which case the line source function reduces to the Planck function, $S_l = B_{\nu_o}$.

However, in general conditions, S_l depends on the level populations n_l and n_u, and these in turn depend on the radiation field. A more general condition for determining these populations is to assume a steady state in which the net processes creating and destroying each level must balance with the net processes creating and destroying the competing level. This balance is known as *statistical equilibrium*, and can be expressed by an equality between the total destruction rates from each of the two levels,

$$n_l \left(B_{lu} \bar{J} + C_{lu} \right) = n_u \left(A_{ul} + B_{ul} \bar{J} + C_{ul} \right) \,. \tag{12.7}$$

Here Clu and Cul represent *collisional* rates for excitation and de-exciatation, and, under the assumption of CRD, the radiative rates now depend on the line-profile-averaged mean-intensity,

$$\bar{J} = \int_{-\infty}^{\infty} \phi(x) J(x) dx \tag{12.8}$$

Typically the free electrons that dominate the collisional rates have themselves a nearly Maxwell-Boltzmann distribution in energy, as in LTE. Thus, by a detailed balance argument, we require a further Einstein relation, now between the collisional exciatation and de-excitation,

$$C_{lu} = \frac{n_u^*}{n_l^*} C_{ul} = e^{-h\nu/kT} C_{ul} \,, \tag{12.9}$$

---

[12]Indeed, in the case of a popluation inversion with $n_l < n_u g_l / g_u$, this stimulated emission can dominate over positive absorption, producing a net *amplification* in intensity along a given beam. Such population inversions are the principle behind a "Light Amplfication by Stimulated Emission of Radiation", or a laser.

where the asterisks denote the LTE populations. Applying this and the statistical equilibrium equation (12.7) in the line source function definition (12.5), we find

$$S_l = \frac{\bar{J} + \epsilon' B_{\nu_o}}{1 + \epsilon'} = (1 - \epsilon)\bar{J} + \epsilon B_{\nu_o} \,, \tag{12.10}$$

where the ratio of collisional to spontaneous decay is

$$\epsilon' \equiv \frac{C_{ul}}{A_{ul}} \left(1 - e^{-h\nu/kT}\right) \,, \tag{12.11}$$

with then the *collisional destruction probability* given by

$$\epsilon \equiv \frac{\epsilon'}{1 + \epsilon'} \,. \tag{12.12}$$

This is similar to the line destruction probability ϵ_l defined above for classical line transfer, except that now it applies to the *entire line*, not just to a single frequency within the line. Otherwise, the meaning is quite similar, with ϵB_{ν_o} representing the *thermal creation* of photons, and $(1 - \epsilon)\bar{J}$ representing the scattering source.

But we now can readily see the essential physical scaling of this destruction probability, namely that since it is depends the electron collisional rate C_{ul}, it scales with the electron density, i.e., $\epsilon \sim \epsilon' \sim C_{ul} \sim n_e$. This implies that at great depth, $\epsilon' \to \infty$, and thus that $\epsilon \to 1$. Again, this leads the high-density regions at great depth toward LTE, $\epsilon \approx 1$ whereas lower density regions in the atmosphere can have $\epsilon \ll 1$, implying a strong scattering component that characterizes NLTE.

But even in this strong scattering, NLTE regime, it is important realize that one cannot disregard the relatively small thermal term ϵB_{ν_o}, since it ultimately provides the source for creative of photons, which are then scattered within the atmosphere.

Indeed, if one sets $\epsilon = 0$, then note that the transfer equation becomes entirely homogeneous, with thus no scale for the radiation field, unless imposed externally through boundary conditions. In actual stellar atmospheres, this scale is indeed set by the small, ϵB_{ν_o} thermal term, which when averaged over the volume of the thermalization depth, provide the ultimate source of the radiation.

However, we shall now see that the scaling for this thermalization depth is somewhat altered in the current case of CRD vs. the previous assumption of coherent scattering.

12.2. Thermalization for Two-Level Line-Transfer with CRD

For photons interacting in a spectral line, the destruction probability per encounter is given by

$$P_d = \frac{C_{ul}}{A_{ul} + C_{ul}} = \epsilon \,. \tag{12.13}$$

This is is to be compared with the probability for direct *escape* of a line photon with scaled frequency x into direction cosine μ from a location with vertical line optical depth τ,

$$P_e(x, \tau, \mu) = e^{-\tau\phi(x)/\mu} \,. \tag{12.14}$$

Averaged over the line profile $\phi(x)$ and all directions μ,

$$P_e(\tau) = \frac{1}{2}\int_{-\infty}^{\infty} dx\phi(x) \int_0^1 e^{-\tau\phi(x)/\mu}\, d\mu \tag{12.15}$$

$$= \frac{1}{2}\int_{-\infty}^{\infty} E_2[\tau\phi(x)]\phi(x)\, dx \,. \tag{12.16}$$

For strong lines with $\tau \gg 1$, let us define a line-edge frequency x_1 by $\phi(x_1) \equiv 1/\tau$. We then find that the exponential integral term in the integrand can be approximated by $E_2 \to 0$ for $x < x_1$, and by $E_2 \to 1$ for $x > x_1$. Physically this states that photons are trapped in the core (with $x < x_1$, but can escape in the line wings, $x > x_1$. Thus the total escape probabilty can be approximated by

$$P_e(\tau) \approx \int_{x_1}^{\infty} \phi(x)\, dx \,. \tag{12.17}$$

The evaluation of this integral can be divided between the case of moderately strong line, for which x_1 is still in the Doppler core of the Voigt profile $\phi(x)$, and the case of very strong lines, for which x_1 lies in the Lorentz damping wings.

For intermediately strong lines with a Doppler profile, we find

$$P_e(\tau) = \frac{1}{2}\mathrm{erfc}(x_1) \approx \frac{e^{-x_1^2}}{2\sqrt{\pi}x_1} \tag{12.18}$$

$$= \frac{\phi(x_1)}{2x_1} = \frac{1}{2x_1\tau} \approx \frac{C}{\tau} \,, \tag{12.19}$$

where in the last equality we note that $C = 1/2x_1 \approx 1/2\sqrt{\ln(\tau/\sqrt{\pi})}$ is nearly just a constant order unity.

If we then define a thermalization depth by setting the escape and destruction probabilities equal, $P_e(\tau_{th}) = P_d$, we find that for CRD line-transfer within the Doppler core the thermalization depth now scales as

$$\tau_{th} = \frac{C}{\epsilon} \,. \tag{12.20}$$

Recall that for coherent scattering, we found above that $\tau_{th} \sim 1/\sqrt{\epsilon}$. For the usual case that $\epsilon \ll 1$, the thermalization depth for CRD line-transfer is thus substantially deeper than in the coherent scattering case. For example, for a quite typical value $\epsilon \approx 10^{-4}$, we find that in CRD, $\tau_{th} \approx 10^4$, or a factor *hundred* greater than the $\tau_{th} \approx 100$ obtained by a coherent scattering model!

The physical reason for this difference stems from the difference in the nature of photon escape in coherent scattering vs. CRD. In coherent scattering, the photons can only escape through an extensive spatial diffusion, a random walk from their point of creation to the $\tau \approx 1$ layer for free photon flight and escape. By contrast, in CRD photons trapped in the very optically thick Doppler core of the line have a chance to be *redistributed* to a frequency in the line wings, where the optical depth can be of order unity or less, thus allowing a *direct* escape in a single flight, without the necessity of a protracted spatial diffusion. This greater "leakage" of thermally created photons means that the escape of radiatio from the surface can be sensed to a much deeper level, implying then a much deeper themalization depth.

Exercise: Show that for very strong lines with saturated Lorentz damping wings, the thermalization depth now scales as $\tau_{th} \sim 1/\epsilon^2$ if one assumes CRD holds through full Voigt profile out to the Lorentz wings.[13] Give a physical explanation for this still deeper thermalization depth scaling.

13. The Energies and Wavelengths of Line Transitions

13.1. The Bohr Atom

The discretization of atomic energy that leads to spectral lines can be understood through the simple Bohr model of the Hydrogen atom. In analogy with planets orbiting the sun, this assumes that electrons of charge $-e$ and mass m_e are in a stable circular orbit around the atomic nucleus (for hydrogen just a single proton) of charge $+e$ whose mass is effectively infinite compared to the electron. The electrostatic attraction between these charges then balances the centrifugal force from the electron's orbital speed v along a circular orbit of radius r,

$$\frac{e^2}{r^2} = \frac{m_e v^2}{r} \,. \tag{13.1}$$

[13]The assumption CRD actually falters for the Lorentz wings, which are better approximated by coherent scattering. As such, the actual thermalization depth for saturated line wings is not so deep in practice.

In classical physics, this orbit could, much like a planet going around the sun, have any arbitrary radius. But in the microscopic world of atoms and electrons, such classical physics has to be modified – indeed replaced – by quantum mechanics. Just as a light wave has its energy quantized into discrete bundles called photons, it turns out that the orbital energy of an electron is also quantized into discrete levels, much like the steps of a staircase. The basic reason stems from the fact that, in the ghostly world of quantum mechanics, electrons are themselves not entirely discrete particles, but rather, much like light, can also have a "wavelike" character. In fact any particle with momentum $p = mv$ has an associated "*de Broglie wavelength*" given by

$$\lambda = \frac{h}{mv}\,, \tag{13.2}$$

where again, h is Planck's constant.

This wavy fuzziness means an orbiting electron cannot be placed at any precise location, but is somewhat spread along the orbit. But then to avoid "interfering with itself", integer multiples n of this wavelength should match the orbital circumference $2\pi r$, implying

$$n\lambda = 2\pi r = \frac{nh}{mv}\,. \tag{13.3}$$

Note that Planck's constant itself has units of speed times distance [14], which represents an *angular momentum*. So another way to view this is that the electron's orbital angular momentum $J = mvr$ must likewise be quantized,

$$J = mvr = n\hbar\,, \tag{13.4}$$

where $\hbar \equiv h/2\pi$ is a standard notation shortcut. The integer index n is known as the *principal quantum number*.

Exercise 2-1: Use eqns. (13.1) and (13.4) to derive the orbital radius r_n in terms of the integer step n.

Exercise 2-2: For an electron and proton that are initially a distance r apart, show that the energy needed to separate them to an arbitrarily large distance is given by $-U(r) = e^2/r$. Use the resulting potential energy $U(r)$ together with the orbital kinetic energy $T = m_e v^2/2$ to derive the expressions in eqn. (13.5) for the total energy $E = U + T$.

---

[14] Or also, energy times time, which when used with Heisenberg's Uncertainty $\Delta E \Delta t \gtrsim h$, will lead us to conclude that an atomic state with finite lifetime t_{life} must have a finite width or "fuzziness" in its energy $\Delta E \sim h/t_{life}$. See the section below on "natural broadening" of spectral lines.

The quantization condition in eqn. (13.3) or (13.4) implies that the orbital radius can only take certain discrete values r_n, numbered by the level n. But instead of radius, it is generally more useful to cast this in terms of the associated orbital *energy*. The total orbital energy is a combination of the *negative potential* energy $U = -e^2/r$, and the *positive kinetic* energy $T = m_e v^2/2$. Using the orbital force balance eqn. (13.1), we find that the total energy is

$$E_n = -\frac{e^2}{2r_n} = -\frac{m_e e^4}{2\hbar^2}\,\frac{1}{n^2} = -\frac{E_1}{n^2}\,, \tag{13.5}$$

where

$$E_1 \equiv \frac{m_e e^4}{2\hbar^2} = 2.2 \times 10^{-11} erg = 13.6\, eV \tag{13.6}$$

denotes the ionization (a.k.a. binding) energy of Hydrogen from the ground state (with $n = 1$). Figure 13 gives a schematic rendition of the energy levels of Hydrogen, measured in *electron Volts* (eV), which is the energy gained when a charge of one electron falls through an electrical potential of one volt.

Exercise 2-3: Confirm the validity of eqn. (13.5) by using eqn. (13.1) to show that $E = U/2 = -T$, where U, T, E are the potential, kinetic, and total energy of an orbiting electron. (Note: this result is sometimes referred to as a corollary of the Virial Theorum for bound systems, which is discussed further below.)

When an electron changes from one level with quantum number m to another with quantum number n, then the associated change in energy is

$$\Delta E_{mn} = E_1 \left(\frac{1}{n^2} - \frac{1}{m^2} \right) . \tag{13.7}$$

13.2. Line Wavelengths for Term Series

Instead of energy, light is more commonly measured in terms of its wavelength $\lambda = c/\nu = hc/E$. Using this conversion in eqn. (13.7), we find the wavelength of a photon emitted by transition from a level m to a lower level n is

$$\lambda_{mn} = \frac{\lambda_1}{\frac{1}{n^2} - \frac{1}{m^2}}\,, \tag{13.8}$$

where

$$\lambda_1 \equiv \frac{hc}{E_1} = \frac{h^3 c}{2\pi^2 m_e e^4} = 91.2\, nm = 912\, \mathring{A} \tag{13.9}$$

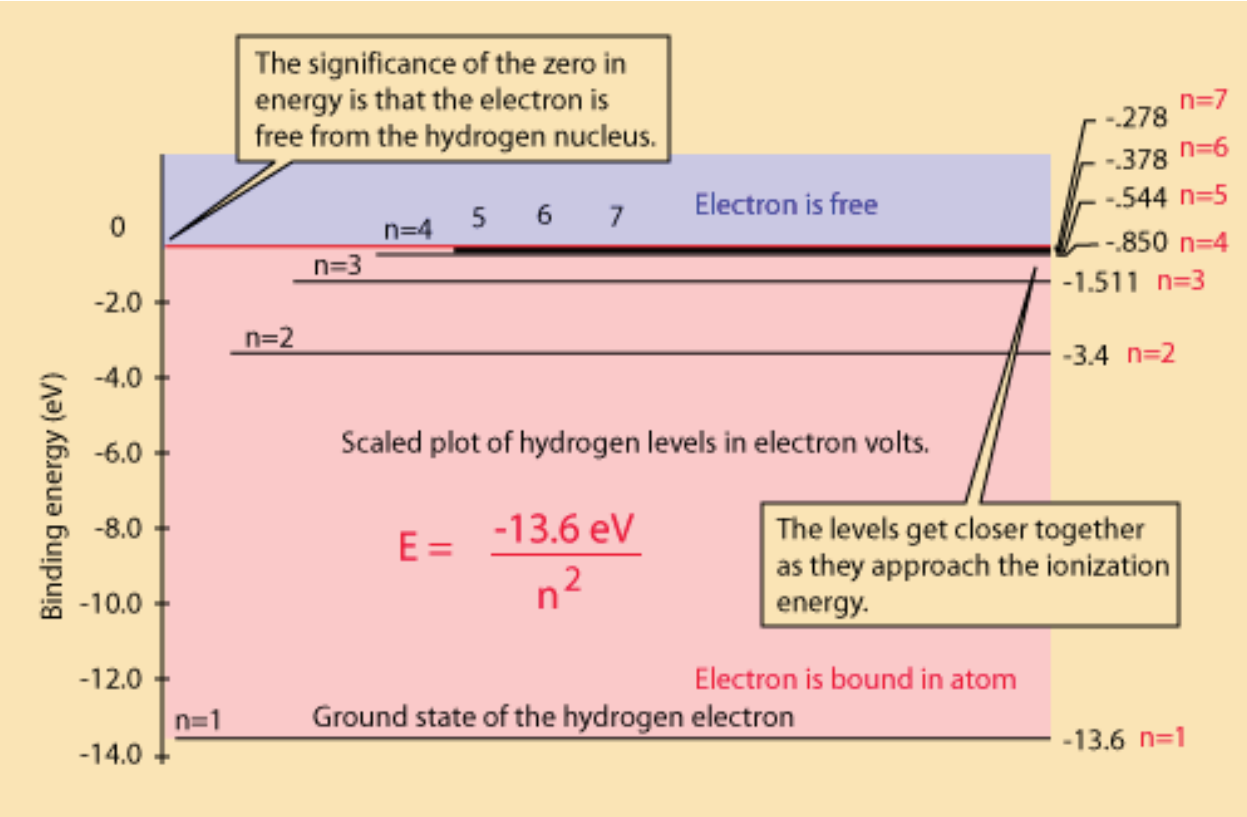

Fig. 13.— The energy levels of the Hydrogen atom. The figure is taken from `http://hyperphysics.phy-astr.gsu.edu/hbase/hyde.html#c3`

is the wavelength at what is known as the *Lyman limit*, corresponding to a transition to the ground state $n = 1$ from an arbitrarily high bound level with $m \to \infty$. Of course, transitions from a lower level m to a higher level n require *absorption* of a photon, with the wavelength now given by the absolute value of eqn. (13.8).

The lower level of a transition defines a *series* of line wavelengths for transitions from all higher levels. For example, the *Lyman series* represents all transition to/from the ground state $n = 1$. Within each series, the transitions are denoted in sequence by a lower case greek letter, e.g. $\lambda_{21} = (4/3)\,912 = 1216\,\AA$ is called Lyman-α, while $\lambda_{31} = (9/8)912 = 1026\,\AA$ is called Lyman-β, etc. The Lyman series all falls in the ultraviolet (UV) part of the spectrum, which due to UV absorption by the earth's atmosphere is generally not possible to observe from ground-based observatories.

More accessible is the *Balmer series*, for transitions between $n = 2$ and higher levels with $m = 3$, 4, etc., which are conventionally denoted Hα, Hβ, etc. These transitions are

pretty well positioned in the middle of the visible, ranging from $\lambda_{32} = 6566\,\mathring{A}$ for Hα to $\lambda_{\infty 2} = 3648\,\mathring{A}$ for the *Balmer limit*.

The Paschen series, with lower level $n = 3$, is generally in the InfraRed (IR) part of the spectrum. Still higher series are at even longer wavelengths.

14. Equilibrium Excitation and Ionization Balance

14.1. Boltzmann equation

A key issue for formation of spectral lines from bound-bound transitions is the balance of processes that excite and de-excite the various energy levels of the atoms. In addition to the photon absorption and emission processes discussed above, atoms can also be excited or de-excited by collisions with other atoms. Since the rate and energy of collisions depends on the gas temperature, the shuffling among the different energy levels also depends sensitively on the temperature.

In *Thermodynamic Equilibrium* (TE), the numbers in each level i is just proportional to the number of quantum mechanical states, g_i, associated with the orbital and spin state of the electrons in that level[15]; but between a lower level i and upper level j with an energy difference ΔE_{ij}, the relative population is also weighted by an exponential term called the *Boltzmann factor*,

$$\frac{n_j}{n_i} = \frac{g_j}{g_i} e^{-\Delta E_{ij}/kT} \,, \tag{14.1}$$

where $k = 1.38 \times 10^{-16} erg/K$ is known as Boltzmann's constant. At low temperature, with the thermal energy much less than the energy difference, $kT \ll \Delta E_{ij}$, there are relatively very few atoms in the more excited level j, $n_j/n_i \to 0$. Conversely, at very high temperature, with the thermal energy much greater than the energy difference, $kT \gg \Delta E_{ij}$, the ratio just becomes set by the statistical weights, $n_j/n_i \to g_j/g_i$.

As the population in excited levels increases with increased temperature, there are thus more and more atoms able to emit photons, once these excited states spontaneously decay to some lower level. This leads to an increased *emission* of the associated line transitions.

On the other hand, at lower temperature, the population balance shifts to lower levels. So when these cool atoms are illuminated by continuum light from hot layers, there is a net

[15]These orbital and spin states are denoted by quantum mechanical number ℓ and m, which thus supplement the principal quantum number n.

absorption of photons at the relevant line wavelengths, leading to a line-absorption spectrum.

14.2. Saha Equation for Ionization Equilibrium

At high temperatures, the energy of collisions can become sufficient to overcome the full binding energy of the atom, allowing the electron to become free, and thus making the atom an *ion*, with a net positive charge. For atoms with more than a single proton, this process of *ionization* can continue through multiple stages up to the number of protons, at which point it is completely stripped of electrons. Between an ionization stage i and the next ionization stage $i+1$, the exchange for any element X can be written as

$$X_{i+1} \leftrightarrow X_i + e^- \,. \tag{14.2}$$

In thermodynamic equilibrium, there develops a statistical balance between the neighboring ionization stages that is quite analogous to the Boltzmann equilibrium for bound levels given in eqn. (14.1). But now the ionized states consist of both ions, with many discrete energy levels, and free electrons, with a kinetic energy $E = p^2/2m_e$ given by their momentum p and mass m_e. The number of *bound* states of an ion in ionization stage i is now given by something called the *partition function*, which we will again write as g_i. But to write the equilibrium balance, we now need also to find an expression for the number of states available to the *free* electron.

For ionization of a stage i with ionization energy ΔE_i, the Boltzmann relation for the ratio of upper vs. lower ionization state can then be written

$$\frac{n_{i+1}(p)}{n_i} = \frac{g_{i+1}}{g_i}\, g_e(p)\; e^{-(\Delta E_i + p^2/2m_e)/kT} \,, \tag{14.3}$$

where $n_{i+1}(p)\,dp$ is the number of ionized atoms with an associated electron of momentum between p and $p+dp$, and $g_e(p)$ is the statistical weight for such electrons, representing the *number of quantum mechanical states* available to them. Because electrons with momentum p have an associated de Broglie wavelength $\lambda_p = h/p$, each electron occupies a minimum volume h^3 in "phase space", with dimensions of length times momentum. For an isotropic momentum distribution, the momentum volume is that for shell of radius p and thickness dp, i.e. $4\pi p^2\,dp$, while the spatial volume is just the inverse of the total density. Accounting for the two possible states of the electron spin, we then find the number of available states is

$$g_e(p)\,dp = \frac{2}{n_e}\frac{4\pi p^2\,dp}{h^3} \,. \tag{14.4}$$

If we define a de Brolie wavelength associated with thermal-speed electrons,

$$\Lambda \equiv \frac{h}{\sqrt{2\pi m_e kT}}\,, \tag{14.5}$$

then after integrating eqn. (14.3) over all p from zero to infinity, we obtain the *Saha-Boltzmann equation* for ionization balance

$$\frac{n_{i+1}}{n_i} = \frac{g_{i+1}}{g_i}\left[\frac{2}{n_e\Lambda^3}\right] e^{-\Delta E_i/kT} \tag{14.6}$$

$$= \frac{g_{i+1}}{g_i}\,\frac{2}{n_e}\left(\frac{2\pi m_e kT}{h^2}\right)^{3/2} e^{-\Delta E_i/kT}\,. \tag{14.7}$$

Throughout a normal star, the electron state factor in square brackets is typically a huge number[16]. For example, for conditions in a stellar atmosphere, it is typically of order 10^{10}. This large number of states acts like a kind of "attractor" for the ionized state. It means the numbers in the more vs. less ionized states can be comparble even when the exponential Boltzman factor is very small, with a thermal energy that is well below the ionization energy, i.e. $kT \approx \Delta E_i/10$.

For example, hydrogen in a stellar atmosphere typically starts to become ionized at a temperature of about $T \approx 10^4 K$, even though the thermal energy is only $kT \approx 0.86$ eV, and thus much less than the hydrogen ionization energy $E_i = 13.6$ eV. But this leads to a Boltzman factor $e^{-13.6/0.86} = 1.4 \times 10^{-7}$ that is roughly offset by this large electron states factor. Since the partition ratio is of order unity, this gives a roughly equal fraction of Hydrogen in neutral and ionized states.

14.3. Absorption Lines and Spectral Type

The line-absorption patterns that appear in a star's spectrum depend on the elemental composition and degree of ionization of the atoms. Because ionization depends sensitively on temperature, the lines in stars with higher (lower) surface temperatures generally come from higher (lower) ionization stages. The effect is so systematic that a judicious classification of the spectral lines from a star can be used to infer the surface temperature. Figure 14 compares the spectra of stars of different surface temperature, showing that this leads to gradual changes and shifts in the detailed pattern of absorption lines. The letters "OBAFGKM"

[16]As discussed later, it only becomes order unity in very compressed conditions, like in the interior of a white dwarf star, which is thus said to be *electron degenerate*.

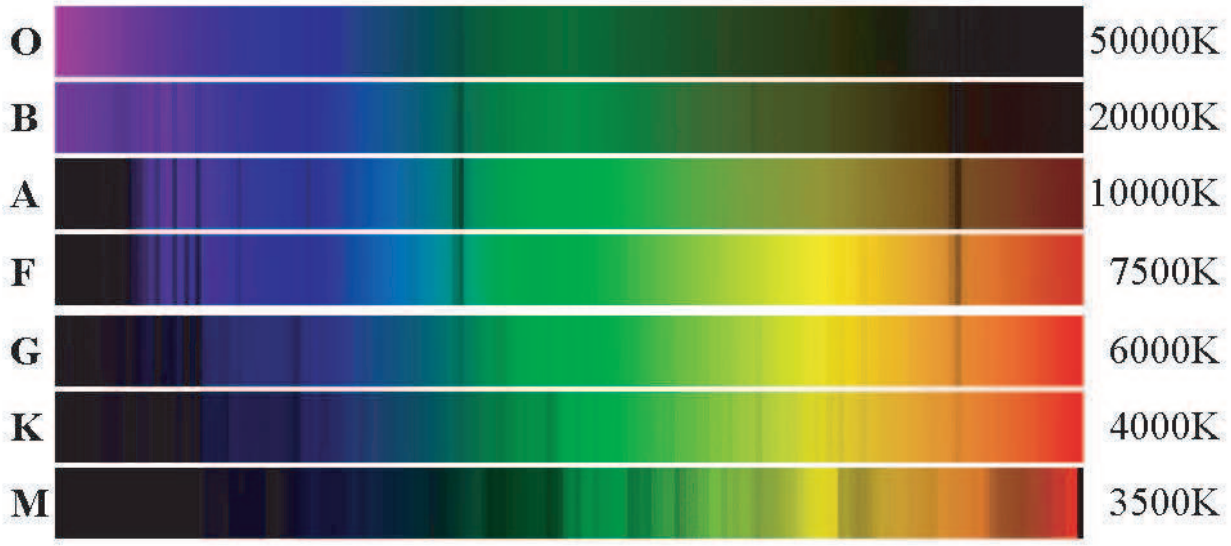

Fig. 14.— Stellar spectra for the full range of spectral types OBAFGKM, corresponding to a range in stellar surface temperature from hot to cool.

represent various categories, known as "spectral class", assigned to stars with different spectral patterns. It turns out that class O is the hottest, with temperatures about 50,000 K, while M is the coolest, with temperatures of ca. 3500 K. The sequence is often remembered through the mneumonic "Oh, Be A Fine Gal/Guy Kiss Me".

Figure 15 shows some further spectra, now broken down into subtypes denoted by an added number from 0 to 9, representing a further delineation of hot to cool within the main spectral type. For example, the sun is a G3 star, with a spectrum somewhat intermediate between the slightly hotter G0 and slightly cooler G5 types shown in the figure. The labels along the top and bottom now also identify the specific elements responsible for the most prominent absorption lines. Note for the high temperature stars, the labels along the top generally correspond to atoms or ions, whereas for cooler stars the labels along the bottom are often for molecules. At high temperature, the higher energy of both the photons and the collisions between the atoms is sufficient to strip off the electrons from atoms, whereas at low temperatures, the energy of the photons and collisions is low enough to allow the much weaker bonds of molecules to still survive.

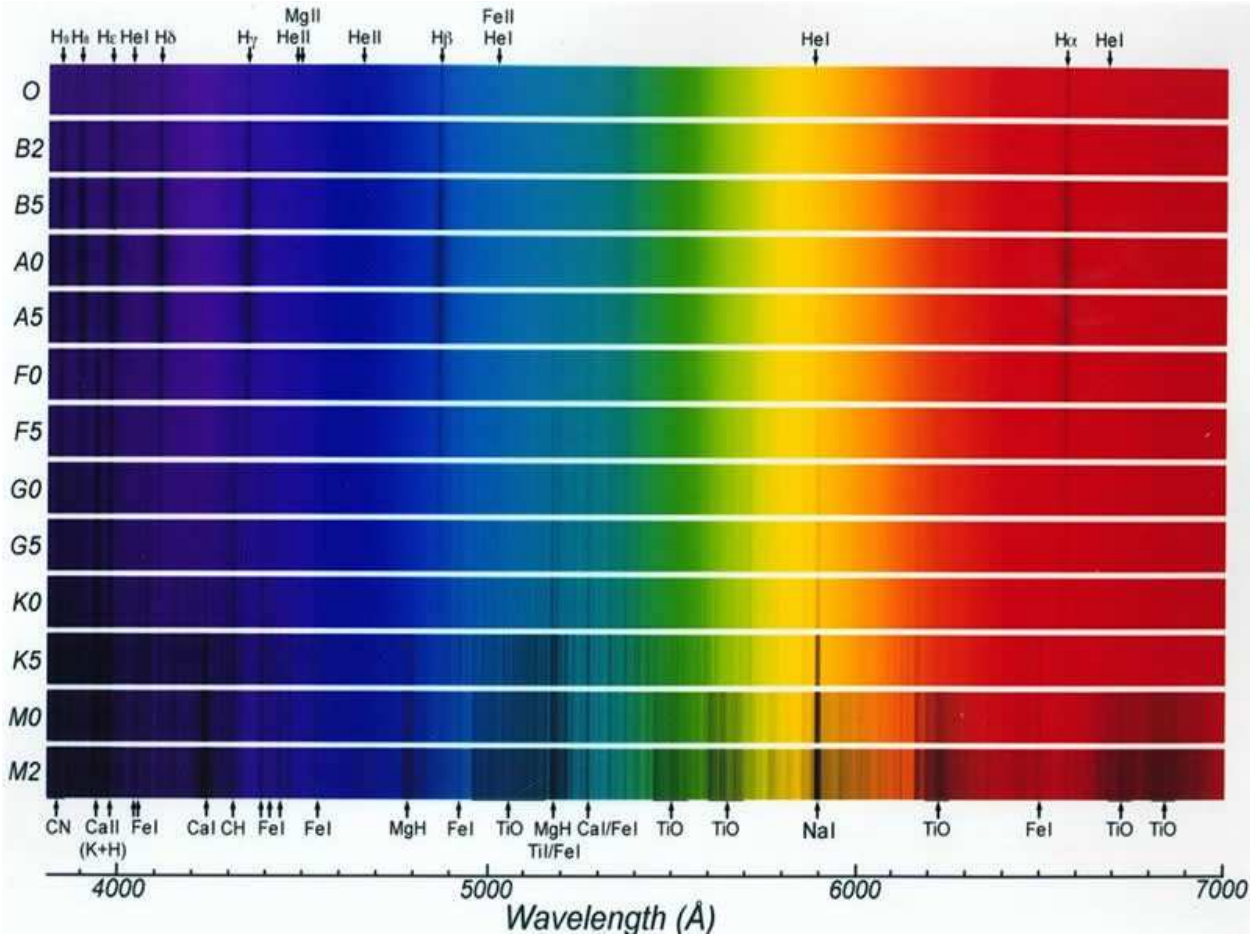

Fig. 15.— Stellar spectra showing various subtypes of the main spectral classes OBAFGKM, denoted by class plus a number ranging from 0 to 9. The labels along the top and bottom identify the specific atom, ion, or molecule responsible for the most prominent absorption lines. For ions the roman numerical denotes degree of ionization, with I representing neutral, II representing singly ionized, etc.

14.4. Luminosity class

The Saha equation shows that ionization depends on density as well as temperature, and for a given temperature, density depends on pressure. Through the equation of hydrostatic equilibrium, the pressure in an atmosphere can be written as $P = mg = \tau g/\kappa$, where the mass column density m is related to the optical depth through the opacity κ by $m = \tau/\kappa$. Thus at the photospheric layers $\tau = 1$, we see that the pressure scales directly with the stellar gravity, which, for given stellar mass, depends in turn on the stellar radius, $g = GM/R^2$.

For a given surface temperature, a larger radius implies a larger surface area and so a larger luminosity, $L \sim \sigma T^4 4\pi R^2$.

The upshot then is that an ionization balance that suggests a lower density – and thus lower pressure, lower gravity, larger radius – also implies a higher luminosity. This is the basis of the *luminosity class* of stellar spectra, conventionally denoted with roman numerals I, II, III, IV and V, denoting a declining luminosity sequence. Class I are called *supergiants*, representing very large, and very luminous stars. Class III are just ordinary *giants*, still large and luminous, but less so. Finally class V are *dwarfs*, representing "normal" stars like the sun.

15. H-R Diagram: Color-Magnitude or Temperature-Luminosity

15.1. H-R Diagram for Stars in Solar Neighborhood

A key diagnostic of stars comes from the Hertzsprung-Russel (H-R) diagram. Observationally, it relates stellar colors to their (absolute) magnitude, or spectral type and luminosity class; physically, it relates surface temperature to luminosity. Figure 16 shows an H-R diagram for a large sample of stars with known luminosities and colors. The horizontal lines show the luminosity classes.

The extended band of stars running from the upper left to lower right is known as the *main sequence*, representing "dwarf" stars of luminosity class V. The reason there are so many stars in this main sequence band is that it represents the long-lived phase when stars are stably burning Hydrogen into Helium in their cores.

The medium horizontal band above the main sequence represent "giant stars" of luminosity class III. They are typically stars that have exhausted hydrogen in their core, and are now getting energy from a combination of hydrogen burning in circum-core shells, and burning Helium into Carbon in their cores.

The relative lack here of still more luminous supergiant stars of luminosity class I stems from both the relative rarity of stars with sufficiently high mass to become this luminous, coupled with the fact that such luminous stars only live for a very short time. As such, there are only a few such massive, luminous stars in the solar neighborhood. Studying them requires broader surveys that encompass a greater fraction of the galaxy.

The band of stars below the main sequence are called *white dwarfs*; they represent the slowly cooling remnant cores of low-mass stars like the sun.

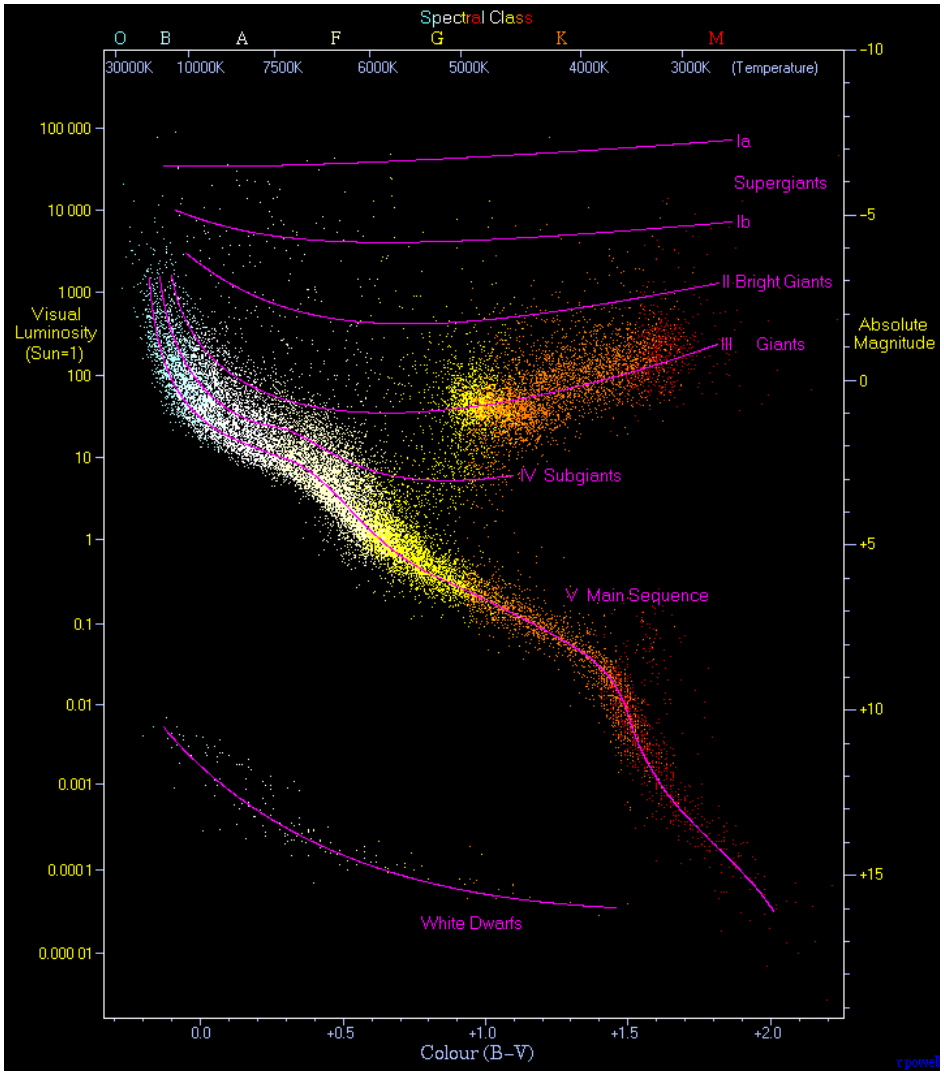

Fig. 16.— H-R diagram relating stellar luminosity to surface temperature. The points include 22,000 stars from the Hipparcos Catalogue together with 1000 low-luminosity stars (red and white dwarfs) from the Gliese Catalogue of Nearby Stars.

This association between position on the H-R diagram, and stellar parameters and evolutionary status, represents a key link between the observable properties from stellar atmosphere and the physical properties associated with the stellar interior. Understanding this link through examination of stellar structure and evolution will constitute the major thrust of our studies of stellar interiors below.

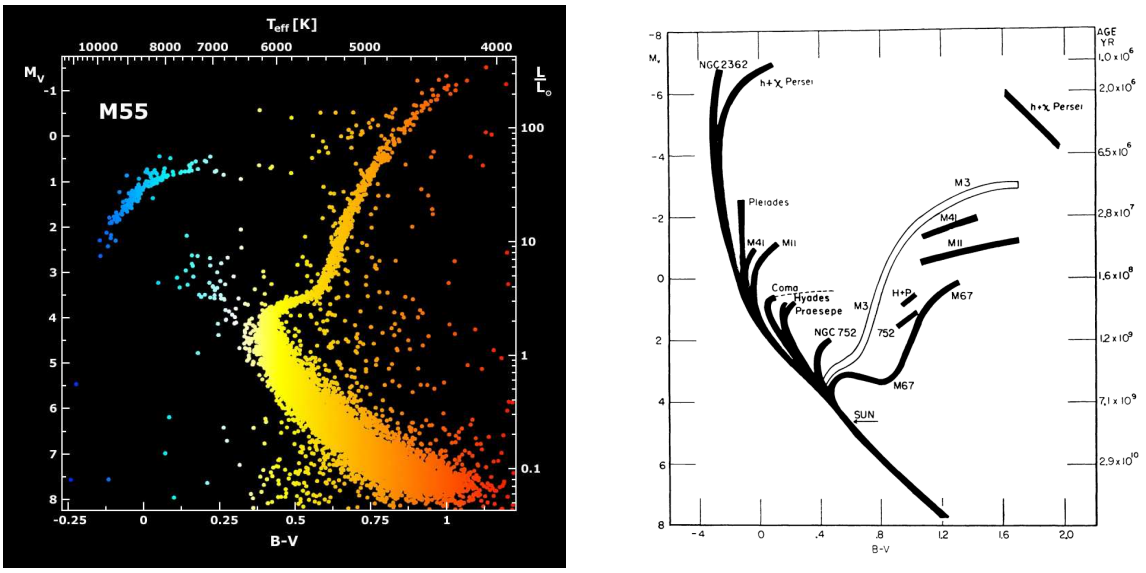

Fig. 17.— Left: H-R diagram for globular cluster M55, showing how stars on the upper main sequence have evolved to lower temperature giant stars. Right: Schematic H-R diagram for clusters, showing the systematic peeling off of the main sequence with increasing cluster age.

15.2. H-R Diagram for Clusters – Evolution of Upper Main Sequence

The above volume-limited sample near the sun consists of stars of a wide range of ages, distances, and perhaps even chemical composition. But stars in a stellar cluster are all at a similar distance, and since the likely formed over a relatively short time span out of the same interstellar cloud, they should all have nearly the same age and composition. The left panel of figure 17 plots an H-R diagram for the globular cluster M55. Note that all the stars in the upper left main sequence have evolved to a vertical branch of cooler stars extending up to the red giants. This reflects the fact that more luminous stars exhaust their hydrogen fuel sooner that dimmer stars. The right panel illustrates this schematically, showing how the turnoff point from the main sequence is an indicator of the cluster age. Plots like this thus provide a direct diagnostic of stellar evolution of stars with different luminosity. As we shall now see, the main sequence luminosity of stars is set primarily by the stellar mass.

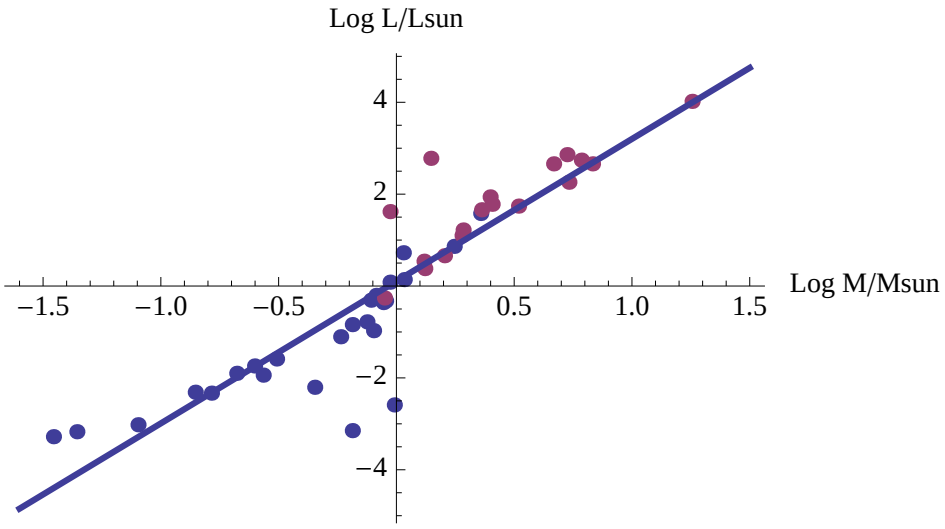

Fig. 18.— A log-log plot of luminosity vs. mass (in solar units) for a sample of astrometric (blue, lower points) binaries and eclipsing (red, upper points) binaries. The best-fit line shown follows the empirical scaling, $\log(L/L_\odot) \approx 0.1 + 3.1 \log(M/M_\odot)$.

16. The Stellar Mass-Luminosity Relation

16.1. Stellar Masses Inferred from Binary Systems

As discussed in sections 6 and 7 of DocONotes1-Stars, the most direct and robust way to infer stellar masses comes from using Kepler's laws to interpret their inferred motion in binary systems, with the most accurate masses derived from astrometric binaries and double line eclipsing binaries.

In astrometric binaries, the positions of the stars can be directly measured as they orbit their common center-of-mass (CM), and since the CM lies at a focus of the elliptical orbit, the inclination of the orbit can be inferred. For a given inclination, measuring the Doppler shift of spectral lines of each star (if bright enough) gives their orbital velocities, which combined with the measured orbital period gives the absolute dimensions of the orbits, the semi-major axes. Through Kepler's third law the orbital period and semi-major axes of each star gives the mass of each component. Furthermore, a comparison of the absolute dimensions with the apparent angular size gives the distance to the binary, allowing apparent magnitudes to be converted to absolute magnitudes and hence luminosities.

In double-line eclipsing binaries, the inclination of the orbit is obtained from the eclipse light curve. The masses can then be obtained in the same way as for the astrometric binaries.

If the distance is not known from trigonometric parallax, a distance estimate can be obtained from the eclipse durations, which give the sizes of the eclipsing stars. If the temperatures of the stars can be obtained from their spectra, combining with the stellar radii gives the stellar luminosity. The distance is then obtained by comparing with the apparent magnitudes.

Figure 18 plots $\log L$ vs. $\log M$ (in solar units) for a sample of astrometric (blue) and ecliping (red) binaries. A key result is that the data can be roughly fit by a straight line in this log-log plot, implying a power-law relation between luminosity and mass,

$$\frac{L}{L_\odot} \approx \left(\frac{M}{M_\odot}\right)^{3.1} . \tag{16.1}$$

16.2. Simple Theoretical Scaling Law for Mass vs. Luminosity

This empirical mass-luminosity relation can roughly explained by considering two basic relations of stellar structure, namely hydrostatic equilibrium and radiative diffusion, as given in eqns. (3.1) and (7.18) above. As in the virial scaling for internal tempeature given in section 3.1, we can use a single point evaluation of the pressure gradient to derive a scaling between interior temperature T, stellar radius R and mass M, and molecular weight μ,

$$\begin{aligned} \frac{dP}{dr} &= -\rho\frac{GM_r}{r^2} \\ \rho\frac{T}{\mu R} &\sim \rho\frac{M}{R^2} \\ T\,R &\sim M\,\mu\,, \end{aligned} \tag{16.2}$$

Likewise, a single point evaluation of the temperature gradient in the radiative diffusion equation gives,

$$\begin{aligned} F(r) &= -\left[\frac{4ac}{3}\frac{T^3}{3\kappa_R\rho}\right]\frac{dT}{dr} \\ \frac{L}{R^2} &\sim \frac{R^3}{\kappa\,M}\frac{T^4}{R} \\ L &\sim \frac{(R\,T)^4}{\kappa\,M} \\ L &\sim \frac{M^3\,\mu^4}{\kappa}\,, \end{aligned} \tag{16.3}$$

where the last scaling uses the hydrostatic equilbrium result to derive the basic scaling law $L \sim M^3$, assuming a fixed molecular weight μ and opacity κ.

We thus see that the empirical scaling found from binary systems plotted in figure 18 can be understood just in terms of the two basic equations for the structure of the stellar envelope, namely hydrostatic balance against gravity, and radiative diffusion transport of the stellar luminosity outward.

Note in particular that it does *not* depend on the details of the nuclear generation of the luminosity in the stellar core! Indeed, this scaling was understood from stellar structure analyses that were done (e.g. by Eddington, and Schwarzschild) in the 1920's, long before nuclear burning was firmly established (in a famous 1957 paper by Burbidge, Burbidge, Fowler and Hoyle).

It is also completely independent of the stellar radius R, which cancels in the above scaling for luminosity.

16.3. Virial Theorum

The hydrostatic balance of star can be used to derive a relation – known as the *virial theorum* – between the internal thermal energy and the graviational binding energy of a star. Detailed derivations are given in Rich Townsend's notes "01-virial.pdf" and Jim MacDonald's "Notes_Part_3.pdf", so here we just give an abridged derivation. Let us first multiply the standard hydrostic equilibrium equation (3.1) by the radius r, and integrate over a mass coordinate $dm = 4\pi r^2 \rho dr$, with m ranging from 0 to M as r goes from 0 to R,

$$
\begin{aligned}
-\int_0^M \frac{Gm}{r}\, dm &= \int_0^M \frac{r}{\rho}\,\frac{dP}{dr}\, dm \qquad (16.4)\\
&= \int_0^M 4\pi r^3 \,\frac{dP}{dm}\, dm \\
&= \left[4\pi r^3 P(r)\right]_{r=0}^{r=R} - \int_0^M \frac{P}{\rho}\, dm \\
&= -3(\gamma-1)\int_0^M u\, dm \\
\Phi &= -3(\gamma-1)U\,. \qquad (16.5)
\end{aligned}
$$

On the left side, $-Gm/r$ is the gravitational potential, defined such that zero potential is at $r \to \infty$; the integrand thus gives the gravitational energy gained by adding each mass shell dm, so that the total integral represents the total gravitational energy Φ. On the right side,

integration by parts leads to the square bracket term, which vanishes at both the center, $r = 0$, and at surface, where the gas pressure effectively become negligible, $P(R) = 0$. For the remaining term, we note that for a perfect gas, $P/\rho = (\gamma - 1)u$, where u is the internal energy-per-unit mass. The integration over mass thus gives the right side in terms of the total internal energy of the star, U. For monotonic gas with $\gamma = 5/3$, we thus find

$$\Phi = -3(\gamma - 1)U = -2U \,, \tag{16.6}$$

This implies that the total stellar energy is given by

$$E \equiv \Phi + U = \frac{3\gamma - 4}{3\gamma - 3}\,\Phi = \frac{\Phi}{2} < 0 \,, \tag{16.7}$$

where again the last equality is for the case of a monotonic gas case $\gamma = 5/3$, which is indeed the most appropriate for stellar interiors.

The virial theorum thus implies that the total energy of a star is negative (meaning it is bound), with a numerical value just half of the gravitational binding energy. This reduction by one-half stems from the positive internal energy, which equals half the absolute value of the gravitational energy.

However, we will discuss later that in very massive stars the internal energy can become dominated by radiation instead of gas. In the limit of a star with pure radiation, we find $\gamma \to 4/3$, which by eqn. (16.7) implies a total energy $E \to 0$. Such a star is no longer gravitationally bound, and so is very unstable. This may be a key factor in setting an upper mass limit of stars, on the order of a few hundred $M_\odot$.

17. Characteristic Timescales

17.1. Shortness of Chemical Burning Timescale for Sun and Stars

When 19th century scientists pondered the possible energy sources for the sun, some first considered whether this could come from the kind of chemical reactions that provide a key energy source (e.g. from fossil fuels like coal) on earth. But such chemical reactions involve transitions of electrons among various bound states of atoms, and, as discussed in the above Bohr model of the Hydrogen, the scale of energy release in such transitions is limited to about an order of electron volt (eV). In contrast, the rest mass energy of the atom itself, consisting protons and neutrons, is typically of order 10 Gev, or 10^{10} times higher. With the associated mass-energy efficiency of $\epsilon \sim 10^{-10}$, we can readily estimate a timescale for

maintaining the solar luminosity from chemical reactions,

$$t_{chem} = \epsilon \frac{M_\odot c^2}{L_\odot} = \epsilon \; 4.5 \times 10^{20} \, sec = \epsilon \; 1.5 \times 10^{13} \, yr \approx 15,000 \, yr \, . \tag{17.1}$$

Even in the 19th century, it was clear, e.g. from geology processes like erosion, that the earth – and so presumably also the sun – had to be much older than this.

17.2. Kelvin-Helmholtz Timescale for Luminosity Powered by Gravity

So let us instead consider a timescale associated with gravitational contraction as the energy source. The above virial relation shows that, as a star undergoes a gradual contraction that roughly maintains hydrostatic equilibrium, half of the gained energy goes into internal energy U of the star. But then the other half is availalble to be radiated away, powering the stellar luminosity. Following the work by Kelvin and Helmholtz, we can thus define an associated gravitational contraction lifetime for the sun

$$t_{KH} \equiv -\frac{\Phi}{L} \, . \tag{17.2}$$

To estimate a value for the gravitational binding energy, let us first consider the somewhat artificial assumption that the sun has a uniform density, given by its mass over volume, $\rho = M_\odot / (4\pi R_\odot^3/3$. Then the equation for gravitational binding energy gives

$$-\Phi = \int_0^{M_\odot} \frac{Gm}{r} \, dm = \frac{16\pi^2}{3} \, G\rho^2 \int_0^R r'^4 \, dr' = \frac{3}{5} \frac{GM_\odot^2}{R_\odot} \, . \tag{17.3}$$

Applying this in eqn. (17.2), we find

$$t_{KH} \approx \frac{3}{5} \frac{GM_\odot^2}{R_\odot L_\odot} \approx \; 30 \, Myr \, . \tag{17.4}$$

Although substantially longer than the chemical burning timescale, this is still much shorter than the geologically inferred minimum age of the earth, which is at least a Byr.

17.3. Nuclear Burning Timescale

We now realize, of course, that the main sequence age of stars like the sun is set by a much longer nuclear burning timescale. When four hydrogen nuclei are fused into a helium nucleus, the helium mass is about 0.7% lower than the original four hydrogen. For nuclear

fusion the above-defined mass-energy burning efficiency is thus $\epsilon \approx 0.007$. But in typical main sequence star, only some core fraction $f = 1/10$ of the stellar mass ever become hot enough to allow hydrogen fusion. Applying this we thus find for the nuclear burning timescale

$$t_{nuc} = \epsilon_{nuc}\, f\, \frac{Mc^2}{L} = 0.007 \times 0.1 \times 1.5 \times 10^{13}\, yr = 10^{10}\, yr\,, \tag{17.5}$$

where the latter equality apples the solar values. This is the basic rationale for the above quote (e.g. eqn. (17.6)) that the sun's main sequence lifetime is about 10 Byr.

17.4. Main Sequence Lifetimes

The above scaling of main-sequence luminosity with a high power of the stellar mass provides a simple explanation for the progressively truncated form of the upper main-sequence in older stellar clusters. Let us make the reaonable assumption that a fixed fraction of the total hydrogen mass of any star is available for nuclear burning into helium in its stellar core. Since then the fuel available scales with the mass, but the burning rate depends on the luminosity. Normalized to the sun, the main-sequence lifetime scales as

$$t_{ms} = t_{ms,\odot}\, \frac{M/M_\odot}{L/L_\odot} \approx 10\, Byr\, \left(\frac{M_\odot}{M}\right)^{2.1}\,. \tag{17.6}$$

The most massive stars, of order $100\, M_\odot$, thus have main-sequence lifetimes about about 1 Myr, much shorter the multi-Byr timescale for solar mass stars.

For cluster H-R diagrams, the above scalings mean that luminosity of stars at the turn-off point of the main sequence, L_{to}, can be used to infer the cluster age,

$$t_{cluster} \approx 10\, Byr\, \left(\frac{L_\odot}{L_{to}}\right)^{0.68}\,. \tag{17.7}$$